UNIVERSITY OF OKLAHOMA

GRADUATE COLLEGE

FUNDAMENTAL STUDIES OF PARDE TOXIN-ANTITOXIN SYSTEMS FOR THEIR POTENTIAL TO IMPACT BACTERIAL CELL GROWTH

A DISSERTATION

SUBMITTED TO THE GRADUATE FACULTY

In partial fulfillment of the requirements for the

Degree of

DOCTOR OF PHILOSOPHY

By

CHIH-HAN TU
Norman, Oklahoma
2025

FUNDAMENTAL STUDIES OF PARDE TOXIN-ANTITOXIN SYSTEMS FOR THEIR POTENTIAL TO IMPACT BACTERIAL CELL GROWTH

A DISSERTATION APPROVED FOR THE

DEPARTMENT OF CHEMISTRY AND BIOCHEMISTRY

BY THE COMMITTEE CONSISTING OF

Dr. Christina Bourne, Chair

Dr. Rakhi Rajan

Dr. Charles Rice

Dr. Andrew Madden

Acknowledgements

First and foremost, I would like to show my deep gratitude to Dr. Bourne. Without her mentorship, patience, and encouragement throughout my entire study, this doctoral dissertation would never become possible. Besides massive support on research, she is also a warmest mentor who cares about me and guide me how to face and overcome difficulties.

In addition, I would like to show my appreciation to my committee members, Dr. Rakhi Rajan, Dr. Charles Rice, and Dr. Andrew Madden. They provide inspired guidance and suggestions on my projects to help me complete my doctoral study.

I also deeply appreciated to my lab partners for their enormous support and assistance in my entire doctoral journey. Dr. Kevin Snead, and Dr. Shengfeng Ruan provided great assistance and guidance on my researches. Dr. Joel Langford and Walter Galie not only give me invaluable suggestion on my projects, but also provided me positive assistance and support on difficulties on research as well as daily life.

Last but not least, I would also like to show my appreciation to my parents and friends for their greatest support through the toughness of the entire journey. Most importantly, I would like to express my sincere gratitude to my parents for their unwavering support and love. Dad and mom, thank you for your encouragement and advice, and for always being there for me.

Table of Contents

List of Figures

List of table

List of Abbreviations

AMR	antimicrobial resistance
HTH	helix-turn-helix
RHH	ribbon-helix-helix
TA	toxin-antitoxin
PSK	postsegregational killing
PaParDE	*Pseudomonas aeruginosa* ParDE
EcParDE	*Escherichia. coli* ParDE
MtParDE	*Mycobacterium tuberculosis* ParDE
VcParDE	*Vibrio cholerae* ParDE
CcParDE	*Caulobacter crescentus* ParDE
MoParDE	*Mesorhizobium opportunistum* ParDE
IPTG	Isopropyl ß-D-1-thiogalactopyranoside
BME	β-Mercaptoethanol
CTD	C-terminal domain
FQ	fluoroquinolones
QPT-1	quinolone pyrimidinetrione
IPYs	imisazopyrazinones
NBTI	novel (or non-fluoroquinolone) bacterial topoisomerase inhibitors
PRP	pentapeptide repeat protein
GdHCl	guanidinium hydrochloride
Sf9	*Spodoptera frugiperda*
PEPPI	Passively Elution Proteins from Polyacrylamide Gel as Intact species
LC-MS	Liquid Chromatography Mass Spectrometry

Abstract

The rise of antimicrobial-resistant bacteria, coupled with a shortage of new antibiotics, has threatened treatment of infections as well as modern medical procedures. To counteract with this burgeoning issue, targeting bacterial toxin-antitoxin (TA) systems, which engage in controlling bacterial cell growth under stress conditions, e.g., antibiotics treatment, presents a promising strategy for developing novel antimicrobial agents to combat resistance. TA systems are widely distributed in prokaryotes and the operon is composed of a small bicistronic locus encoding antitoxin and toxin genes. In the case of type II ParDE TA systems, the ParE toxin protein selectively inhibits DNA gyrase, an essential type II bacterial topoisomerase, by stabilizing gyrase-mediated DNA cleavage complex, leading to double strand DNA break. The toxicity of ParE protein can be neutralized by its co-encoded cognate ParD antitoxin protein through direct protein-protein interaction. The work presented in this dissertation aim to provides deeper insights to understand the structural properties of the ParDE TA systems and the impact on bacterial cell growth and resulting influence on mutation driven from ParE-mediated gyrase inhibition.

Chapter II of this work focuses on the impact of VcParE toxins induced expression in the native host, *Vibrio cholerae* (Vc). The results showed that strong expression of VcParE toxins caused cell death, likely arising from extensive DNA break generated by inhibition of gyrase, and overwhelming the repair machinery. However, lower levels of ParE expression could be tolerated, and the induced DNA breaks was able to be repaired, permitting cell survival. As it is known that this type of repair can be error-prone, the result confirmed increases in mutation frequency after lower induction of VcParE toxins. Importantly, however, this did not correlate with decreasing antibiotics susceptibility. Overall these results indicate that VcParE toxins are potent inhibitors of DNA gyrase in bacterial cells, and that damage generated by gyrase inhibition do not lead to increase in antibiotic resistance.

Chapter III of this work explore the feasibility to obtain purified ParE toxins following reported methods and developed an optimized purification approach. We tried various expression and purification strategies, including denaturation-refolding of the ParDE complex, in vitro protein synthesis, bulky fusion protein expression and co-transformation with gyrase, to overcome ParE toxicity and obtain sufficient protein for future characterization. Our result showed that co-transformation with gyrase was effective to lessen VcParE1 toxicity and the purified VcParE1 proved to be active in the inhibition of gyrase-mediated supercoiling assay. The approach developed in this chapter enables us to obtain quantitive VcParE1 for future structural studies to further elucidate the structure of ParE-gyrase complex.

Chapter IV of this work investigates the intrinsic degradation of the PaParD1 antitoxin, analyzing factors influencing its stability. Our result indicated that the degradation of PaParD1 is affected by temperature, pH value, and concentration, with maximal degradation observed at physiological pH and temperature. Higher concentrations of PaParD1 also increased degradation rate. We also established the effect of ionic strength on PaParD1 dimerization and degradation, with increased degradation rate as the ratio of monomeric PaParD1 increased. While initial hypothesis suggested a glutamine-mediated cleavage mechanism, mutagenesis experiments revealed no direct role for glutamine in PaParD1 degradation. To further identify protein speices appearing in the PaParD1 degradation process, Mass spectrometry was used and identified unexpectedly co-purifying DnaK chaperone which potentially modulate PaParD1 stability. In aggregate, Chapter IV provides optimal conditions for PaParD1 stability for *in vitro* storage, and propose a dynamic PaParD1 dimerization in varied ionic strength,

offering a foundation for future research on TA system regulation.

Overall, the study of this dissertation advanced the understanding of ParDE TA systems and their potential for antimicrobial development. ParE toxins were shown to strongly inhibit DNA gyrase, causing DNA damage and cell death, though lower level of expression increased mutation frequency but did not accumulate to become antibiotic resistance. Additionally, the approach of co-transformation with gyrase developed in this dissertation is able to produce decent quantity of active VcParE1, enabling future structural studies for the ParE-gyrase complex. Lastly, investigation of the intrinsic stability of the PaParD1 revealed core conditions affecting its degradation, including temperature, pH, concentration, and ionic strength. The co-purifying DnaK chaperone is also identified and may function in modulating PaParD1 stability. Taken together, the research in this dissertation extend the understanding of ParDE TA system, from the structural to functional properties, providing a foundation for future studies on their regulatory mechanisms as well as potential application in antimicrobial development.

Chapter I: Introduction

The emergence of antimicrobial resistant pathogenic bacteria and shortage of antibiotics

The emergence of antimicrobial resistant pathogenic bacteria coupled with the shortage of novel antibiotics jeopardizes treatment options for infections.[1, 2] It has been reported that antimicrobial resistance was associated with 1.27 million global deaths and directly contributed to 4.95 million deaths in 2019.[3] Antimicrobial resistance poses a risk to modern medicine by not only making infectious diseases even more difficult to treat, but also compounds complications to medical procedures, like surgery or chemotherapy[4] Due to the elevated threats of infectious disease, from both increased cases of bacterial resistance toward currently used therapeutics and decreased number of newly developed antibiotics, it is urgent to address the need for novel antimicrobial strategies.

Bacterial toxin-antitoxin (TA) systems are linked closely to antimicrobial resistance (AMR) because of their involvement to bacterial persistence, stress adaptation and the maintenance of plasmids carrying resistant genes.[5-7] When bacterial cells encounter stringent conditions, including antibiotics treatment, host immune response, TA systems play a vital role in the reduction of bacterial metabolic activities, pausing cell growth and promoting a persister state.[6, 8] Therefore, targeting TA systems likely bring an alternative strategy for developing novel antimicrobial agents. Due to their wide distribution in bacterial genomes, especially in pathogenic bacteria,[9] and their diverse impacts in disrupting fundamental biological processes,[10] exploiting TA systems provide novel treatment options to overcome conventional resistance mechanisms and reduce prevalence of AMR issues.

The bacterial TA system

TA systems are widely distributed in prokaryotes, usually encoded in an operon with small bicistronic loci consisting of an antitoxin and a toxin gene.[11, 12] Toxins of the TA system bind to different essential targets, including tRNAs, mRNAs, ribosomes and DNA gyrase. The antitoxin gene encodes either a protein or RNA with an unstable structure, and this neutralizes the cognate toxin protein.[11, 13, 14] The classification of a TA systems is based on the nature of the antitoxin and the mode it neutralizes the toxin. Currently, there are eight types of TA system that have been classified.[11]

Among them, type I, III and VIII systems encode RNA antitoxins. In type I systems, RNA antitoxins are antisense RNAs complementary to the toxin mRNA which functions to silence toxin expression[15-17]. In type III systems, the RNA antitoxins are small pseudoknot RNAs that neutralize their cognate toxin proteins by directly binding and forming RNA-protein complex.[18, 19] In type VIII systems, the RNA antitoxins act as an antisense RNA or recruit a Cas protein by emulating a CRISPR RNA to repress the expression of the cognate toxin RNA.[20, 21]

On the other hand, type II, IV, V, VI and VII systems encode protein antitoxins. In type II systems, the neutralization is mediated through direct interactions between protein antitoxins and their cognate toxin proteins.[12, 22, 23] In type IV systems, the protein antitoxins protect or reverse toxin-mediated modifications the cellular targets of the cognate toxins.[24-26] In type V systems, antitoxins act as endoribonucleases to degrade the mRNA of their cognate toxin.[27] In type VI systems, the protein antitoxins facilitate the degradation of ATP-

dependent protease by binding to their cognate toxin proteins.[28] In type VII systems, the protein antitoxins process post-translational modifications on their cognate toxin proteins to inactivate their activity.[29-31] Type II TA systems are the most prevalent in bacterial genomes compared to type I, III, IV, VII and VIII. There is only one single representative system identified as Type V and VI system, respectively.

TA systems were first discovered in plasmids, functioning by promoting the retention of plasmids via a phenomenon known as postsegregational killing(PSK).[32, 33] Briefly, due to the unstable property of antitoxins in these Type II systems, cells failing to inherit TA-encoded plasmids are killed as they are unable to neutralize remaining toxins. Later on, TA systems were also identified in bacterial chromosomes, mostly found associated with integrated mobile genetic elements, including transposons, integrative and conjugative elements or prophage, or were found to be established their own small genomic islands.[34-36] Unlike the plasmid-encoded TA systems which have a clear role on ensuring plasmid inheritance, the function for chromosomal TA systems is still under debate. So far, they have been proposed to play roles in i) regulating cell growth or inducing cell death in stress condition;[16, 37] ii) phage defense; [38, 39] iii) anti-addiction[40] and iv) pathogenesis.[9, 41, 42] The function of chromosomal TA systems was originally considered to mediate cell growth when cells are subjected to stringent conditions.[43] Such conditions cause elevated level of un-neutralized toxin due to a decrease in the level of antitoxin via degradation in cells. For instance, the PepA1 toxin from the type I PepA1-SprA1$_{AS}$ TA system has been shown to increase in expression while the level of SprA1$_{AS}$ antitoxin decreased in acid and oxidative stress.[16, 37] Conversely, phage defense is also a commonly proposed function for chromosomal TA systems.[38] The type II PfiT-PfiA TA system encoded in Pf prophages was shown to inhibit Pf4 phage production in *Pseudomonas aeruginosa*.[39] Additionally, models propose the chromosomal TA system functions as an anti-addiction modules due to the fact that chromosomal antitoxins may neutralize toxins from mobile genetic elements, such as plasmids or bacteriophage, to protect host cells against PSK.[40] The chromosomal CcdA antitoxin from *Erwinia chrysanthemi* was reported to neutralize the CcdB toxin from F1 plasmids.[44] Lastly, chromosomal TA systems have also been associated with pathogenicity. In *Mycobacteria*, there are only five TA systems encoded in the non-pathogenic *M. smegmatis* genome while there are approximately 88 TA systems encoded in the pathogenic *M. tuberculosis* H37Rv.[9] The VapBC TA systems, in particular, have been reported to contribute to the bacterium's pathogenicity.[9, 41] Taken together, the chromosomal TA systems have been proposed to be involved in multiple functions and mechanisms. With many examples supporting these functions and mechanisms, chromosomal TA systems are a robust field with researchers beginning to uncover their role in prokaryotes.

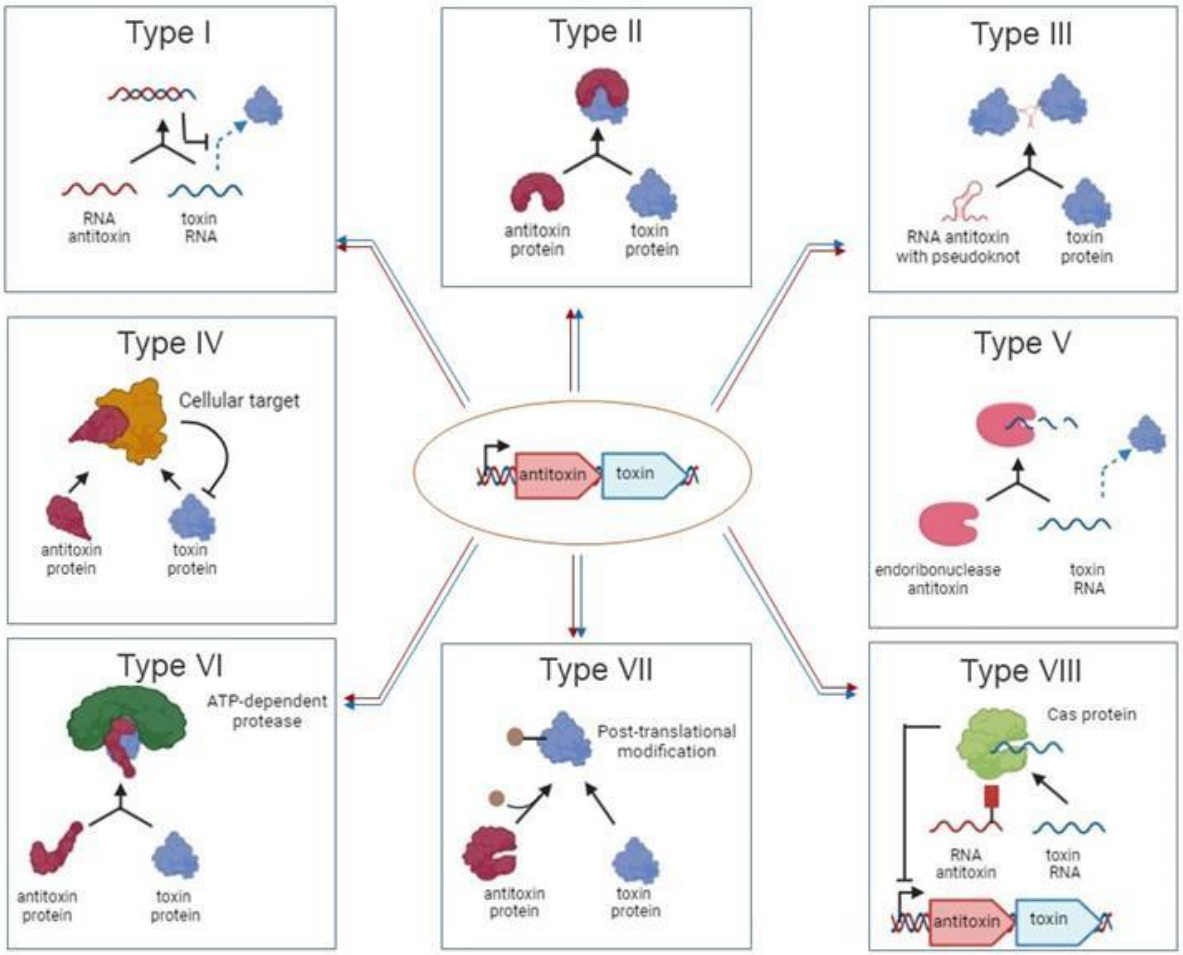

Figure. 1.1. The eight types of toxin-antitoxin (TA) system. A TA system is a module encoding an antitoxin and a toxin gene, in which the antitoxin gene is usually preceding the toxin gene. Currently, there are eight types of TA system that have been categorized. Type I systems encode RNA antitoxins neutralizing the cognate toxin by silencing its expression. Type II systems encode protein antitoxins that neutralize the cognate toxin through direct protein-protein interaction. Type III systems encode RNA antitoxins that sequester the cognate toxin by direct RNA-protein interaction. Type IV systems encode protein antitoxins that protect the cellular target from the toxin. The type V system encodes an endoribonuclease antitoxin that digests the toxin RNA. The type VI system encodes a protein antitoxin that interacts with toxin protein to facilitate the degradation by ATP-dependent protease. Type VII systems encode a protein antitoxin that post-translationally modifies the toxin. Type VIII systems encode RNA antitoxins that recruit a Cas protein to repress the expression of the cognate toxin RNA.

The Type II ParDE TA system

The ParDE TA system is a Type II TA system, in which the protein ParD antitoxin neutralizes the protein ParE toxin through direct protein-protein interactions (Figure 1.2.)[45] The ParD antitoxin is relatively unstable, either exhibiting an unstable structures or is easily targeted and degraded by ATP-dependent proteases.[45] Conversely, the ParE toxin contains a stable structure and has been identified to inhibit DNA gyrase by stalling the gyrase-mediated DNA cleavage complex, leading to persistence of double-strand DNA breaks.[22, 46, 47]

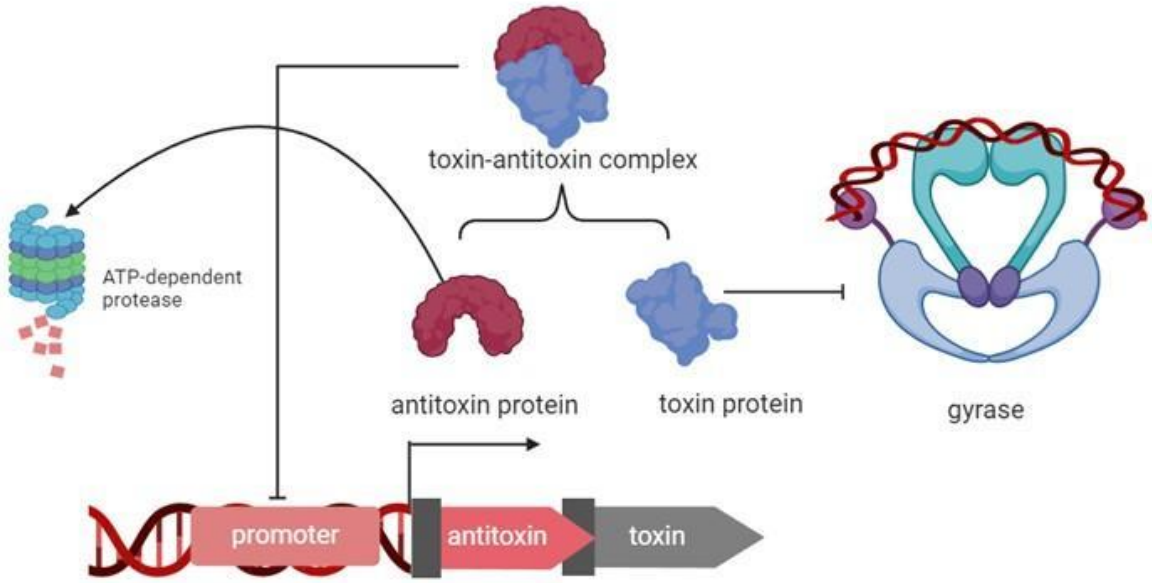

Figure. 1.2. Overview of type II ParDE TA system. The type II ParDE TA system is encoded in an operon containing the ParD antitoxin and ParE toxin genes. The ParD antitoxin is an unstable protein, exhibiting an unstable structure and being easily degraded by ATP-dependent protease, but functions in neutralizing ParE toxin via direct protein-protein interactions. The ParDE complex can return to self-regulate the TA operon by binding to a repressor site in the promoter. On the other hand, the ParE toxin is a relatively stable protein, targeting DNA gyrase, which is an essential enzyme for prokaryotic cells.

Although the sequence identity is low, the structures of type II TA systems are conserved and classified into several superfamilies.[40, 48, 49] While the C-terminus of an antitoxin is specific to the cognate toxin co-encoded with that antitoxin, the DNA binding motif is highly conserved in antitoxin families and can be categorized into antitoxin families based on motifs, like helix-turn-helix (HTH), ribbon-helix-helix (RHH) and Abr-like DNA binding domain. The structure of the ParD antitoxin exhibits an N-terminal RHH DNA binding motif involved in autoregulation of the TA operon, and an unstructured C-terminal ParE binding motif that becomes structured upon binding to the cognate ParE toxin.[50, 51] On the other hand, the toxin proteins are classified into a RelE/ParE-type clan, a PIN-type clan, and a CcdB/PemK-type clan.[40] The ParE toxin belongs to the most prevalent toxin families, the RelE/ParE-type superfamily. The toxin proteins in this superfamily often exhibit a microbial RNase fold but vary at the C - terminus as well as the specific residues comprising the active site[52, 53]. Despite most of the toxin members in the RelE/ParE superfamily functioning as RNA cleaving enzymes,[53] the ParE toxins acts as a gyrase inhibitor with uncharacterized mechanisms that appear devoid of a catalytic component.[46, 47, 54]

To date, there are eight crystal structures of ParDE complexes that have been resolved with no

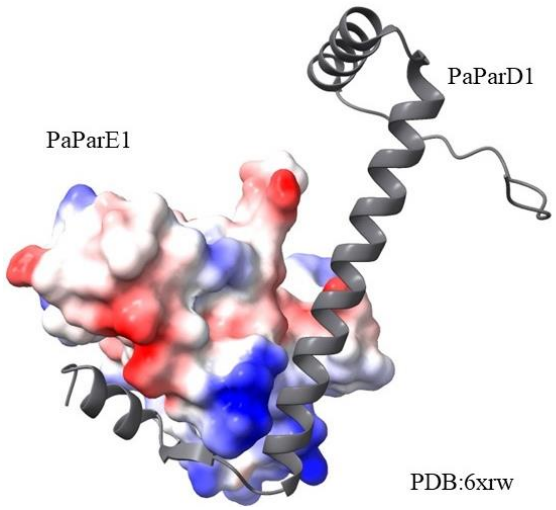

Figure 1.3. The structure of ParDE complex. Despite having low sequence identity, the ParDE complex exhibits highly conserved structure among different ParDE TA systems. The interaction surface is extensive and highly specific so that the occurrence of cross interaction between different ParDE systems is rare. The PaParD1 is represented as a grey ribbon. The PaParE1 is represented as a Coulombic surface.

success in structure determination for the free ParE toxin or in complex with the target DNA gyrase.[45, 50, 55-59] The structures of these ParDE complexes are highly conserved and the contact area between the toxin and antitoxin is approximately 20% of both ParE and ParD surface.[60] However, the interaction between ParE and ParD is highly specific. The occurrence of cross interaction is rare even when there are multiple ParDE pairs in the same cells.[55, 60, 61] Also, the stoichiometry of some ParDE complexes is different. Unlike most ParDE complexes that usually form 2:2 stoichiometry,[45, 50, 59, 60] the ParDE2 complex from *V. cholerae* exhibits the $ParD2_6$-$ParE2_2$ hetero-octamer stoichiometry that performs the strongest promoter binding compared to the ParD2 homodimer and $ParD2_2$-$ParE2_2$ hetero-tetramer, indicating the hetero-octamer contains the most potent repression on the ParDE2 expression.[58] Interestingly, the hetero-tetrameric form of ParDE2 complex, instead, cannot fully bind to the operator due to the steric hindrance and in turn abrogates the repression.[58] The ParDE1 complex from *M. tuberculosis* also forms a special $ParD1_4$-$ParE1_2$ hetero-hexamer and exhibits a dynamic equilibrium between hetero-hexameric and hetero-tetrameric complex in solution, incorporated with release of the ParE1 toxin.[59] The ParDE complex from *M. opportunistum* further forms a $ParD3_4$-$ParE3_4$ stoichiometry in solution.[60] Last but not least, the PaaA2-ParE2 complex from *E.coli* assembles into a hetero-hexadecamer in solution although the PaaA2 antitoxin is truncated and lacks the DNA-binding RHH motif.[55] Taken together, the structure of the ParD antitoxin binding to the cognate ParE toxin is highly conserved among ParDE TA systems but the interaction is highly specific. The C-terminal domain of ParD antitoxins function in ParE toxin binding while the N-terminal domains of ParD antitoxin are vital for the formation of higher-order stoichiometries.

DNA gyrase and the inhibitory sites

DNA gyrase belongs to the type II topoisomerase family, which functions in regulating DNA topology, including relaxing positive DNA supercoils, introducing negative DNA supercoils, and decatenating interlinked DNA molecules.[62-65] DNA gyrase is composed of two subunits, GyrA and GyrB, and together forms an active A_2B_2 heterotetramer of approximately 370 kDa.[66] DNA gyrase contains three functionally important interfaces: the "N-gate", the "DNA-gate", and the "C-gate". The N-gate includes an ATP binding site in GyrB that, when fully occupied, traps the DNA T-segment.[67, 68]. The DNA-gate is composed of a DNA-binding winged helix domain (WHD), as well as the tower domain of GyrA and TOPORIM domain of GyrB, functioning in DNA cleavage and re-ligation. Particularly, the WHD domain of GyrA contains the catalytic tyrosine residue and is the domain interacting with GyrB TOPORIM domain to form the active gyrase heterotetramer.[66, 69, 70] The C-gate consists of the coiled coil region of GyrA which forms an exit for the leaving of DNA strands.[66] The

formation of protein-protein interfaces by the WHD domains and by the coiled coil domains contribute to the stabilization of the GyrA dimer.[69]

As DNA replication or transcription occurs, "positive" supercoils accumulate ahead of replication forks or transcription bubbles while "negative" supercoils accumulate behind due to unwinding of the DNA duplex. [71, 72] Therefore, to maintain the topological homeostasis, DNA gyrase relaxes positive supercoils and introduces negative supercoils through a strand-passage mechanism.[62, 72] This process is achieved by breaking both strands of a bound DNA segment ("G" or gate segment) to allow the adjacent second DNA segment ("T" or transported segment) to pass through this gate and cleaved DNA using energy from ATP hydrolysis (Figure 1.4.) The catalytic cycle is initiated when DNA gyrase wraps the G-segment dsDNA around the gyrase two C-terminal domains (CTDs). The T-segment is locked in an area between the ATP binding domains of Gyrase B subunits (GyrB) once two ATP molecules bind. A magnesium ion is coordinated with the GyrB subunits and used to stabilize charges to promote the cleavage of a phosphodiester bond in each DNA strand through transesterification.[64, 72, 73] Cleavage is mediated by a catalytic tyrosine residue on each GyrA subunit, resulting in a covalently bound 5' end of G-segment. The T-segment subsequently passes through the G-gate gap with energy provided by hydrolysis of one of the two bound ATPs. Once the T-segment is passed, the DNA break is ligated to restore the integrity of the DNA substrate. The DNA molecule is then released from the gyrase C-gate as the second ATP is hydrolyzed, and the gyrase enzyme resets for another cycle.[64]

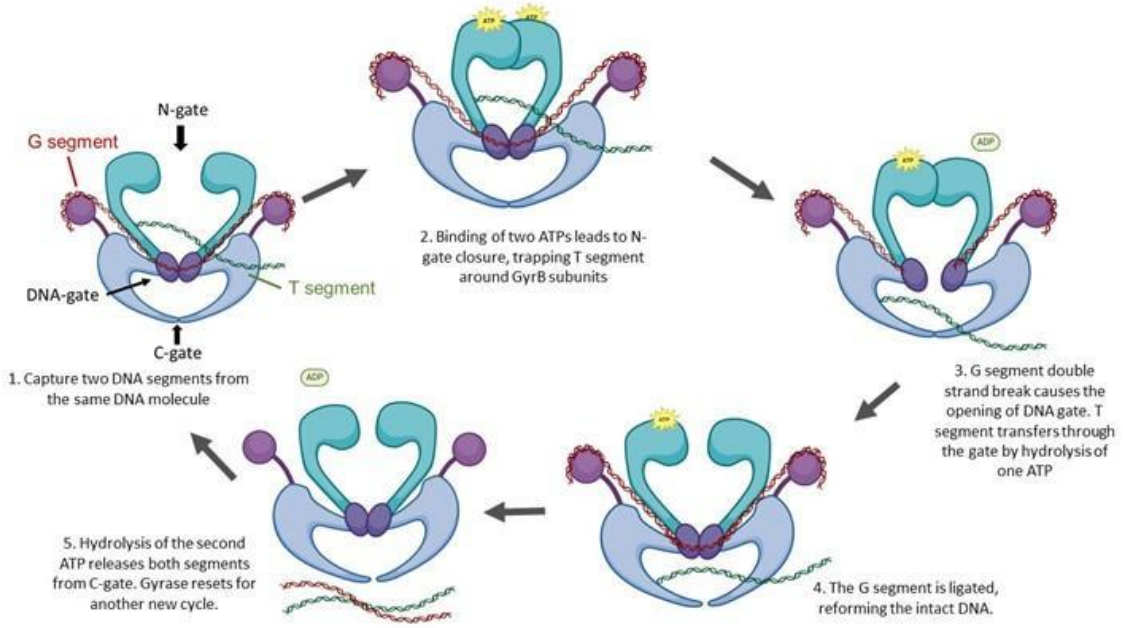

Figure. 1.4. Catalytic cycle of DNA gyrase. 1. The cycle begins when two segments of double-stranded DNA are captured. The "G-segment" is wrapped around the C-terminal domains of the GyrA subunits, while the "T-segment" is positioned within the ATP binding domain of the GyrB subunits. **2.** Binding of two ATPs causes a conformational change of GyrB, resulting in the closure of N-gate, trapping T-segment within the GyrB subunits. **3.** A double strand break in the G-segment is induced by the GyrA active site, leading to the opening of DNA gate. Hydrolysis of one ATP drives the T-segment to pass through to the lower chamber in GyrA. **4.** As the T-segment passes through, the G-segment is ligated, reforming the intact DNA. **5.** Both segments are released from C-gate as the second ATP is hydrolyzed. Gyrase resets for another cycle with the re-opening of N-gate in GyrB subunits.

The overall structure of DNA gyrase is highly conserved across species, but with some subtle discrepancies in both GyrA and GyrB subunits from different species.[74] As figure 5 presents, GyrB from gram negative bacteria, such as *E.coli*, contains an inserted globular structure of 170 amino acids, with the TOPRIM domain that is absent in Gram positive bacteria and *Mycobacteria*.[75] This structure imparts extra contacts with the coiled coil domain of GyrA and may contribute to DNA binding and interdomain interaction.[70, 74, 75] The GyrB from Mycobacteria contains a "C-loop", a short insertion in the ATPase domain, which interacts with another loop exhibiting negative charge in the tower domain of GyrA that might be important for stabilization of the resting state of gyrase with N-gate opening.[76] GyrA from *E. coli* has an extra globular domain in the coiled-coil domain that does not exist in Gram positive bacteria and Mycobacteria.[70] Though the function of this globular domain is still unclear, it is speculated that it might contribute to stabilization of the C-gate.[70, 74] Lastly, the C-terminal domain of GyrA is highly conserved and mediates the DNA wrapping and supercoiling activity.[77, 78]

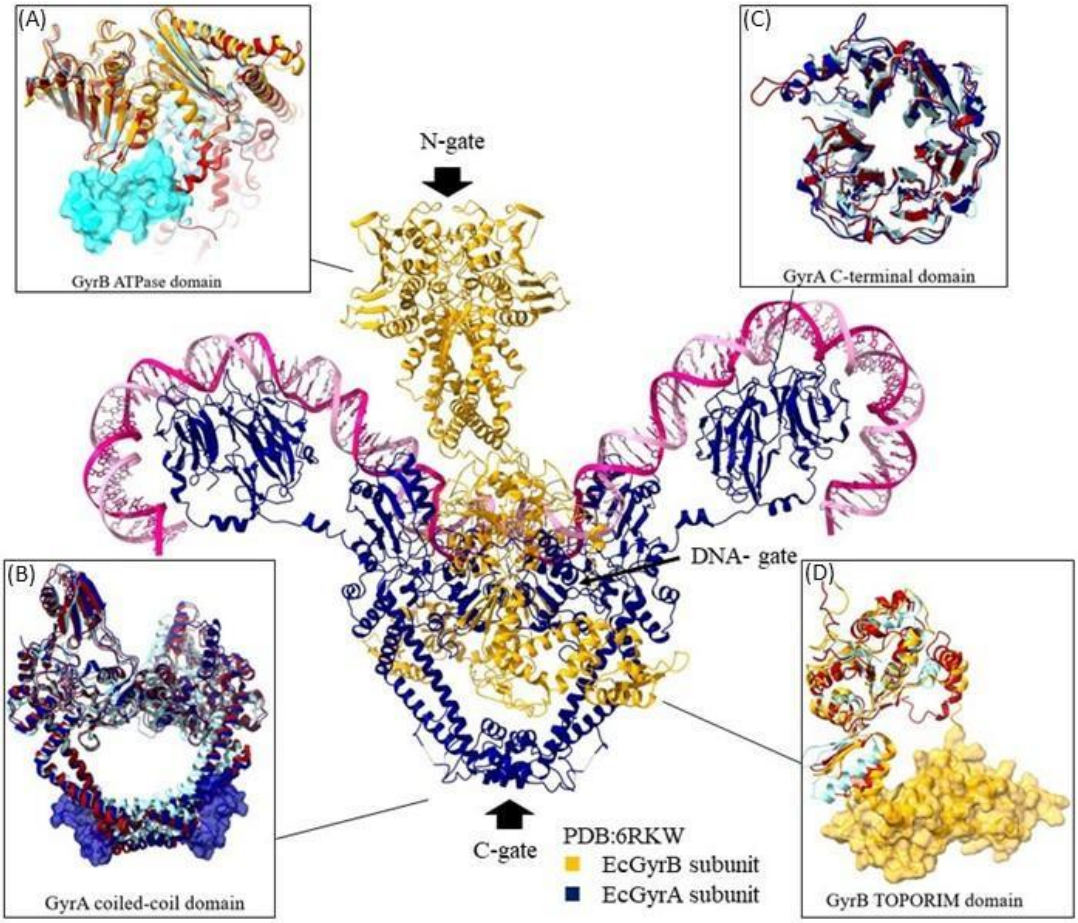

Figure. 1.5. Species-specific structural variation of gyrase subunits. The overall structure of gyrase is highly conserved, however, there are still some distinct structures in different organisms. The center shows the complete structure of *E. coli* gyrase (PDB: 6RKW.[66])The GyrB subunit is shown in yellow ribbon and the GyrA subunit is shown in blue ribbon (A) Superimposition of the GyrB ATPase domains from *M. tuberculosis* (PDB: 6GAV[76], shown in cyan ribbon), *E.coli* (PDB: 6RKW[66], shown in yellow ribbon) and *B. subtilis* (AlphaFold prediction, shown in red ribbon.) and an extra C-loop from M. tuberculosis is highlighted in cyan surface. (B) Superimposition of the GyrA coiled-coil domain from *M. tuberculosis* (PDB: 3ILW,[79] shown in cyan ribbon), *E. coli* (PDB:6RKW[66], shown in blue ribbon) and *B. subtilis* (PDB: 4DDQ[80], shown in red ribbon) and an additional globular structure in the coiled coil domain of *E. coli* GyrA is displayed in blue surface. (C) Superimposition of GyrA C-terminal domain from *M. tuberculosis* (PDB: 4G3N,[81] shown in cyan ribbon), *E. coli* (PDB: 6RKW,[66] shown in blue ribbon) and *B. subtilis* (AlphaFold prediction, shown in red ribbon) (D) Superimposition of GyrB TOPRIM domain from *M. tuberculosis* (3IG0[82], shown in cyan ribbon) *E.coli* (PDB: 6RKW[66], shown in yellow ribbon) and *B. subtilis*(PDB: AlphaFold prediction, shown in red ribbon) and an extra structure in *E. coli* GyrB is highlighted in yellow surface.

Even though the structures of gyrase subunits exhibit some difference among organisms, it is feasible to assemble a functional enzyme using different gyrase subunits. Weidlich and Klostermeier compared the activity of homologous gyrases from *E. coli*, *B. subtilis* and *M. tuberculosis* and from heterologous versions.[74] They initially compared the activity of each gyrase and found that both gyrases from *E. coli* and *B. subtilis* have higher efficiencies of DNA-stimulated ATP hydrolysis, DNA supercoiling, and decatenating activities, while the gyrase from *M. tuberculosis* presented a lower activity on all mentioned activities.[74] Heterologous gyrase, formed by mixing GyrA and GyrB subunits from different bacteria, generally exhibited lower activity than the non-heterologous versions except for the reconstruction of GyrA subunits from *M. tuberculosis* and GyrB from *B. subtilis*.[74] Overall, this study showed the possibility of interdomain communication between different gyrase subunits and suggests that species-specific structures may restrict the efficiency of activities when tested with non-heterologous gyrase enzymes.

Due to its essential role in bacteria cells as well as absence in human cells, gyrase has become an ideal target for developing antimicrobial strategies.[62] Inhibition of gyrase activity also reduces the accessibility of DNA for the transcription and translation activities, affecting gene expression.[79, 80] Furthermore, generating a temporary DNA double strand break, which is potentially harmful to cells, is a required step for gyrase function.[81] Therefore, one of effective antimicrobial schemes is to stabilize the DNA-gyrase intermediate complex resulting in persistent DNA breakage.

Many gyrase-inhibiting compounds are shown to bind at the cleavage site and directly block the re-ligation of cleaved DNA[73, 82]. However, some compounds also stabilize the DNA-gyrase cleavage complex using distinct binding sites distal to the cleaved DNA. The binding of those compounds trigger allosteric effects that pause the action of gyrase,[83, 84] indicating that different conformations of gyrase in its catalytic cycle are able to be targeted by different compounds. Currently, three binding sites on gyrase are classified to stabilize the DNA-cleavage complex.[62]

Site I

Site I is in the cleavage site of the DNA molecule.[62] Compounds targeting this site often bind at both cleavage sites to physically block DNA re-ligating in a steric manner. They also interact with the WHD domain of GyrA and/or TOPRIM domain of GyrB.[85] Fluoroquinolones (FQ), the quinolone pyrimidinetrione (QPT-1), eptoside and imidazopyrazinones (IPYs) are examples of well characterized compound families that target this site.[85-87]

Site II

DNA molecules and GyrA subunits form a pocket which makes up site II.[62] Compounds binding at this site are often referred as" Novel (or non-fluoroquinolone) bacterial topoisomerase inhibitors (NBTI)".[83] Although NBTIs do not exhibit a common scaffold, they share some characteristics that allow them to fit into this site. One portion of these inhibitors sits in a pocket formed by interactions of the two GyrA subunits and the other portion sits in the middle of the cleaved DNA molecule between the two cleavage sites. Both portions are connected by a central linker that usually contains a basic nitrogen.[83] Gepotidacin, a current phase III approved gyrase antibiotic, belongs to NBTI. [88] Gepotidacin also occupies at the pocket between two GyrA subunits and the scissile DNA bonds to cause DNA single strand break.[88, 89]

Site III

Site III is a hinge pocket located in the GyrA and GyrB subunits and is away from the DNA molecule.[90] Thiophene 1 is an example of a compound that binds at this site. Compounds situating at this site likely induce an allosteric mechanism to stabilize the DNA-gyrase cleavage complex and prevent it from progression into a relaxed state.[90]

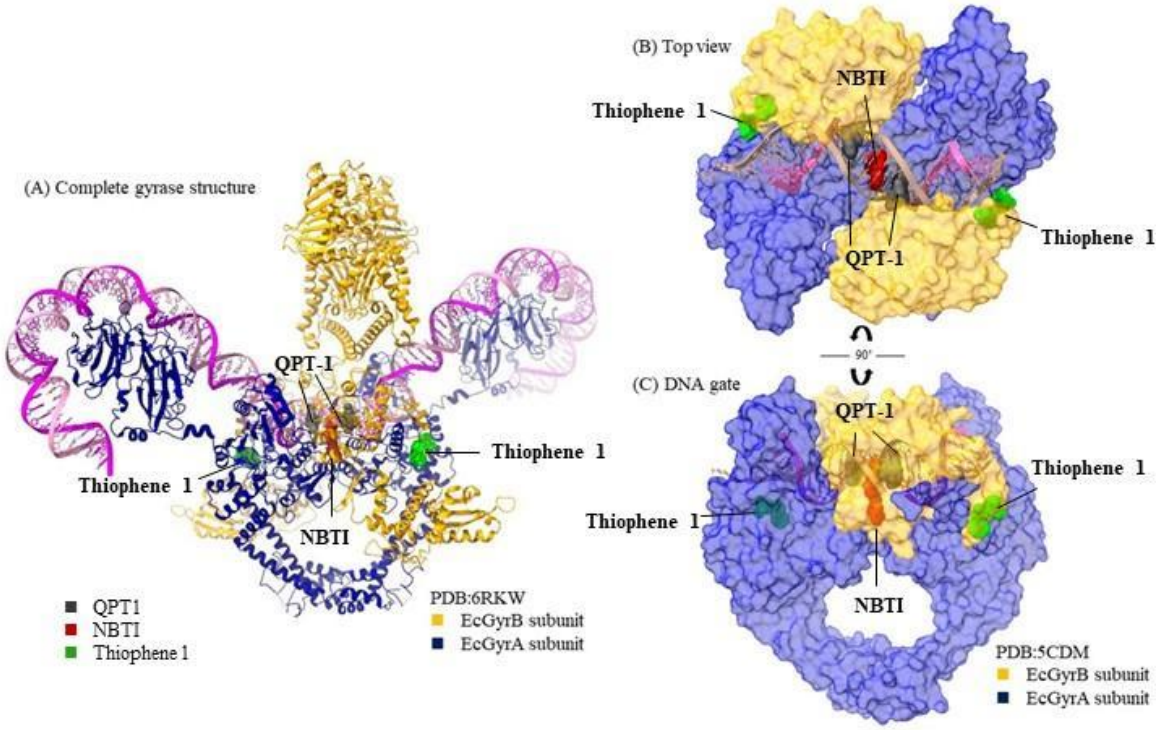

Figure 1.6. The binding of gyrase inhibitors that stabilize the gyrase-mediated DNA cleavage complex. The binding of QPT-1 is at Site 1, while binding of NBTI is at Site 2 and binding of thiophene 1 is at Site 3. (A) The overall structure of *E. coli* gyrase (PDB entry: 6RKW[66], GyrB is shown in yellow ribbon, and GyrA is shown in blue ribbon) superposed with QPT-1 (PDB: 5CDM[85], shown in grey surface), NBTI (PDB entry: 2XCS[83], shown in red surface) and thiophene 1 (PDB entry: 5NPK[84], shown in green surface) to highlight the three main pockets targeted for gyrase inhibition. (B) Top view of the binding pockets, also shown in (C) for a closer view of the DNA gate. The PDB entry of the structure shown in (B) and (C) is 5CDM[70], with GyrB in yellow surface and GyrA in blue surface.

While numerous small molecules are designed to target gyrase and act as antibacterial agents, small proteins have also been identified to have a gyrase-inhibiting effect.[64] Because bacterial chromosomal replication, as well as transcriptional homeostasis, are significantly dependent on gyrase activity, microbes have evolved protein-based gyrase inhibitors to impact growth of competitors for retention of selfish genes. Some of these protein inhibitors mimic antibacterial agents, such as Microcin B17, CcdB and ParE, produce a double strand DNA break when inhibiting gyrase that can persist and lead to cell death;[11, 63, 91] whereas other inhibitors, including MfpA, Qnr and GyrI, perform a reversible and non-damaging mode of gyrase, with no stabilization of the DNA breaks, suggesting a regulatory role on bacterial growth or potentially a protective role against damaging inhibition.[92, 93]

Microcin B17

Microcin B17(MccB17) is a modified peptide, which contains oxazole and thiazole heterocycles, potently inhibits DNA gyrase.[63] The mccB17 operon is encoded in single-copy

plasmids carried by *E. coli*. [63] The operon also includes an immunity protein, similar to pentapeptide repeat MfpA, and a synthetase complex for mccB17 post-translational modifications.[94, 95] MccB17 can be secreted to target neighboring bacteria when growth condition becomes challenging. The producing cells are unaffected by generating the immunity protein to neutralize MccB17.[95] Serines and cysteines in the C- terminus of the MccB17 precursor are post-translational modified to form oxazole and thiazole heterocycles, respectively, and is required for MccB17 toxicity. Removing the leader peptide in the N-terminal domain by an endogenous protease is the final step to generate an active MccB17 peptide.[94, 96]

The molecular mechanism of how MccB17 interacting with gyrase is still elusive, however, mutagenesis studies provide some insights. Mutation of W751 in GyrB, a residue located close to the DNA gate, has been shown to impart resistance to MccB17.[97] In addition, GyrB K447E and S83W mutations, which are known to generate quinolone-resistance, also impact MccB17 activity, suggesting that the binding site of MccB17 may partially overlap with that of quinolones.[98] Pierrat et al., showed that MccB17 inhibits gyrase only when the DNA substrate is a linear DNA fragment with a length of more than 150 base pairs. At this length, a DNA molecule is wrapped around the C-terminal domain of GyrA with sufficient remaining DNA to be positioned as the T segment at the N-gate.[98] They also indicated that MccB17 is able to block the passage of T segment through the DNA gate, and that it can also inhibit the relaxation activity of gyrase.[98] Taken together, these studies suggest that MccB17 may bind to gyrase during strand passage.

Pentapeptide repeat protein (PRP) family

PRPs mimic helical structures, such as a DNA molecule, by forming a three-dimensional structure with repeating patterns that is analogous to a beta solenoid fold.[99] The sequence of PRPs exhibit a regular repeat of five amino acids that projects the side chains of the first and third residue inward while the side chains of second, fourth, and fifth residues outward. These recurring segments of five amino acids are positioned along the primary sequence to be linked into four regions of sequence variation forming one "turn" of the solenoid.[64] The PRPs typically have a dimeric form through the interaction of C-terminal helices, leaving the N-terminus as a free region of the pentapeptide repeat protein. Among the PRP family, the MfpA and Qnr proteins have been identified to interact with DNA gyrase.[99, 100]

MfpA

The mycobacterial fluoroquinolone resistance protein A (MfpA) gene is a chromosomal gene that was first identified in *M. smegmatis* by genomic screening.[101] The *mfpA* gene not only exists in the genome of at least 19 species of *Mycobacterium*, but can also be found in 10 other *Actinobacteria* species with at least 40% homology.[102] The MfpA protein from *M. smegmatis* ($MfpA_{Ms}$) belongs to the pentapeptide repeat protein(PRP) family, and encodes 192 amino acids.[103] It is the first solved PRP structure, and it displays a right-handed quadrilateral β-helix structure that resembles the B-form of DNA[103, 104]. MfpA is also found in *M. tuberculosis* ($MfpA_{Mt}$) and it exhibits 67% identity with $MfpA_{Ms}$.[103] It has been shown that MfpA binds to DNA gyrase and inhibits supercoiling activity at high doses[99, 103]

The $MfpA_{Ms}$ has been proposed to interact with the ATPase domain of gyrase.[99] Feng et al., showed that the gyrase protecting effect of $MfpA_{Ms}$ against fluoroquinolone (FQs) was absent without ATP or in the presence of unhydrolizable ADPNP, suggesting that the hydrolysis of ATP is required for $MfpA_{Ms}$ to protect gyrase from FQs.[99] The $MfpA_{Ms}$ was also shown to

activate the ATPase activity of MsGyrB47 and might compete with linear DNA for binding with gyrase.[99] They further solved the crystal structure of $MfpA_{Ms}$ complexed with MsGyrB47, i.e., the ATPase domain of *M. smegmatis* GyrB subunit, and identified one interface between the C- terminal end of MsGyrB47 and one subunit of the $MfpA_{Ms}$ dimer that forms critical interactions and is necessary for protection against FQs.[99] Taken together, $MfpA_{Ms}$ acts as a DNA T-segment that emulates the interactions with ATPase domain of MsGyrB subunit to stimulate ATP hydrolysis. The ATPase domain subsequently triggers a conformational change which leads to the opening of the blocked DNA gate, and expel the binding of FQs, allowing re-ligation of the DNA G-segment. [99]

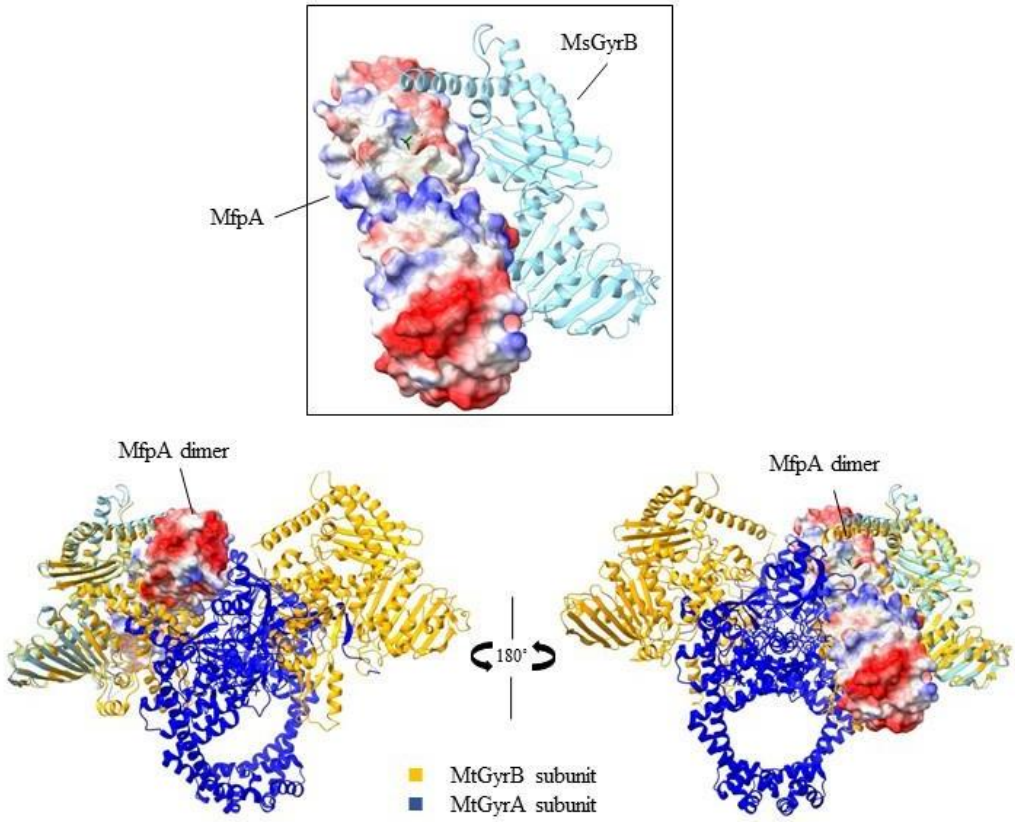

Figure 1.7. The complexed structure of the pentapeptide repeat protein MfpA binding to Gyrase. The structure of MfpA exhibits a conserved dimeric solenoid fold and has a charge distribution that mimics DNA. Superposition of the MfpA-GyrB complex (PDB: 6ZT5[99]) with the *M. tuberculosis* GyrBA fusion (PDB: 6GAV[76] highlights the length of MfpA, (represented as Coulombic surface), that extends to the active site of GyrA.

Qnr

The Qnr protein contains 218 amino acids and belongs to the pentapeptide repeat protein(PRP) family. This gene was first identified on a multi-resistance plasmid, pMG252, from a clinical isolate of *Klebsiella pneumonia*.[105] Qnr homologs were subsequently discovered on the chromosome of several Gram-positive and Gram-negative bacteria.[106] The sequences of Qnr homologs generally exhibits more than 65% similarity and could be categorized into seven families, including QnrA, QnrB, QnrC ,QnrD, QnrE, QnrS and QnrVC.[106, 107] Although they vary in size, ranging from 214 to 221 amino acids, all Qnr proteins function in protecting gyrase and topoisomerase IV in a similar mechanism.[108] The structure of Qnr proteins exhibits a dimeric right-handed quadrilateral β-helix with a similar size and surface charge to

the B form of DNA.[100, 109] In particular, two projecting loops are characteristic features conserved among all plasmid-based and some chromosomally encoded Qnr variants.[109] Multiple lines of experimentation indicate that Qnr can bind to the GyrA subunit, the GyrB subunit, and the gyrase A_2B_2 without the presence of DNA or quinolones.[110, 111] Hegde et al., showed that EfsQnr was able to inhibit gyrase supercoiling activity but poorly inhibited relaxation activity.[100] They further showed that *E. coli* cells expressing EfsQnr were able to divide, but seemed not to separate, i.e., daughter cells formed clusters connected with an external appendage-like structure[100], suggesting that the activity of the related topoisomerase IV was inhibited.

Studies have shown a protection effect of Qnr from quinolones-mediated inhibition.[93, 105, 106] Jacoby et al., indicated that Qnr also protected against synthetic compounds exhibiting structural similarity to quinolone[93]. However, Qnr did not protect from GyrA-targeting simocyclinone D8 that affects DNA binding. Moreover, Qnr did not affect either synthetic or non-synthetic GyrB inhibitors.[93] Taken together, Qnr shows protective effects for gyrase against compounds which are able to stabilize the cleaved state of the DNA-gyrase complex.

Although the protective effect of Qnr against quinolones has been described, the biological function of Qnr remains unknown. The first description of *qnr* genes is from 1930s, which is earlier than the discovery of quinolones in the 1960s[112]. Additionally, *qnr* genes are ubiquitous among various bacterial hosts, implying other functions than protecting from quinolone antimicrobials. One plausible Qnr function is hypothesized to be involved in responding to DNA damage. A LexA-binding site is within the promoter region of all *qnrB* alleles, implying that the expression of QnrB might be regulated in a LexA/RecA-dependent manner in SOS response, a DNA damage-induced regulatory mechanism.[113] Qnr might also play an adaptive role for bacteria to survive in a stringent environment. Kim et al., showed that *qnrA2* gene is overexpressed with cold shock in *Shewanella algae*.[114] In spite of having available evidence, more are needed to further probe biological roles of Qnr.

GyrI

The gyrase inhibitory protein, GyrI, also known as SbmC, is a chromosomally encoded gyrase regulator identified in *E. coli*.[92, 115] The *gyrI* gene is in an SOS regulon induced in the presence of DNA-damaging agents or when the cells enter into the stationary phase.[116] GyrI is a polypeptide containing 157 residues with a molecular mass around 18 kDa and the crystal structure has been determined.[117] The structure of GyrI consists of two four-stranded antiparallel β-sheets and two α-helices, with a pseudo two-fold symmetry.[117]

GyrI has been shown to inhibit both supercoiling and relaxation activity of DNA gyrase. Unlike some gyrase inhibitors, such as quinolone, that stabilize the DNA-gyrase complex and cause persistent DNA cleavage, GyrI does not induce DNA cleavage. Instead, GyrI decreases the DNA-gyrase complex because it is shown that GyrI inhibits gyrase prior to, or at the stage of, DNA binding[92]. Nakanishi et al., also indicated that GyrI exhibits higher affinity with the gyrase holoenzyme compared to either GyrA or GyrB alone[115].

GyrI is considered a protective antidote against proteinaceous inhibitors of gyrase. *In vitro* gyrase assays show that the cleavage products caused by microcin B17 and CcdB decreased in the presence of GyrI.[92] Furthermore, cells expressing GyrI continued to grow in the presence of microcin B17, highlighting the defensive role of GyrI on resisting proteinaceous inhibitors of gyrase[92].

CcdB

The *ccd* operon, which was first identified on the F plasmid, is a typical Type II toxin-antitoxin module encoding a CcdB toxin protein and the antidote, CcdA antitoxin protein.[118-120] CcdA and CcdB are co-expressed and CcdA neutralizes CcdB by forming a non-covalent complex.[118, 121] The CcdAB complex is able to autoregulate its expression.[121] CcdA forms an unstable structure and is easily degraded by ATP-dependent proteases.[122] Upon losing the plasmid encoding *ccdAB*, the remnant CcdB is able to act on its target, DNA gyrase[33]. Like quinolones, CcdB has been shown to poison gyrase by stabilizing the DNA-gyrase cleavage complex and thus inhibiting supercoiling activity.[91] However, the inhibition mechanism of CcdB is different to that of quinolones.

An available crystal structure and accompanying biochemical assay indicate that CcdB binds to the GyrA subunit.[91] Side chain interactions of R492 of GyrA and W99 of CcdB play important roles during complex formation. Furthermore, the side chain of R462 of GyrA also forms a hydrogen bond with that of N95 of CcdB. Thus, a single mutation, R492C, in GyrA confirms resistance to CcdB[91]. In addition to the interaction on R492 of GyrA, I101 at the C-terminus of CcdB complements a hydrophobic crevice formed by L383, L461, I379 and A457 on the GyrA surface. A small conformation change occurs upon formation of the CcdB-GyrA complex. The C-terminus(G100-I101) of CcdB flips 180˚, and N95 and W99 also undergo conformational changes to allow W99 to become more accessible to interact with R462 of GyrA.[91] Meanwhile, the side chain of R462 of GyrA also undergoes a rotameric shift to interact with CcdB W99.[91] Dao-Thi et al., superimposed the complex of CcdB and GyrA14(a truncated form of GyrA with only C-gate) onto a GyrA59 structure (a truncated form of GyrA with the C-terminal coiled-coil domains removed) with a closed DNA gate and observed that there was a significant steric hindrance between the tower domain of GyrA59 and CcdB; however, CcdB can fit into the identical position at GyrA59 with DNA-gate opening.[91] In this work the authors also suggest that CcdB can interact with gyrase in the absence of DNA, inhibiting the enzyme by keeping the catalytic tyrosines far apart in a conformation not compatible with catalyzing cleavage of the G segment.[91] Taken together, CcdB binds to the C-gate of gyrase and acts as a road block to prevent the passage of T segment as well as the re-ligation of the G segment, disrupting the conformation of DNA-gyrase cleavage complex.

CcdB can bind to both free gyrase as well as the DNA-gyrase cleavage complex, inhibiting the catalytic cycle, however, the inhibition can be rescued by CcdA in a process termed rejuvenation.[123] The binding of CcdA to the CcdB dimer triggers a significant distortion of CcdB dimer interface, inducing the rearrangement of CcdB surface from gyrase-binding surface to the CcdA-binding surface.[123] This rearrangement also involves the conformational change of W99 of CcdB, which disrupts the interaction with GyrA.[91, 123]

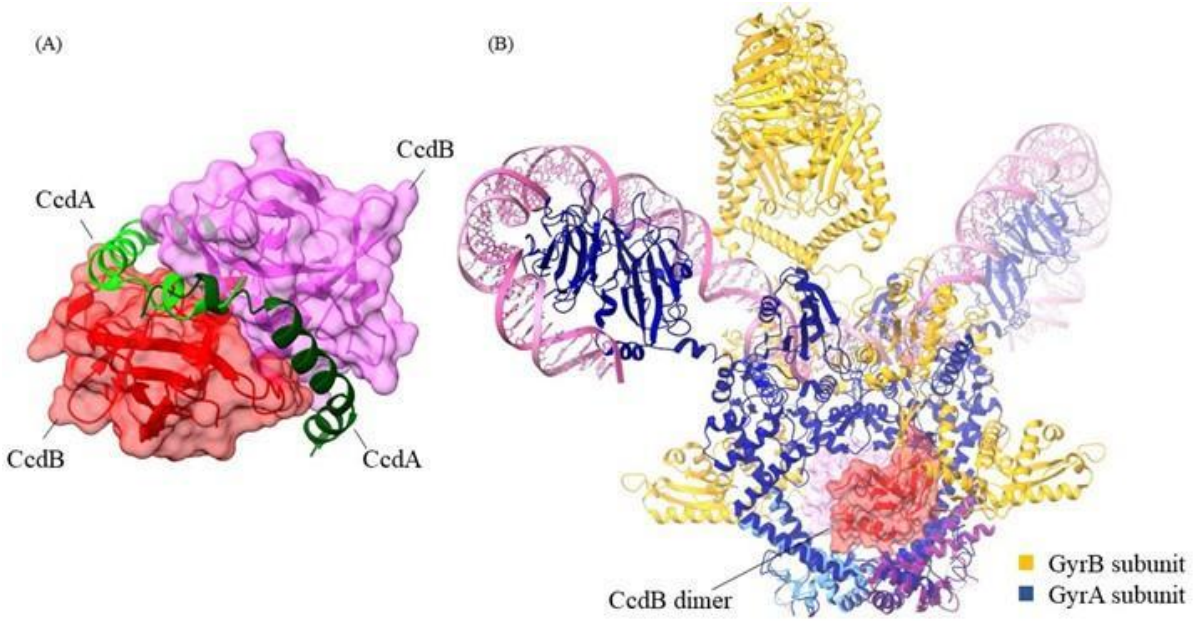

Figure 1.8. The dimeric CcdB toxin binds to the C-gate in GyrA to block the release of DNA fragments, leading to the accumulation of double strand breaks. (A) The structure of CcdAB complex. (PDB: 3G7Z[123], CcdB are shown in red and magenta surfaces. CcdA is shown in green ribbon) (B) Superposition of *E. coli* GyrA and F plasmid CcdB (PDB: 1X75[91], CcdB are shown in red and magenta surfaces. GyrA14 is shown in cyan and purple ribbons.) with *E. coli* gyrase (PDB: 6RKW[66]. GyrA is shown in blue ribbon. GyrB is shown in yellow ribbon. DNA is shown in pink ribbon.)

The interaction between ParE toxin and gyrase

The bacterial toxins CcdB and ParE both inhibit gyrase. While the inhibition mechanism of the CcdB toxin has been well established, the mechanism for gyrase inhibition by ParE toxins still remains unclear. Members of the ParE toxin family exhibit a highly conserved structure but the sequence similarity between them is low, which likely contributes to the varying levels of inhibition against gyrase.[22, 54, 61] From *in vitro* reaction, the half maximal inhibitory concentration (IC_{50}) of VcParE2 is 1.2μM, whereas PaParE is 3.7μM against *E. coli* gyrase. [22, 47] Studies have revealed conflicting data about ParE- gyrase interactions, including ParE toxins binding to different gyrase subunits and whether ATP is required for the ParE inhibition.[46, 47, 61] Yuan et al., demonstrated that strains resistant to nalidixic acid, a quinolone type antibiotic, are still sensitive to the ParE toxin.[47] In contrast, MtParE2 was been shown to contain a higher affinity to MtGyrB (around 4.75μM) while the affinity to MtGyrA is much lower (approx. 922μM).[46] EcParE2 also shows no interaction with EcGyrA.[55] In aggregate, current studies on the molecular mechanism of ParE toxin inhibition of DNA gyrase appear to conflict, and a comprehensive mechanism cannot be determined.

The background described in Chapter I of this dissertation establishes the rationale for the significance of the research discussed in the subsequent chapters. The major caveats in the field of TA systems to be addressed in this work include: (1) Whether bacterial cells expressing the ParE toxin increase mutation frequency and generate antibiotics resistance. (2) An effective method to produce sufficient quantity of ParE toxins (3) Why does degradation still occur in the purified ParD antitoxin?

Chapter II of this dissertation demonstrates the feasibility of leveraging the ParE toxin as antibacterial without generating any resistance. Chapter III focuses on developing an effective method to obtain descent amount of purified ParE toxins for further characterization, and Chapter IV investigates the condition that impact the integrity of purified ParD antitoxin.

Reference

1. Alcock, B.P., et al., *CARD 2023: expanded curation, support for machine learning, and resistome prediction at the Comprehensive Antibiotic Resistance Database.* Nucleic Acids Res, 2023. **51**(D1): p. D690-d699.
2. Shafiq, N., et al., *Shortage of essential antimicrobials: a major challenge to global health security.* BMJ Glob Health, 2021. **6**(11).
3. Antimicrobial Resistance, C., *Global burden of bacterial antimicrobial resistance in 2019: a systematic analysis.* Lancet, 2022. **399**(10325): p. 629-655.
4. Birgand, G., P. Dhar, and A. Holmes, *The threat of antimicrobial resistance in surgical care: the surgeon's role and ownership of antimicrobial stewardship.* Br J Surg, 2023. **110**(12): p. 1567-1569.
5. Pedersen, K., S.K. Christensen, and K. Gerdes, *Rapid induction and reversal of a bacteriostatic condition by controlled expression of toxins and antitoxins.* Mol Microbiol, 2002. **45**(2): p. 501-10.
6. Wen, Y., E. Behiels, and B. Devreese, *Toxin–Antitoxin systems: their role in persistence, biofilm formation, and pathogenicity.* Pathogens and Disease, 2014. **70**(3): p. 240-249.
7. Kamruzzaman, M. and J. Iredell, *A ParDE-family toxin antitoxin system in major resistance plasmids of Enterobacteriaceae confers antibiotic and heat tolerance.* Sci Rep, 2019. **9**(1): p. 9872.
8. Yang, Q.E. and T.R. Walsh, *Toxin-antitoxin systems and their role in disseminating*

and maintaining antimicrobial resistance. FEMS Microbiol Rev, 2017. **41**(3): p. 343-353.
9. Ramage, H.R., L.E. Connolly, and J.S. Cox, *Comprehensive functional analysis of Mycobacterium tuberculosis toxin-antitoxin systems: implications for pathogenesis, stress responses, and evolution.* PLoS Genet, 2009. **5**(12): p. e1000767.
10. Yamaguchi, Y., J.H. Park, and M. Inouye, *Toxin-antitoxin systems in bacteria and archaea.* Annu Rev Genet, 2011. **45**: p. 61-79.
11. Jurėnas, D., et al., *Biology and evolution of bacterial toxin-antitoxin systems.* Nat Rev Microbiol, 2022. **20**(6): p. 335-350.
12. Fraikin, N., F. Goormaghtigh, and L. Van Melderen, *Type II Toxin-Antitoxin Systems: Evolution and Revolutions.* J Bacteriol, 2020. **202**(7).
13. Park, S.J., W.S. Son, and B.J. Lee, *Structural overview of toxin-antitoxin systems in infectious bacteria: a target for developing antimicrobial agents.* Biochim Biophys Acta, 2013. **1834**(6): p. 1155-67.
14. Chan, W.T., D. Balsa, and M. Espinosa, *One cannot rule them all: Are bacterial toxins-antitoxins druggable?* FEMS Microbiol Rev, 2015. **39**(4): p. 522-40.
15. Gerdes, K., et al., *Translational control and differential RNA decay are key elements regulating postsegregational expression of the killer protein encoded by the parB locus of plasmid R1.* J Mol Biol, 1988. **203**(1): p. 119-29.
16. Weaver, K., *The Fst/Ldr Family of Type I TA System Toxins: Potential Roles in Stress Response, Metabolism and Pathogenesis.* Toxins (Basel), 2020. **12**(8).
17. Kawano, M., et al., *Molecular characterization of long direct repeat (LDR) sequences expressing a stable mRNA encoding for a 35-amino-acid cell-killing peptide and a cis-encoded small antisense RNA in Escherichia coli.* Mol Microbiol, 2002. **45**(2): p. 333-49.
18. Fineran, P.C., et al., *The phage abortive infection system, ToxIN, functions as a protein-RNA toxin-antitoxin pair.* Proc Natl Acad Sci U S A, 2009. **106**(3): p. 894-9.
19. Goeders, N., et al., *Structure, Evolution, and Functions of Bacterial Type III Toxin-Antitoxin Systems.* Toxins (Basel), 2016. **8**(10).
20. Choi, J.S., et al., *The small RNA, SdsR, acts as a novel type of toxin in Escherichia coli.* RNA Biol, 2018. **15**(10): p. 1319-1335.
21. Li, M., et al., *Toxin-antitoxin RNA pairs safeguard CRISPR-Cas systems.* Science, 2021. **372**(6541).
22. Muthuramalingam, M., et al., *The toxin from a ParDE toxin-antitoxin system found in Pseudomonas aeruginosa offers protection to cells challenged with anti-gyrase antibiotics.* Mol Microbiol, 2019. **111**(2): p. 441-454.
23. Xie, Y., et al., *TADB 2.0: an updated database of bacterial type II toxin-antitoxin loci.* Nucleic Acids Res, 2018. **46**(D1): p. D749-D753.
24. Jimmy, S., et al., *A widespread toxin-antitoxin system exploiting growth control via alarmone signaling.* Proc Natl Acad Sci U S A, 2020. **117**(19): p. 10500-10510.
25. Masuda, H., et al., *YeeU enhances the bundling of cytoskeletal polymers of MreB and FtsZ, antagonizing the CbtA (YeeV) toxicity in Escherichia coli.* Mol Microbiol, 2012. **84**(5): p. 979-89.
26. Jankevicius, G., et al., *The Toxin-Antitoxin System DarTG Catalyzes Reversible ADP-Ribosylation of DNA.* Mol Cell, 2016. **64**(6): p. 1109-1116.
27. Wang, X., et al., *A new type V toxin-antitoxin system where mRNA for toxin GhoT is cleaved by antitoxin GhoS.* Nat Chem Biol, 2012. **8**(10): p. 855-61.
28. Aakre, C.D., et al., *A bacterial toxin inhibits DNA replication elongation through a direct interaction with the β sliding clamp.* Mol Cell, 2013. **52**(5): p. 617-28.
29. Wang, X., et al., *Type VII Toxin/Antitoxin Classification System for Antitoxins that*

Enzymatically Neutralize Toxins. Trends Microbiol, 2021. **29**(5): p. 388-393.
30. Yu, X., et al., *Characterization of a toxin-antitoxin system in Mycobacterium tuberculosis suggests neutralization by phosphorylation as the antitoxicity mechanism.* Commun Biol, 2020. **3**(1): p. 216.
31. Songailiene, I., et al., *HEPN-MNT Toxin-Antitoxin System: The HEPN Ribonuclease Is Neutralized by OligoAMPylation.* Mol Cell, 2020. **80**(6): p. 955-970.e7.
32. Gerdes, K., P.B. Rasmussen, and S. Molin, *Unique type of plasmid maintenance function: postsegregational killing of plasmid-free cells.* Proc Natl Acad Sci U S A, 1986. **83**(10): p. 3116-20.
33. Ogura, T. and S. Hiraga, *Mini-F plasmid genes that couple host cell division to plasmid proliferation.* Proc Natl Acad Sci U S A, 1983. **80**(15): p. 4784-8.
34. Guglielmini, J. and L. Van Melderen, *Bacterial toxin-antitoxin systems: Translation inhibitors everywhere.* Mob Genet Elements, 2011. **1**(4): p. 283-290.
35. Yuan, J., Y. Yamaichi, and M.K. Waldor, *The three vibrio cholerae chromosome II-encoded ParE toxins degrade chromosome I following loss of chromosome II.* J Bacteriol, 2011. **193**(3): p. 611-9.
36. Shmidov, E., et al., *PrrT/A, a Pseudomonas aeruginosa Bacterial Encoded Toxin-Antitoxin System Involved in Prophage Regulation and Biofilm Formation.* Microbiol Spectr, 2022. **10**(3): p. e0118222.
37. Sayed, N., et al., *Functional and structural insights of a Staphylococcus aureus apoptotic-like membrane peptide from a toxin-antitoxin module.* J Biol Chem, 2012. **287**(52): p. 43454-63.
38. Azam, A.H. and Y. Tanji, *Bacteriophage-host arm race: an update on the mechanism of phage resistance in bacteria and revenge of the phage with the perspective for phage therapy.* Appl Microbiol Biotechnol, 2019. **103**(5): p. 2121-2131.
39. Li, Y., et al., *Prophage encoding toxin/antitoxin system PfiT/PfiA inhibits Pf4 production in Pseudomonas aeruginosa.* Microb Biotechnol, 2020. **13**(4): p. 1132-1144.
40. Tu, C.H., et al., *Evaluating the Potential for Cross-Interactions of Antitoxins in Type II TA Systems.* Toxins (Basel), 2020. **12**(6).
41. Agarwal, S., et al., *VapBC22 toxin-antitoxin system from Mycobacterium tuberculosis is required for pathogenesis and modulation of host immune response.* Sci Adv, 2020. **6**(23): p. eaba6944.
42. Sonika, S., et al., *Toxin-antitoxin systems in bacterial pathogenesis.* Heliyon, 2023. **9**(4): p. e14220.
43. Magnuson, R.D., *Hypothetical functions of toxin-antitoxin systems.* J Bacteriol, 2007. **189**(17): p. 6089-92.
44. Saavedra De Bast, M., N. Mine, and L. Van Melderen, *Chromosomal toxin-antitoxin systems may act as antiaddiction modules.* J Bacteriol, 2008. **190**(13): p. 4603-9.
45. Snead, K.J., L.L. Moore, and C.R. Bourne, *ParD Antitoxin Hotspot Alters a Disorder-to-Order Transition upon Binding to Its Cognate ParE Toxin, Lessening Its Interaction Affinity and Increasing Its Protease Degradation Kinetics.* Biochemistry, 2022. **61**(1): p. 34-45.
46. Gupta, M., et al., *The Chromosomal parDE2 Toxin-Antitoxin System of Mycobacterium tuberculosis H37Rv: Genetic and Functional Characterization.* Front Microbiol, 2016. **7**: p. 886.
47. Yuan, J., et al., *Vibrio cholerae ParE2 poisons DNA gyrase via a mechanism distinct from other gyrase inhibitors.* J Biol Chem, 2010. **285**(51): p. 40397-408.
48. Leplae, R., et al., *Diversity of bacterial type II toxin-antitoxin systems: a comprehensive search and functional analysis of novel families.* Nucleic Acids Res, 2011. **39**(13): p.

5513-25.
49. Goeders, N. and L. Van Melderen, *Toxin-Antitoxin Systems as Multilevel Interaction Systems.* Toxins, 2014. **6**(1): p. 304-324.
50. Dalton, K.M. and S. Crosson, *A conserved mode of protein recognition and binding in a ParD-ParE toxin-antitoxin complex.* Biochemistry, 2010. **49**(10): p. 2205-15.
51. Garcia-Rodriguez, G., et al., *Entropic pressure controls the oligomerization of the Vibrio cholerae ParD2 antitoxin.* Acta Crystallogr D Struct Biol, 2021. **77**(Pt 7): p. 904-920.
52. Schureck, M.A., et al., *Defining the mRNA recognition signature of a bacterial toxin protein.* Proc Natl Acad Sci U S A, 2015. **112**(45): p. 13862-7.
53. Jurėnas, D. and L. Van Melderen, *The Variety in the Common Theme of Translation Inhibition by Type II Toxin-Antitoxin Systems.* Front Genet, 2020. **11**: p. 262.
54. Ames, J.R., et al., *Expression of different ParE toxins results in conserved phenotypes with distinguishable classes of toxicity.* Microbiologyopen, 2019. **8**(10): p. e902.
55. Sterckx, Y.G., et al., *A unique hetero-hexadecameric architecture displayed by the Escherichia coli O157 PaaA2-ParE2 antitoxin-toxin complex.* J Mol Biol, 2016. **428**(8): p. 1589-603.
56. Zhou, J., et al., *Insights into the Neutralization and DNA Binding of Toxin-Antitoxin System ParE(SO)-CopA(SO) by Structure-Function Studies.* Microorganisms, 2021. **9**(12).
57. Lite, T.V., et al., *Uncovering the basis of protein-protein interaction specificity with a combinatorially complete library.* Elife, 2020. **9**.
58. Garcia-Rodriguez, G., et al., *Toxin:antitoxin ratio sensing autoregulation of the Vibrio cholerae parDE2 module.* Sci Adv, 2024. **10**(1): p. eadj2403.
59. Beck, I.N., et al., *Toxin release by conditional remodelling of ParDE1 from Mycobacterium tuberculosis leads to gyrase inhibition.* Nucleic Acids Res, 2023.
60. Aakre, C.D., et al., *Evolving new protein-protein interaction specificity through promiscuous intermediates.* Cell, 2015. **163**(3): p. 594-606.
61. Fiebig, A., et al., *Interaction specificity, toxicity and regulation of a paralogous set of ParE/RelE-family toxin-antitoxin systems.* Mol Microbiol, 2010. **77**(1): p. 236-51.
62. Bax, B.D., et al., *DNA Topoisomerase Inhibitors: Trapping a DNA-Cleaving Machine in Motion.* J Mol Biol, 2019. **431**(18): p. 3427-3449.
63. Collin, F. and A. Maxwell, *The Microbial Toxin Microcin B17: Prospects for the Development of New Antibacterial Agents.* J Mol Biol, 2019. **431**(18): p. 3400-3426.
64. Ruan, S., C.H. Tu, and C.R. Bourne, *Friend or Foe: Protein Inhibitors of DNA Gyrase.* Biology (Basel), 2024. **13**(2).
65. Salman, M., et al., *Targeting novel sites in DNA gyrase for development of anti-microbials.* Brief Funct Genomics, 2023. **22**(2): p. 180-194.
66. Vanden Broeck, A., et al., *Cryo-EM structure of the complete E. coli DNA gyrase nucleoprotein complex.* Nat Commun, 2019. **10**(1): p. 4935.
67. Wigley, D.B., et al., *Crystal structure of an N-terminal fragment of the DNA gyrase B protein.* Nature, 1991. **351**(6328): p. 624-9.
68. Brino, L., et al., *Dimerization of Escherichia coli DNA-gyrase B provides a structural mechanism for activating the ATPase catalytic center.* J Biol Chem, 2000. **275**(13): p. 9468-75.
69. Morais Cabral, J.H., et al., *Crystal structure of the breakage-reunion domain of DNA gyrase.* Nature, 1997. **388**(6645): p. 903-6.
70. Schoeffler, A.J., A.P. May, and J.M. Berger, *A domain insertion in Escherichia coli GyrB adopts a novel fold that plays a critical role in gyrase function.* Nucleic Acids Research, 2010. **38**(21): p. 7830-7844.

71. Espeli, O. and K.J. Marians, *Untangling intracellular DNA topology.* Mol Microbiol, 2004. **52**(4): p. 925-31.
72. Wang, J.C., *Cellular roles of DNA topoisomerases: a molecular perspective.* Nat Rev Mol Cell Biol, 2002. **3**(6): p. 430-40.
73. Michalczyk, E., et al., *Molecular mechanism of topoisomerase poisoning by the peptide antibiotic albicidin.* Nat Catal, 2023. **6**(1): p. 52-67.
74. Weidlich, D. and D. Klostermeier, *Functional interactions between gyrase subunits are optimized in a species-specific manner.* J Biol Chem, 2020. **295**(8): p. 2299-2312.
75. Schoeffler, A.J., A.P. May, and J.M. Berger, *A domain insertion in Escherichia coli GyrB adopts a novel fold that plays a critical role in gyrase function.* Nucleic Acids Res, 2010. **38**(21): p. 7830-44.
76. Petrella, S., et al., *Overall Structures of Mycobacterium tuberculosis DNA Gyrase Reveal the Role of a Corynebacteriales GyrB-Specific Insert in ATPase Activity.* Structure, 2019. **27**(4): p. 579-589.e5.
77. Tretter, E.M. and J.M. Berger, *Mechanisms for defining supercoiling set point of DNA gyrase orthologs: II. The shape of the GyrA subunit C-terminal domain (CTD) is not a sole determinant for controlling supercoiling efficiency.* J Biol Chem, 2012. **287**(22): p. 18645-54.
78. Lanz, M.A., M. Farhat, and D. Klostermeier, *The acidic C-terminal tail of the GyrA subunit moderates the DNA supercoiling activity of Bacillus subtilis gyrase.* J Biol Chem, 2014. **289**(18): p. 12275-85.
79. Bielińska, A. and D. Hulanicka, *Effect of DNA gyrase inhibitors and urea on the expression of cysB, the regulatory gene of the cysteine regulon.* J Gen Microbiol, 1986. **132**(9): p. 2571-6.
80. Briffotaux, J., S. Liu, and B. Gicquel, *Genome-Wide Transcriptional Responses of Mycobacterium to Antibiotics.* Front Microbiol, 2019. **10**: p. 249.
81. Bush, N.G., K. Evans-Roberts, and A. Maxwell, *DNA Topoisomerases.* EcoSal Plus, 2015. **6**(2).
82. Jacoby, G.A., *Mechanisms of resistance to quinolones.* Clin Infect Dis, 2005. **41 Suppl 2**: p. S120-6.
83. Bax, B.D., et al., *Type IIA topoisomerase inhibition by a new class of antibacterial agents.* Nature, 2010. **466**(7309): p. 935-40.
84. Chan, P.F., et al., *Thiophene antibacterials that allosterically stabilize DNA-cleavage complexes with DNA gyrase.* Proceedings of the National Academy of Sciences, 2017. **114**(22): p. E4492-E4500.
85. Chan, P.F., et al., *Structural basis of DNA gyrase inhibition by antibacterial QPT-1, anticancer drug etoposide and moxifloxacin.* Nat Commun, 2015. **6**: p. 10048.
86. Aldred, K.J., R.J. Kerns, and N. Osheroff, *Mechanism of quinolone action and resistance.* Biochemistry, 2014. **53**(10): p. 1565-74.
87. Germe, T., et al., *A new class of antibacterials, the imidazopyrazinones, reveal structural transitions involved in DNA gyrase poisoning and mechanisms of resistance.* Nucleic Acids Res, 2018. **46**(8): p. 4114-4128.
88. Gibson, E.G., et al., *Mechanistic and Structural Basis for the Actions of the Antibacterial Gepotidacin against Staphylococcus aureus Gyrase.* ACS Infect Dis, 2019. **5**(4): p. 570-581.
89. Nicholls, R.A., et al., *How Do Gepotidacin and Zoliflodacin Stabilize DNA-Cleavage Complexes with Bacterial Type IIA Topoisomerases? 2. A Single Moving Metal Mechanism.* Int J Mol Sci, 2024. **26**(1).
90. Chan, P.F., et al., *Thiophene antibacterials that allosterically stabilize DNA-cleavage complexes with DNA gyrase.* Proc Natl Acad Sci U S A, 2017. **114**(22): p. E4492-

e4500.
91. Dao-Thi, M.H., et al., *Molecular basis of gyrase poisoning by the addiction toxin CcdB.* J Mol Biol, 2005. **348**(5): p. 1091-102.
92. Chatterji, M. and V. Nagaraja, *GyrI: a counter-defensive strategy against proteinaceous inhibitors of DNA gyrase.* EMBO Rep, 2002. **3**(3): p. 261-7.
93. Jacoby, G.A., M.A. Corcoran, and D.C. Hooper, *Protective effect of Qnr on agents other than quinolones that target DNA gyrase.* Antimicrob Agents Chemother, 2015. **59**(11): p. 6689-95.
94. Yorgey, P., et al., *Posttranslational modifications in microcin B17 define an additional class of DNA gyrase inhibitor.* Proc Natl Acad Sci U S A, 1994. **91**(10): p. 4519-23.
95. Montero, C., et al., *Intrinsic Resistance of Mycobacterium smegmatis to Fluoroquinolones May Be Influenced by New Pentapeptide Protein MfpA.* Antimicrobial Agents and Chemotherapy, 2001. **45**(12): p. 3387-3392.
96. Bayer, A., et al., *Posttranslational Backbone Modifications in the Ribosomal Biosynthesis of the Glycine-Rich Antibiotic Microcin B17.* Angewandte Chemie International Edition in English, 1993. **32**(9): p. 1336-1339.
97. Vizan, J.L., et al., *The peptide antibiotic microcin B17 induces double-strand cleavage of DNA mediated by E. coli DNA gyrase.* EMBO J, 1991. **10**(2): p. 467-76.
98. Pierrat, O.A. and A. Maxwell, *The action of the bacterial toxin microcin B17. Insight into the cleavage-religation reaction of DNA gyrase.* J Biol Chem, 2003. **278**(37): p. 35016-23.
99. Feng, L., et al., *The pentapeptide-repeat protein, MfpA, interacts with mycobacterial DNA gyrase as a DNA T-segment mimic.* Proc Natl Acad Sci U S A, 2021. **118**(11).
100. Hegde, S.S., et al., *Structural and biochemical analysis of the pentapeptide repeat protein EfsQnr, a potent DNA gyrase inhibitor.* Antimicrob Agents Chemother, 2011. **55**(1): p. 110-7.
101. Montero, C., et al., *Intrinsic resistance of Mycobacterium smegmatis to fluoroquinolones may be influenced by new pentapeptide protein MfpA.* Antimicrob Agents Chemother, 2001. **45**(12): p. 3387-92.
102. Jacoby, G.A. and D.C. Hooper, *Phylogenetic analysis of chromosomally determined qnr and related proteins.* Antimicrob Agents Chemother, 2013. **57**(4): p. 1930-4.
103. Merens, A., et al., *The pentapeptide repeat proteins MfpAMt and QnrB4 exhibit opposite effects on DNA gyrase catalytic reactions and on the ternary gyrase-DNA-quinolone complex.* J Bacteriol, 2009. **191**(5): p. 1587-94.
104. Hegde, S.S., et al., *A fluoroquinolone resistance protein from Mycobacterium tuberculosis that mimics DNA.* Science, 2005. **308**(5727): p. 1480-3.
105. Martínez-Martínez, L., A. Pascual, and G.A. Jacoby, *Quinolone resistance from a transferable plasmid.* Lancet, 1998. **351**(9105): p. 797-9.
106. Hooper, D.C. and G.A. Jacoby, *Topoisomerase Inhibitors: Fluoroquinolone Mechanisms of Action and Resistance.* Cold Spring Harb Perspect Med, 2016. **6**(9).
107. Jacoby, G., et al., *qnr Gene nomenclature.* Antimicrob Agents Chemother, 2008. **52**(7): p. 2297-9.
108. Strahilevitz, J., et al., *Plasmid-mediated quinolone resistance: a multifaceted threat.* Clin Microbiol Rev, 2009. **22**(4): p. 664-89.
109. Vetting, M.W., et al., *Structure of QnrB1, a plasmid-mediated fluoroquinolone resistance factor.* J Biol Chem, 2011. **286**(28): p. 25265-73.
110. Tran, J.H., G.A. Jacoby, and D.C. Hooper, *Interaction of the plasmid-encoded quinolone resistance protein Qnr with Escherichia coli DNA gyrase.* Antimicrob Agents Chemother, 2005. **49**(1): p. 118-25.
111. Kim, E.S., et al., *Interactions between QnrB, QnrB mutants, and DNA gyrase.*

Antimicrob Agents Chemother, 2015. **59**(9): p. 5413-9.
112. Saga, T., et al., *Characterization of qnrB-like genes in Citrobacter species of the American Type Culture Collection.* Antimicrob Agents Chemother, 2013. **57**(6): p. 2863-6.
113. Da Re, S., et al., *The SOS response promotes qnrB quinolone-resistance determinant expression.* EMBO Rep, 2009. **10**(8): p. 929-33.
114. Kim, H.B., et al., *Cold shock induces qnrA expression in Shewanella algae.* Antimicrob Agents Chemother, 2011. **55**(1): p. 414-6.
115. Nakanishi, A., S. Imajoh-Ohmi, and F. Hanaoka, *Characterization of the interaction between DNA gyrase inhibitor and DNA gyrase of Escherichia coli.* J Biol Chem, 2002. **277**(11): p. 8949-54.
116. Baquero, M.R., et al., *sbmC, a stationary-phase induced SOS Escherichia coli gene, whose product protects cells from the DNA replication inhibitor microcin B17.* Mol Microbiol, 1995. **18**(2): p. 301-11.
117. Romanowski, M.J., S.A. Gibney, and S.K. Burley, *Crystal structure of the Escherichia coli SbmC protein that protects cells from the DNA replication inhibitor microcin B17.* Proteins: Structure, Function, and Bioinformatics, 2002. **47**(3): p. 403-407.
118. Bernard, P. and M. Couturier, *Cell killing by the F plasmid CcdB protein involves poisoning of DNA-topoisomerase II complexes.* J Mol Biol, 1992. **226**(3): p. 735-45.
119. Miki, T., et al., *Control of segregation of chromosomal DNA by sex factor F in Escherichia coli. Mutants of DNA gyrase subunit A suppress letD (ccdB) product growth inhibition.* J Mol Biol, 1992. **225**(1): p. 39-52.
120. Engelberg-Kulka, H. and G. Glaser, *Addiction modules and programmed cell death and antideath in bacterial cultures.* Annu Rev Microbiol, 1999. **53**: p. 43-70.
121. de Feyter, R., C. Wallace, and D. Lane, *Autoregulation of the ccd operon in the F plasmid.* Mol Gen Genet, 1989. **218**(3): p. 481-6.
122. Van Melderen, L., P. Bernard, and M. Couturier, *Lon-dependent proteolysis of CcdA is the key control for activation of CcdB in plasmid-free segregant bacteria.* Mol Microbiol, 1994. **11**(6): p. 1151-7.
123. De Jonge, N., et al., *Rejuvenation of CcdB-poisoned gyrase by an intrinsically disordered protein domain.* Mol Cell, 2009. **35**(2): p. 154-63.

Chapter II: Investigation of VcParE-mediated toxicity in the native host cell, V*ibrio cholerae*, and the effect on mutagenic frequency

Chih-Han Tu, Christina R. Bourne

Department of Chemistry and Biochemistry, University of Oklahoma, Norman OK USA

The following work was published in ASM Journal of Bacteriology. I collected and processed all of the data, figures and tables regarding to VcParDE1, VcParDE2 TA systems, and the section regarding to chimeric ParE toxins. Writing of the manuscript was performed by myself with assistance from Dr. Christina Bourne. For the dissertation, I re-wrote the entire chapter. Editing and feedback on all writing was provided by Dr. Christina Bourne.

Introduction

Bacterial toxin-antitoxin (TA) systems are widely distributed in prokaryotic genomes as operons consisting of small bicistronic loci encoding an antitoxin and toxin gene.[1-4] TA systems were first identified in plasmids, functioning in an phenomenon called postsegregational killing (PSK),which ensures successful plasmid inheritance to daughter cells.[5] Later, TA systems were also found in bacterial chromosomes; however, their function is still debated. Nonetheless, studies link chromosomal TA systems to be involved in stress response, biofilm formation, phage defense and maintenance of mobile genetic elements.[6-9]

The type of TA system is categorized based on the nature of antitoxin and the mode of interaction between them. Currently eight different classes of TA systems have been classified[10]. The ParDE TA system of interest in this work belongs to type II TA system. Both ParD antitoxin and ParE toxin are proteins, and ParD antitoxins neutralize ParE toxins through direct protein-protein interaction.[1, 3, 11] ParE toxins have been shown to poison DNA gyrase and the inhibiton might be different from other known inhibitors, including the well-studied CcdB TA system toxin and quinolone antibiotics.[4] However, current studies on the molecular mechanism of how ParE toxins inhibit DNA gyrase appear to conflict, and therefore, cannot be integrated into a comprehensive model.

DNA gyrase is an essential type II bacterial topoisomerase, composed of two GyrA and GyrB subunits, forming an A_2B_2 heterotetramer that binds two helices of double-stranded DNA substrate.[12] Gyrase functions in regulating DNA topology by negatively supercoiling DNA through introducing a reversible double-strand break and passing one DNA segment across the other in an ATP dependent manner.[13] This change in DNA topology catalyzed by DNA gyrase is necessary as prokaryotic cells undergo DNA replication or transcription.[12, 14] The absence of DNA gyrase in eukaryotic cells make it a promising target for developing novel antibiotics. Since persistent double-strand breaks are fatal to cells, inhibitors blocking strand ligation after gyrase-induced DNA cleavage are potent inhibitors of bacterial growth. Additionally, DNA gyrase exhibits high sequence and structural similarity among different species, which make it a feasible target for a broad range of bacterial pathogens.[15] Several antimicrobial agents, including fluoroquinolones, as well as natural products including Microcin B17, albicidin, and simocyclinone are known to bind to and inhibit gyrase.[16-18] However, the resulting gyrase-inhibition-induced double strand break triggers the SOS response, a potentially error-prone DNA repair mechanism, that potentially produces resistant strains.[19-22] Within the GyrA subunit, defined mutational hotspots termed the quinolone resistance determining region (QRDR), are documented to arise directly from use of quinolone

antibiotics.[23]

The structure of ParE toxins is highly conserved even though the sequence conservation among them is low.[1] Superposition of ParE structures reveals they are highly conserved except for the C terminus. Several studies state that the mutation of specific residues or even truncations of the C-terminal region decrease ParE toxicity.[24-26] Fiebig et al., showed that truncation of C-terminus of a ParE toxin from *Caulobacter crescentus* reduced its toxicity and stability.[26] ParE toxins have been demonstrated to inhibit both gyrase-mediated supercoiling activity *in vitro* and induce a filamentous morphology, a hallmark of gyrase inhibition, as cells express ParE toxins.[2, 4, 27, 28] However, whether the ParE-induced gyrase inhibition triggers mutations and if those mutations accumulate to cause antibiotic resistance remains unknown. In this study, two ParE toxins cloned from the *Vibrio cholerae* N16961 chromosome were tested to assess the extent of toxicity in the native host. Our results show that induced expression of both VcParE1 and VcParE2 toxins led to a significant decrease in cell viability and VcParE2 exerts a higher toxicity compared to VcParE1. Moreover, this study also reveals that cells expressing either VcParE1 or VcParE2 toxins have an increased mutation frequency, but importantly, that these mutations did not impact antibiotic susceptibility. Building from these and others results, we sought to determine if the C-terminus of ParE toxins specifically impact the resulting cell viability.[24-26] Overall, our data demonstrate that expression of ParE toxins can increase the mutation frequency but these mutations are likely distributed randomly through the genome and so do not contribute to the development of antibiotic resistance. Furthermore, we show that while the C-terminus of ParE may be required for toxin activity, it is not sufficient to explain the observed different potencies of gyrase inhibition.

Method

Sequence alignments and homology model

The sequence similarity and identity of each ParE toxin were calculated from alignments generated from structure based superpositions in Chimera.[29] Formatting of this alignments were generated using ESPript 3.0.[30]

Bacterial strains and culture conditions

The strain of *Vibrio cholerae* utilized in this study is El Tor clinical isolate, N16961(ATCC). Cultures were grown at 37°C, either on agar plates or shaking at 200rpm. LB media was used as the growth media for the overnight liquid cultures, with 2.5% w/v agar added for solid agar plates. M9 minimal media (Table S2) was used in the later outgrowth for viability assay, to monitor the mutation frequency, and for detection of antibiotic susceptibility. When necessary, growth media was supplemented with chloramphenicol (CHL, 25μg/mL) and/ or with arabinose (0.02%, 0.2%)

Table 1. Bacterial strains and vectors used in this study

Strains	Description	Source of Reference
Vibrio cholerae N16961	Genomic DNA source, experimental strain	Obtained through BEI Resources, NIAID, NIH (NR-147; ATCC 39315)
Escherichia coli K-12 MG1655	F- lambda- *ilvG- rfb*-50 *rph*-1, experimental strain	Dr. Tyrrell Conway (Oklahoma State University)

Escherichia coli K-12 NovaBlue	F'[proA+B+ lacIqZΔM15::Tn10] endA1 hsdR17 (rK12– mK12+) supE44 thi-1 recA1 gyrA96 relA1 lac (TetR)	Novagen

Plasmid	Description	Source of Reference
pBAD	p15A origin of replication, araBAD promter, Cm^r, acceptor of Vc ParDE genes	Dr. Mattew Waldor (Harvard Medical School)
p15b	T7 promoter, Amp^r, acceptor of PaParE1 genes	Invitrogen

Recombinant Plasmid construction and transformation

The *VcparDE1* and *VcparDE2* genes were cloned from *V. cholerae* gDNA and inserted after the ribosome binding site in the pBAD33 vector using HiFi DNA Assembly kit (NEB) (**Table 1**.) The chimeric ParE constructs were generated by replacing the sequence of the C-terminus of the ParE1 toxins from *P. aeruginosa* encoded in p15b vector to that of the ParE toxins from *C. crescentus* and *V. cholerae* via Q5 mutagenesis kits (NEB). Verification of the resulting constructs was done by DNA sequencing. Electroporation was used to transform the plasmids into competent *V. cholerae* N16961 cells.[31]

A standardized protocol was used to prepare *V. cholerae* N16961 and *E. coli* MG1655 competent cells. An overnight culture was inoculated into fresh LB media at a 1:20 ratio and incubated at 37˚C, 200rpm until the OD_{600} reached 0.5 to 0.7. The culture was cooled on ice for 20min then harvested by centrifuging at 4000 x g for 15min at 4˚C. The cells were subsequently washed twice with 2mM calcium chloride and then resuspended in 10% glycerol. Electroporation was used to transform plasmids into *V. cholerae*. A 50μL aliquot of competent cells was mixed with 40ng plasmid encoding desired gene and incubated on ice for 1min. The mixture was transferred into a cold electroporation cuvette with a gap of 2mm and the cuvette was placed into a MicroPulser which was operated at 1.8kV. The cells were recovered by adding 1mL S.O.C. outgrowth media (NEB) and incubated at 37˚C for 3 h without shaking. For *E. coli* cells, the transformation processed via heat shock. A 50μL aliquot of competent cells was mixed with 0.1 - 100ng plasmid encoding the desired gene(s) and incubated on ice for 30min. The mixture was then transferred into an incubator maintained at 42˚C and incubated for 30s. The cells were recovered after storing on ice for 5min by adding 1mL S.O.C. outgrowth media (NEB) and incubated at 37˚C for 1 h with shaking. For all transformations, verification of successful transformation was evaluated by growth of cultures on selective plates. Resulting strains were isolated from single colonies and stored as glycerol stocks at -80˚C.

Measurement of Viability

Cultures were inoculated from frozen glycerol stocks into LB media supplemented with chloramphenicol and 1% glucose, and grown overnight (16-18 hr) at 37˚C, 200rpm. These dense cultures were diluted at a 1:20 ratio into M9 media supplemented with 1% glucose and divided into four tubes with equal volumes for protein induction. The expression of proteins was induced by adding 0%, 0.02%, 0.2% and 2% of arabinose into designated tubes. At given time points, aliquots of cultures were collected, serially diluted, and plated onto selective plates containing 1% glucose and chloramphenicol. Viable cell colonies were counted and corrected for both dilutions and the volume plated to determine the colony-forming units (CFUs) per mL.

Determination of minimum inhibitory concentration (MIC)

The MIC values for rifampicin (RIF) and ciprofloxacin (CIP) were determined in two ways. A broth microdilution method used 96-well round bottom microtiter plates. The first well contained 100μL of the stock solutions ([RIF]: 500μg/mL and [CIP]: 1μg/mL). The second to twelfth well added the following amount of the stock antibiotics: 50, 45, 40, 35, 30, 25, 20, 15, 10, 5 and 0 μL. Each well was then supplemented with the test -media (40, 45, 50, 55, 60, 65, 70, 75, 80, 85 and 90μL) to reach a total volume of 90μL in each well. Overnight cultures were diluted at a 1:20 ratio into M9 media and incubated at 37°C, 200rpm until the OD_{600} reached 0.2. 10μL of these cultures were subsequently inoculated into each well to make the final volume of 100μL. The MIC of each antibiotic was determined by visually inspecting cell pellets and the MIC was defined as the lowest concentration of antibiotic with no visible cell growth. The second method to determine the MIC is using standardized antibiotics-impregnated strip. Overnight cultures were streaked on selective plates containing 1% glucose and chloramphenicol. Antibiotic strips containing rifampicin (0.016 to 256 mg/L, Liofilchem) or Ciprofloxacin (0.002 to 32 μg/mL, bioMérieux) were placed onto the center of the plate. These plates were incubated at 37°C for 18h without shaking, after which time the MIC was determined by visual inspection for the antibiotic concentration corresponding to the boundary between a resulting cleared area and bacterial growth.

Fluctuation assay

Dense cultures were obtained by inoculation of frozen glycerol stocks into M9 media supplemented with chloramphenicol and 1% glucose, and grown overnight (16-18 hr) at 37°C, 200rpm. The cultures were diluted 10,000-fold in M9 media with chloramphenicol and incubated at 37°C, 200rpm. As the OD_{600} reached ~0.2, the diluted culture was subsequently divided into aliquots and, as indicated, 0.02% or 0.2% of arabinose was added to induce expression. A control culture containing 3.5ng/mL CIP (0.05 times the MIC) was included to mimic the expected inhibition of gyrase. Aliquots were incubated at 37°C, 200rpm for ~8hr before sampling. To increase the density, cells were pelleted and the resulting cell pellet was resuspended in the remaining 10% of the original volume. Of these resuspended cells, 90% were plated on rifampicin-containing plates (150 μg/mL, 2 times the MIC) and 10% of aliquots were serially diluted and plated onto selective plates containing chloramphenicol to determine the CFUs. The mutation frequency was determined by calculating the ratio of the number of colony forming units per volume on the rifampicin-containing plate (i.e., mutants) and on the chloramphenicol-containing plate (i.e. total possible cell units).

Antibiotics susceptibility

The preparation of cultures is depicted in the procedure of fluctuation assay. After the 8hr incubation, the cultures were pelleted. 90% of supernatant was removed and the cell pellet was resuspended in the remaining volume. The dense culture was streaked on selective plates containing 1% glucose and chloramphenicol. Standard antibiotic stripes containing azithromycin (0.16 to 256 μg/mL, bioMérieux), doxycycline (0.16 to 256 μg/mL, bioMérieux) or levofloxacin (32 to 0.002 μg/mL, bioMérieux) were placed onto the center of the plate. After incubation at 37°C overnight (18-24h), the antibiotics susceptibilities (MIC values) were determined from the scale on the strips at the point where bacterial growth began.

Result

Expression of VcParE1 and VcParE2 toxins in *Vibrio cholerae* N16961 results in decreased cell viability, while antitoxins do not impact growth and can effectively neutralize toxin function.

To test the toxic effects of VcParE1 and VcParE2 toxins in their native host, (i.e., *V. cholerae*), pBAD33 constructs encoding VcParD1, VcParE1, VcParDE1, VcParD2, VcParE2 or VcParDE2 were transformed into competent cells via electroporation. Because the addition of high concentrations of L-arabinose (e.g., >1%) to *V. cholerae* leads to the formation of non-proliferating spheroplasts,[32] we limited induction of protein expression to 0.02%, and 0.2% arabinose. Resulting colony-forming units (CFU/mL) were used to assess the potential toxic effect of each overexpressed protein.

Values were compared to a vector control (EV) lacking an inserted protein sequence. It is expected that cells transformed with EV would have no decrease on CFU counts as compared to the 0h time point, i.e., no negative value on Δlog(CFU/mL). Induction of VcParD1 and VcParD2 (Figure. 2.1) exerted essentially no toxicity but with modest effect on cell growth, as compared to the EV. In contrast, induction of either VcParE1 or VcParE2 toxins (Figure. 2.1) showed decreased cell survival within the first 2hr of induction. At 0.2% induction, VcParE1 triggered a 4-log reduction after 8hr induction as compared to EV and overall stagnated growth (Figure. 2.1C). In particular, VcParE2 exhibited an even stronger toxicity than VcParE1. In the 0.2% induction, VcParE2 mediated a 5.3-log reduction by the 4hr time point as compared to EV (Figure. 2.1F). The toxic effect of both VcParE1 and VcParE2 could be neutralized when co-expressed with their cognate VcParD1 and VcParD2 antitoxin, respectively, with resulting CFU counts closely matching those of the vector controls.

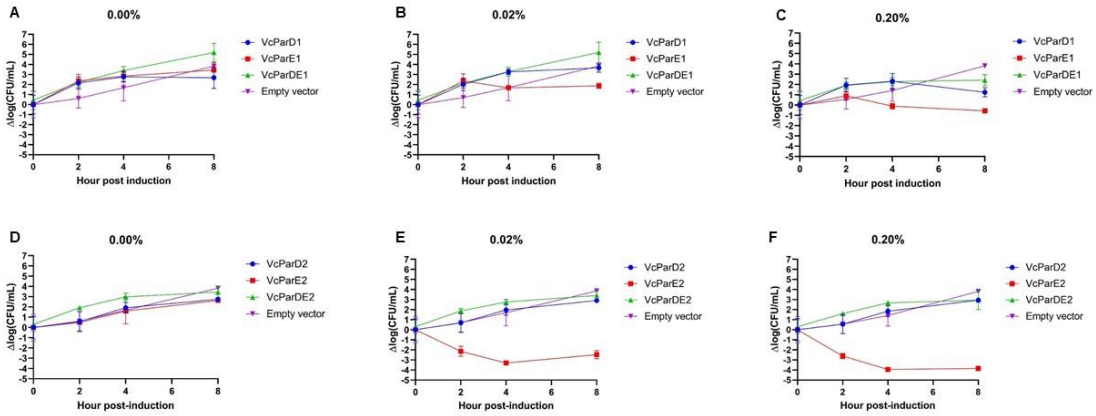

Figure. 2.1. Expression of VcParE1 and VcParE2 toxins cause decreases in CFU counts for *V. cholerae* N16961. Induction of VcParE1 (B and C) and VcParE2 (E and F) expression in *V. cholerae* resulted in decrease in CFUs as compared to the uninduced control cultures (A, D). Measurement were conducted with 3 biological replicates; average values for the change in CFU counts are graphed with standard error of the mean (SEM).

Induced expression of VcParE toxins in surrogate host *E. coli* MG1655 also leads to decreases in cell viability.

In addition to having toxic effects on the native host, VcParE1 and VcParE2 can also exert toxicity to *E. coli* MG1655 cultures. As measured with the native host, VcParE2 exhibited stronger toxicity to *E. coli* as compared to VcParE1. As Figure 2.2 indicated, a 2% induction of VcParE1 caused an approximately 3-log decrease in CFU counts at the time point of 4h as compared to 0% induction, while the 2% induction of VcParE2 resulted in approximately 4-log decrease in CFU counts at the time point of 4h as compared to 0% induction.

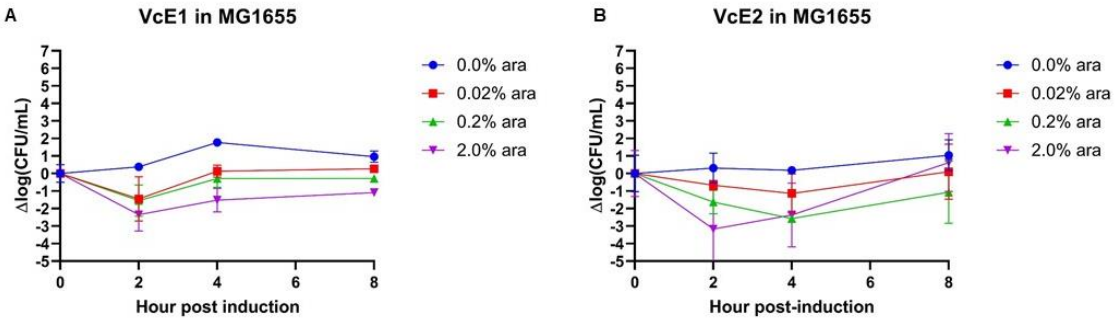

Figure. 2.2. Expression of VcParE1 and VcParE2 toxins cause decreases in CFU counts for *E. coli* MG1655. Expression of VcParE1 (A) and VcParE2 (B) in *E. coli* with increased induction concentrations (0 to 2%) caused decreased CFU counts.

Deducing molecular features of ParE important for toxicity.

As Figure 2.2 shows, expression of VcParE1 and VcParE2 toxins in *E. coli* MG1655 led to varying levels of toxicity. Based on the superposition of ParE toxins (Figure 2.3), the three-dimensional structure of ParE toxins is highly conserved except for the C-terminus.[33-35] Therefore, generating chimeric ParE with C terminus from other ParE toxins was the next step in this study. Since the ParE1 toxin from *Pseudomonas aeruginosa* (Pa) is not toxic to cells, and it contains the shortest C terminus,[1] it is an ideal model for switching the C-terminal amino acids to analyze if the toxicity increases. Based on the sequence alignment and structural superposition (Figure 2.3), the C-terminal region was replaced by that of the highly toxic VcParE2 toxin and with another highly toxic ParE toxin from *Caulobacter crescentus*(Cc). The chimeric ParE toxins were transformed to *E. coli* NovaBlue (DE3), a *recA*- strain established to be more sensitive to DNA break, with an aim of maximizing potential toxicity and expression, to assess and quantify the growth condition via CFU counts.[2]

As Figure 2.4A indicates, switching the amino acid sequences at the C terminus did not cause a significant difference in CFU counts measured after induction of toxin expression. For the parent PaParE1 and chimeric toxins, there is an approximate 2-fold decrease in CFU values at 8hrs after induction as compared to the EV. The expression levels of these chimeric ParE toxins were comparable or stronger than the wild type PaParE1, as figure 4B shows. These results indicate that adding or swapping the C-terminus between ParE toxins does not appear to impact toxicity upon induction, even with comparable or better expression levels.

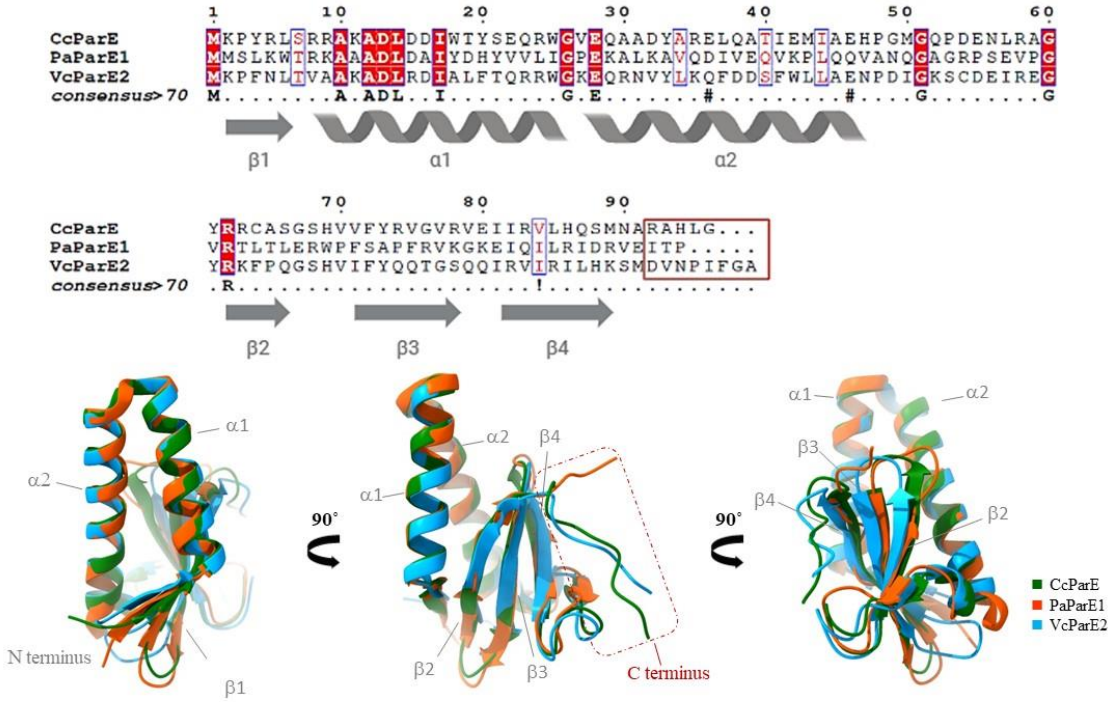

Figure. 2.3. Structural and sequence alignments of CcParE, PaParE1 and VcParE2 toxins. **(A)** Sequences are aligned based on the structural superposition, carried out using UCSF Chimera, and the alignment was formatted with ESPript 3.0 [4]. Residues with a similarity score exceeding 70% are considered highly similar and are colored in red and framed in blue. The C terminus of each ParE toxin is enclosed by a red rectangle. **(B)** The three-dimensional structures of ParE toxins were superimposed in ChimeraX; note, the antitoxins were removed from the superposition and images for clarity. The corresponding ParD antitoxins make direct and extensive contacts with the C-terminal regions of ParE toxins. (CcParE PDB 3KXE[33]; PaParE1 PDB: 6XRW[34]; VcParE2 PDB: 7R5A[35]). The C-terminus of the ParE toxins is highlighted by a dashed red rectangle.

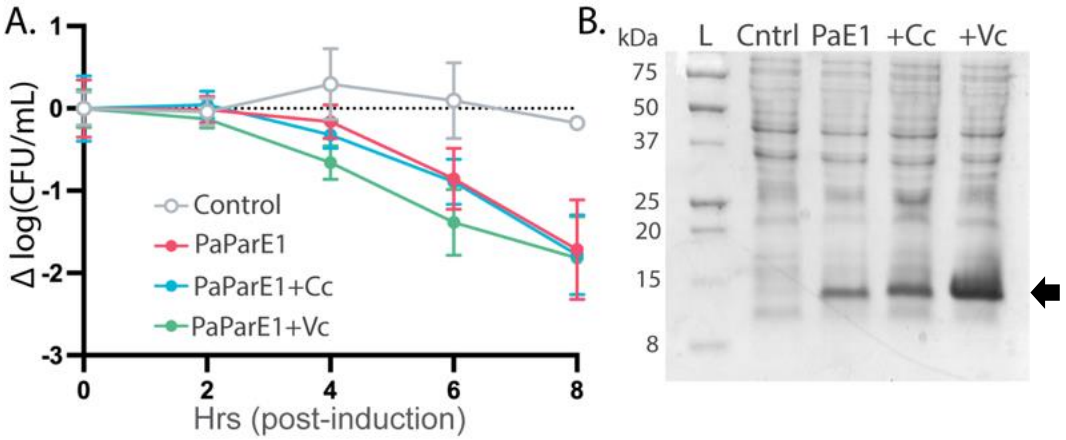

Figure. 2.4. Switching the C-terminus of ParE toxins does not impact or induce differences in toxicity. **(A)** *E. coli* cells expressing wild type PaParE1, PaParE1 with VcParE2 C-terminus ("PaParE1-Vc) and PaParE1 with CcParE1C-terminus ("PaParE1-Cc") does not significantly alter resulting CFU counts. **(B)** The expression level of each ParE1 was detected by electrophoresis. Based on intensity of each bend, the PaParE1-Vc protein (black arrow) does appear to have somewhat enhanced expression. Equivalent numbers of *E. coli* cells expressing toxins were used for this PAGE analysis.

Induction of VcParE1 and VcParE2 significantly increases the mutation frequency

To assess if expression of VcParE1 and VcParE2 toxins also trigger the accumulation of genomic mutations in *V. cholerae*, the mutation frequency was measured with and without toxin induction. From the viability analysis, induction of the ParE toxins for 8hrs is the strongest induction time point, giving the greatest loss of viability, and should reflect the effect of ParE-induced DNA breakage and repair on the bacteria cells. Because Ciprofloxacin has an analogous impact on gyrase inhibition as ParE toxin, it was selected as an appropriate control for mutations arising from repair following gyrase inhibition by sub-MIC treatments. Rifampicin (RIF) is used as a reporter because single point mutations in the *rpoB* gene, which encodes the beta subunit of RNA polymerase, can produce resistance and because of this, RIF is commonly used in the detection of mutation frequencies.[21, 36, 37] The number of mutants within the total population was determined by comparing the colony forming units arising from growth on plates with 2x the MIC value of RIF (Table 2.2.) with those forming on the plates containing only selection antibiotics for the plasmid harboring the inducible cassette.

Table 2.2. Minimum Inhibitory Concentrations (MIC, μg/mL) of RIF and CIP against the bacterial strain in test media used in the current studies.

Unit: μγ/mL	Rifampicin			Ciprofloxacin		
Strain	microtiter plates	Antibiotic stripe	Reference	microtiter plates	Antibiotic stripe	Reference
V. cholerae N16961	75	0.19	1	0.07	<0.002	0.079

The MIC was first determined via antibiotic strips. However, the MIC obtained from the strips could not provide useful values for testing mutation frequency. The resulting growth showed no difference between untreated and CIP-treated cells. Moreover, cells overgrew on the plate

containing either 0.75 μg/mL or 1.25 μg/mL of RIF that cannot be counted for CFU. Thus, the MIC was alternatively determined via microtiter plates. Cells treated with 0.05 times the MIC (0.035 μg/mL) decreased approx. 1000 times on CFU counts compared to untreated one. The growth of cells on the plate containing two times MIC (150 μg/mL) of RIF now can count the CFU.

As anticipated, treatment with 0.5 times the MIC of ciprofloxacin (Table 2.2) strongly increases the frequency of mutations in *V. cholerae* (Figure 2.5), from a basal value of 6 per 10^{-9} up to approx. 6 per 10^{-7}. Induction of VcParE1 or VcParE2 also significantly increased the mutation frequency, and this rise was dose dependent and consistent with the observed increase in toxicity (Figure 2.1.) For VcParE1, 0.2% induction triggers approx. 1.4 per 10^{-7} while the 0.02% induction level had a more modest increase, resulting in approx. 1 per 10^{-8}. VcParE2 leads to a higher mutation frequency than either VcParE1 or CIP, resulting in approx. 2 per 10^{-4}. Overall, these results demonstrate an increased mutation frequency in response to inhibition of DNA gyrase and consistent with the trends observed for loss of viability.

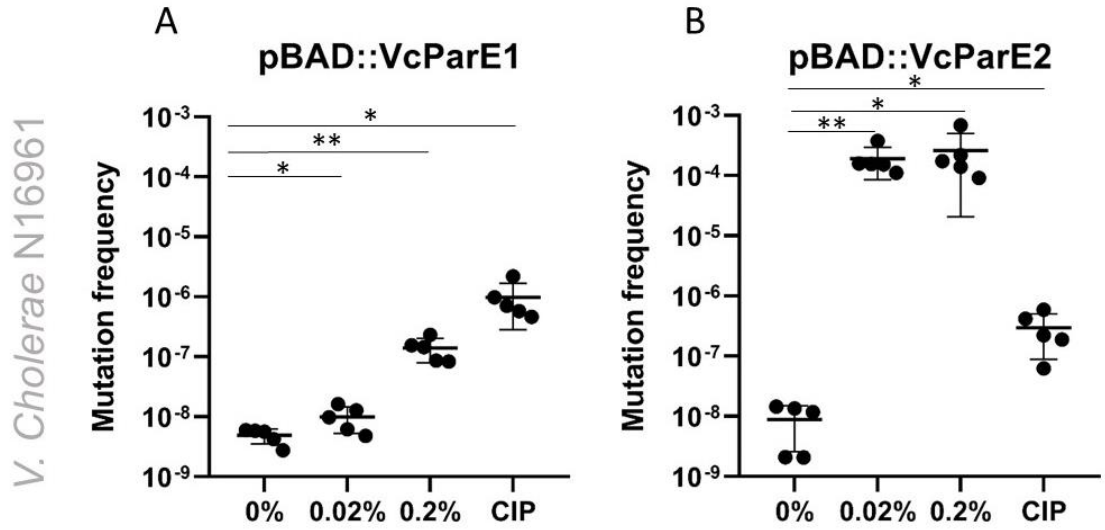

Figure. 2.5. Mutation frequency is significantly increased as *V. cholerae* is induced to express VcParE1 and VcParE2. (A) Induction of VcParE1, (B) Induction of VcParE2. Both VcParE1 and VcParE2 strongly increase the mutation frequency in *V. cholerae*. Measurement were conducted with at least 5 biological replicates; average values for the change in CFU counts are graphed with standard error of the mean (SEM). One asterisk indicates P-value is between 0.01 to 0.01 and two asterisks indicate P-value is between 0.001 to 0.01.

No significant changes in antibiotics susceptibility when *V. cholerae* is induced to express VcParE1 or VcParE2

As induction of VcParE1 and VcParE2 results in increased mutagenesis, it is intriguing to investigate whether the mutations can accumulate to the point of causing antibiotic resistance. The same cultures used for analyzing mutation frequency are also used in this assessment. The antibiotic strips containing azithromycin (AZM), or doxycycline (DOX), which are commonly utilized to treat *V. cholerae* infection, or the gyrase inhibiting antibiotic, levofloxacin (LEV), were applied to determine the minimal inhibitory concentration (MIC). As Table 2.3 shows, the MIC of all antibiotics do not have significant changes as cells expressing either VcParE1 or VcParE2, compared to the 0% induction. Taken together, *V. cholerae* cells expressing VcParE1 and VcParE2 toxins increase mutation frequency, but the mutations do not

accumulate to become antibiotic resistant.

Table 2.3. MIC of selected antibiotics on *V. cholerae* expressing VcParE1 and VcParE2.

Strain and treatment	Arabinose	AZM	DOX	LEV
N16961 expressing VcParE1	0%	0.38±0.00	0.21±0.03	0.01±0.00
	0.02%	0.44±0.06	0.23±0.03	0.01±0.002
	0.20%	0.44±0.06	0.25±0.09	0.01±0.006
N16961 expressing VcParE2	0%	0.5±0.17	0.38±0.00	0.02±0.01
	0.02%	0.57±0.19	0.24±0.14	0.01±0.002
	0.20%	0.88±0.13	0.16±0.09	0.004±0.00
N16961 + Ciprofloxacin	0%	0.75±0.54	0.38±0.1	0.01±0.002

Discussion

DNA gyrase affects the process of DNA replication and transcription, which in turn determines the overall rate of cell growth. If DNA gyrase can be inhibited during the steps involved in DNA topological change, permanent double-strand breaks can accumulate, which results in reducing cell viability. [1, 2] Together with the absence of DNA gyrase in eukaryotic cells, DNA gyrase is promising for developing novel antibacterial strategies.[12, 38] However, multiple studies show that antibiotics targeting gyrase significantly increase the mutation frequency, leading to the formation of resistance strains.[23, 39-41] Bacterial TA systems have been deemed potential targets for antibacterial strategies[42]. In particular, type II ParDE TA systems have been recognized to target DNA gyrase but the effect of inducing mutagenesis when cells express ParE toxins remain unknown.

In this study, the toxic effects of VcParE1 and VcParE2 toxins have been assessed in both native host, *V. cholerae* N16961, and in *E. coli* MG1655. ParE-induced gyrase inhibition causes DNA breaks, which results in a filamentous morphology of cells. Such filamented cells have been reported to impact light scattering and lead to an issue on the effectiveness of comparing culture turbidity via spectrophotometric instruments. Thus, we used CFU counts to indicate the effect of toxicity of each overexpressed protein. As Figures 2.1 and 2.2 indicate, in both cell types, VcParE2 exerts more toxicity than VcParE1. The 0.2% induction with arabinose of VcParE2 in *V. cholerae* led to 5.3-log decrease in CFU counts whereas the same induction of VcParE1 in *V. cholerae* led to 4-log decrease in CFU counts after 4h. Similarly, the 2.0% induction of VcParE2 in *E. coli* caused a 4-log decrease in CFU counts but the same induction of VcParE1 caused approximately 3-log decrease in CFU counts after 4h. Those results also indicate that *V. cholerae* cells are more sensitive to the toxic effect of VcParE1 and VcParE2 than *E. coli* cells. Our previous result of *in vitro* gyrase activity showed that the half-maximal inhibitory concentration (IC_{50}) of PaParE1 is higher in *P. aeruginosa* derived gyrase (IC_{50} = 11.7μM) than *E. coli* derived gyrase (IC_{50} = 3.7μM), suggesting PaParE1 exerts more effective inhibition against *E. coli* gyrase.[2] However, expression of PaParE1 in both *E. coli* MG1655 and *P. aeruginosa* PA14 as well as PAO1 do not impact cell growth (data not shown), implying that both *E. coli* and *P. aeruginosa* cells contain certain mechanisms for repairing double strand break. In the current study, it is possible that *E. coli* cells have better tolerance toward double strand break compared to that of *V. cholerae*, as the decrease of CFU count is

less in *E. coli* cells than that of *V. cholerae* cells.

The toxic effect of both VcParE1 and VcParE2 toxins can be neutralized by their cognate antitoxins, VcParD1 and VcParD2, respectively. Intriguingly, although expression of both VcParE1 and VcParE2 toxins decreased CFU counts significantly, cells were not completely eliminated and even returned to grow. The growth of the *E. coli* cultures expressing VcParE1 and VcParE2 toxins regrew to values equivalent to the control sample between 8h to 24h (data not shown). This phenomenon has been documented by our lab as potentially arising from an altered plasmid copy number whereby *E. coli* cells limit production of induced toxin proteins by decreasing the number of toxin-encoding plasmids.[43] However, the plasmid used in the current studies has a different origin of replication, and it is not clear if a similar cause is responsible for the observed effect. This could be explicated by our recent study that cells alter the plasmid copy number if the plasmid encodes genes which are unfavorable to cells, to this point where there is no significant effect on cell growth. The impact of the plasmid decreases after several generations and eventually exerts no significant effect on cell growth.[43]

Even though ParE toxins exhibit highly conserved three-dimensional structures, the level of toxicity among different ParE toxins varies. Therefore, PaParE1, a toxin exhibiting the least toxicity as well as containing the shortest C-terminus, was selected to analyze the role of the C-terminal amino acid sequence of ParE toxins to their potency. The C-terminus of VcParE2 and of CcParE1 were switched to the PaParE1 toxin to monitor the toxicity of the chimeric ParE by counting the CFU. Our results indicate that the CFU counts had no significant difference between wild type ParE1 toxin and chimeric ParE toxins. However, Fiebig et al., showed that truncations of the C-terminus from CcParE1 reduced its toxicity and protein stability. [26] Klemenc̆ic̆ et al., also discovered a ParE/ParD-like TA module in *Microcystis aeruginosa* and found that the C-terminal truncated toxin also attenuated its toxicity and the yield of the protein is low, implying that truncating C-terminus results in an unstable structure.[25] Taken together, the C-terminus is critical for ParE structural stability, and truncating the C-terminus leads to reduced toxicity. Combined with our results, the C-terminus might not directly contribute to the ParE toxicity, but it is necessary for the structural stability.

The estimation of mutation frequency when cells express VcParE1 and VcParE2 toxins was also conducted in this study. Inducing DNA double-strand breaks are one critical step in the gyrase mechanism. Antibacterial agents targeting gyrase usually stabilize the DNA-gyrase complex, inhibiting its progression through later parts of the gyrase mechanism, leading to permanent DNA breakage. Cells in turn often undergo error-prone repair mechanisms, e.g., SOS response, leading to an increased mutation frequency.[21, 22, 44] The SOS response and mutation frequency have also been detected and measured when *V. cholerae* was treated with sub-MICs of antibiotics. In particular, given the sub-MIC of ciprofloxacin, *V. cholerae* induced SOS response, resulting in increased mutation frequency.[21] As Figure 5 shows, our estimated mutation frequency of untreated *V. cholerae* as well as ciprofloxacin resulted in comparable values to published literature, in which the mutation frequency of *V. cholerae* without any treatment is around $2x10^{-8}$ and raises to approx. $2.6 x10^{-6}$ when treated with similar amount of CIP.[21] Based on this, we further measured the mutation frequency as *V. cholerae* expressed VcParE1 and VcParE2. Our results indicate that expression of both VcParE1 and VcParE2 increased mutation frequency. Moreover, the stronger the toxicity the ParE exhibited, the higher the mutation frequency it produced. Interestingly, cells expressing VcParE2 presented an even higher mutation frequency than treatment with sub-MIC ciprofloxacin. Taken together, our results demonstrate that *V. cholerae* expressing VcParE1 or VcParE2 toxins also raise the probability of mutagenesis and the ParE toxin containing stronger toxicity (*i.e.*, VcParE2)

induces a higher mutation frequency.

As ParE-induced mutagenesis has been established, we further analyzed if *V. cholerae* expressing VcParE toxins affects antibiotic susceptibility. Our results indicate that expression of VcParE1 and VcParE2 toxins did not show significant differences in the MIC analysis for clinically used antibiotics. Noteworthy, due to the potent toxicity, cells expressing VcParE2 appeared to form smaller colonies compared to control colonies. The cell density of each set was normalized and incubated for longer time, however, the cell expressing VcParE2 still did not grow as well as the control. Nonetheless, the MIC for each set was still determined, as Table 2.3 shows.

In conclusion, VcParE1 and VcParE2 toxins have been shown to inhibit DNA gyrase, causing persistent DNA double-strand breaks.[3, 4] As Figure 6 presents, our results confirm that bothVcParE1 and VcParE2 toxins are toxic to both *E. coli* MG1655 and the host cell, *V. cholerae* N16961. Higher dosage of both toxins suppress bacterial growth, or even kill cells. Conversely, moderate dosage of either toxin allows cells to undergo error-prone DNA repair, resulting in elevated mutation frequencies. Although ParE-induced mutagenesis occurs in bacterial cells, these seems to arise sporadically and do not contribute to the acquisition of antibiotic resistance.

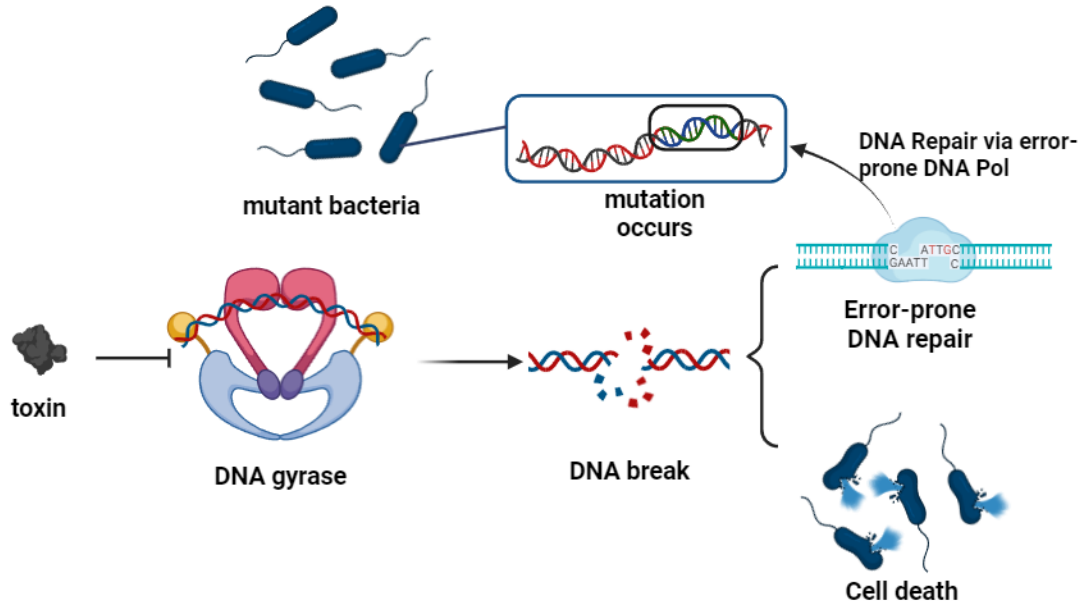

Figure. 2.6. Moderate dosage of the ParE toxin induces mutagenesis. The ParE toxin inhibits DNA gyrase, resulting in DNA breakage. Bacterial cells are either dead or undergo DNA repair via error-prone DNA polymerase, causing the mutagenesis to occur.

Data Availability

All data are included in this manuscript and supplement document; DNA clones for constructs made in this work are available upon request

Author Contributions

C.H.T. collected all data reported in this manuscript; C.H.T. and C.R.B. participated in the project design, data processing, manuscript drafting, and editing.

Acknowledgements

We thank the Protein Production Characterization Core facility (supported by Institutional Development Awards from the National Institute of General Medical Sciences of the National Institutes of Health Grants P20GM103640 and P30GM145423, the OU Vice President for Research and Partnerships, and the OU College of Arts and Sciences) for access to equipment. The funding souces is Department of Defense Congressionally Directed Medical Research Program Discovery Award PR192335, the OU Vice President for Research and Partnerships, and the University of Oklahoma Libraries' Open Access Fund.

Reference

1. Ames, J.R., et al., *Expression of different ParE toxins results in conserved phenotypes with distinguishable classes of toxicity.* Microbiologyopen, 2019. **8**(10): p. e902.
2. Muthuramalingam, M., et al., *The toxin from a ParDE toxin-antitoxin system found in Pseudomonas aeruginosa offers protection to cells challenged with anti-gyrase antibiotics.* Mol Microbiol, 2019. **111**(2): p. 441-454.
3. Yuan, J., Y. Yamaichi, and M.K. Waldor, *The three vibrio cholerae chromosome II-encoded ParE toxins degrade chromosome I following loss of chromosome II.* J Bacteriol, 2011. **193**(3): p. 611-9.
4. Yuan, J., et al., *Vibrio cholerae ParE2 poisons DNA gyrase via a mechanism distinct from other gyrase inhibitors.* J Biol Chem, 2010. **285**(51): p. 40397-408.
5. Gerdes, K., P.B. Rasmussen, and S. Molin, *Unique type of plasmid maintenance function: postsegregational killing of plasmid-free cells.* Proc Natl Acad Sci U S A, 1986. **83**(10): p. 3116-20.
6. Shmidov, E., et al., *PrrT/A, a Pseudomonas aeruginosa Bacterial Encoded Toxin-Antitoxin System Involved in Prophage Regulation and Biofilm Formation.* Microbiol Spectr, 2022. **10**(3): p. e0118222.
7. Wood, T.L. and T.K. Wood, *The HigB/HigA toxin/antitoxin system of Pseudomonas aeruginosa influences the virulence factors pyochelin, pyocyanin, and biofilm formation.* Microbiologyopen, 2016. **5**(3): p. 499-511.
8. Otsuka, Y. and T. Yonesaki, *Dmd of bacteriophage T4 functions as an antitoxin against Escherichia coli LsoA and RnlA toxins.* Mol Microbiol, 2012. **83**(4): p. 669-81.
9. Kamruzzaman, M. and J. Iredell, *A ParDE-family toxin antitoxin system in major resistance plasmids of Enterobacteriaceae confers antibiotic and heat tolerance.* Sci Rep, 2019. **9**(1): p. 9872.
10. Jurėnas, D., et al., *Biology and evolution of bacterial toxin-antitoxin systems.* Nat Rev Microbiol, 2022. **20**(6): p. 335-350.
11. Tu, C.H., et al., *Evaluating the Potential for Cross-Interactions of Antitoxins in Type II TA Systems.* Toxins (Basel), 2020. **12**(6).
12. Vanden Broeck, A., et al., *Cryo-EM structure of the complete E. coli DNA gyrase nucleoprotein complex.* Nat Commun, 2019. **10**(1): p. 4935.
13. Ruan, S., C.H. Tu, and C.R. Bourne, *Friend or Foe: Protein Inhibitors of DNA Gyrase.* Biology (Basel), 2024. **13**(2).
14. Basu, A., A.C. Parente, and Z. Bryant, *Structural Dynamics and Mechanochemical Coupling in DNA Gyrase.* J Mol Biol, 2016. **428**(9 Pt B): p. 1833-45.
15. Salman, M., et al., *Targeting novel sites in DNA gyrase for development of anti-microbials.* Brief Funct Genomics, 2023. **22**(2): p. 180-194.
16. Collin, F. and A. Maxwell, *The Microbial Toxin Microcin B17: Prospects for the Development of New Antibacterial Agents.* J Mol Biol, 2019. **431**(18): p. 3400-3426.

17. Michalczyk, E., et al., *Molecular mechanism of topoisomerase poisoning by the peptide antibiotic albicidin.* Nat Catal, 2023. **6**(1): p. 52-67.
18. Edwards, M.J., et al., *A crystal structure of the bifunctional antibiotic simocyclinone D8, bound to DNA gyrase.* Science, 2009. **326**(5958): p. 1415-8.
19. Tippin, B., P. Pham, and M.F. Goodman, *Error-prone replication for better or worse.* Trends Microbiol, 2004. **12**(6): p. 288-95.
20. Goodman, M.F., *Error-prone repair DNA polymerases in prokaryotes and eukaryotes.* Annu Rev Biochem, 2002. **71**: p. 17-50.
21. Baharoglu, Z. and D. Mazel, *Vibrio cholerae triggers SOS and mutagenesis in response to a wide range of antibiotics: a route towards multiresistance.* Antimicrob Agents Chemother, 2011. **55**(5): p. 2438-41.
22. Ysern, P., et al., *Induction of SOS genes in Escherichia coli and mutagenesis in Salmonella typhimurium by fluoroquinolones.* Mutagenesis, 1990. **5**(1): p. 63-6.
23. Hooper, D.C. and G.A. Jacoby, *Mechanisms of drug resistance: quinolone resistance.* Ann N Y Acad Sci, 2015. **1354**(1): p. 12-31.
24. Gupta, K., et al., *Contribution of the Chromosomal ccdAB Operon to Bacterial Drug Tolerance.* J Bacteriol, 2017. **199**(19).
25. Klemenčič, M., A. Halužan Vasle, and M. Dolinar, *The Cysteine Protease MaOC1, a Prokaryotic Caspase Homolog, Cleaves the Antitoxin of a Type II Toxin-Antitoxin System.* Front Microbiol, 2021. **12**: p. 635684.
26. Fiebig, A., et al., *Interaction specificity, toxicity and regulation of a paralogous set of ParE/RelE-family toxin-antitoxin systems.* Mol Microbiol, 2010. **77**(1): p. 236-51.
27. Beck, I.N., et al., *Toxin release by conditional remodelling of ParDE1 from Mycobacterium tuberculosis leads to gyrase inhibition.* Nucleic Acids Res, 2023.
28. Roberts, R.C., A.R. Ström, and D.R. Helinski, *The parDE operon of the broad-host-range plasmid RK2 specifies growth inhibition associated with plasmid loss.* J Mol Biol, 1994. **237**(1): p. 35-51.
29. Pettersen, E.F., et al., *UCSF Chimera--a visualization system for exploratory research and analysis.* J Comput Chem, 2004. **25**(13): p. 1605-12.
30. Robert, X. and P. Gouet, *Deciphering key features in protein structures with the new ENDscript server.* Nucleic Acids Research, 2014. **42**(W1): p. W320-W324.
31. Panda, D.K., U. Dasgupta, and J. Das, *Transformation of Vibrio cholerae by plasmid DNA.* Gene, 1991. **105**(1): p. 107-11.
32. Espinosa, E., et al., *L-arabinose induces the formation of viable non-proliferating spheroplasts in Vibrio cholerae.* Appl Environ Microbiol, 2020.
33. Dalton, K.M. and S. Crosson, *A conserved mode of protein recognition and binding in a ParD-ParE toxin-antitoxin complex.* Biochemistry, 2010. **49**(10): p. 2205-15.
34. Snead, K.J., L.L. Moore, and C.R. Bourne, *ParD Antitoxin Hotspot Alters a Disorder-to-Order Transition upon Binding to Its Cognate ParE Toxin, Lessening Its Interaction Affinity and Increasing Its Protease Degradation Kinetics.* Biochemistry, 2022. **61**(1): p. 34-45.
35. Garcia-Rodriguez, G., et al., *Toxin:antitoxin ratio sensing autoregulation of the Vibrio cholerae parDE2 module.* Sci Adv, 2024. **10**(1): p. eadj2403.
36. Taddei, F., I. Matic, and M. Radman, *cAMP-dependent SOS induction and mutagenesis in resting bacterial populations.* Proc Natl Acad Sci U S A, 1995. **92**(25): p. 11736-40.
37. Leehan, J.D. and W.L. Nicholson, *The Spectrum of Spontaneous Rifampin Resistance Mutations in the Bacillus subtilis rpoB Gene Depends on the Growth Environment.* Applied and Environmental Microbiology, 2021. **87**(22): p. e01237-21.
38. Wang, J.C., *Cellular roles of DNA topoisomerases: a molecular perspective.* Nat Rev Mol Cell Biol, 2002. **3**(6): p. 430-40.

39. Collins, J.A. and N. Osheroff, *Gyrase and Topoisomerase IV: Recycling Old Targets for New Antibacterials to Combat Fluoroquinolone Resistance.* ACS Infect Dis, 2024. **10**(4): p. 1097-1115.
40. Gillespie, S.H., et al., *Fluoroquinolone resistance in Streptococcus pneumoniae: evidence that gyrA mutations arise at a lower rate and that mutation in gyrA or parC predisposes to further mutation.* Microb Drug Resist, 2003. **9**(1): p. 17-24.
41. Farhat, M.R., et al., *Gyrase Mutations Are Associated with Variable Levels of Fluoroquinolone Resistance in Mycobacterium tuberculosis.* J Clin Microbiol, 2016. **54**(3): p. 727-33.
42. Równicki, M., et al., *Targeting Type II Toxin-Antitoxin Systems as Antibacterial Strategies.* Toxins (Basel), 2020. **12**(9).
43. Ruan, S. and C.R. Bourne, *Escherichia coli cells evade inducible parE toxin expression by reducing plasmid copy number.* Microbiol Spectr, 2024: p. e0397323.
44. Mesak, L.R. and J. Davies, *Phenotypic changes in ciprofloxacin-resistant Staphylococcus aureus.* Res Microbiol, 2009. **160**(10): p. 785-91.

Chapter III: Optimizing the Expression and Purification of ParE toxins using *E. coli* system

Chih-Han Tu, Christina R. Bourne

Department of Chemistry and Biochemistry, University of Oklahoma, Norman OK USA

This chapter represents unpublished data conducted in the Bourne lab.

I collected and processed all of the data, figures for the manuscript. All figures were produced by myself. Writing of the manuscript was performed by myself with assistance from Dr. Christina Bourne. Editing and feedback on all writing was provided by Dr. Christina Bourne.

Introduction

Toxin-antitoxin (TA) systems are small operons composed of an antitoxin and a toxin gene.[1] They are widely distributed in the prokaryotic genomes with one or several copies of TA loci and are found in nearly all bacterial and archaeal chromosomes.[2, 3] TA systems are categorized into eight classes based on the inhibitory mechanism of toxin and the nature of antitoxin neutralization.[1] Among TA systems, the "type II" are the most prevalent and well-characterized, in which both toxin and antitoxin are proteins and the neutralization is through direct protein-protein interaction.[4] The ParDE TA system is one of the earliest identified type II TA systems when it was discovered to be harbored on the broad-host range RK2 plasmid and functions in promoting the maintenance of the plasmid.[5] The *parDE* operon has also been found in bacterial chromosomes but the function is still debated.[6-8] The overall structure of ParDE complex is highly conserved, but the sequence identity is typically low.[9] In addition, the interaction between ParD antitoxin and ParE toxin is highly specific to those co-encoded in a single operon, or "cognate" pairs. Evidence suggests that cross interaction between non-cognate ParD and ParE proteins, even when multiple ParDE operons are in the same cell, is rare.[10-12] While the ParD antitoxin protein is labile, either containing an unstable structure or being easily degraded by AAA+ proteases,[13, 14] the ParE toxin protein is stable and has been shown to function as a DNA gyrase inhibitor via stabilizing the gyrase-DNA cleavage complex, resulting in the persistence of double-strand DNA breaks.[9, 15-17]

DNA gyrase belongs to the type II topoisomerase family and is essential to bacteria to relieve torsional stress that accumulates in the circular genome, but is lacking in human cells. It is composed of two copies of two different protein chains (GyrA and GyrB), together forming an "A_2B_2" heterotetramer.[18, 19] The function of DNA gyrase is to maintain the homeostasis of DNA topology to prevent DNA entanglement when cells undergo DNA replication and transcription. The process is ATP-dependent and is achieved via temporarily cleaving both strands of bound DNA segment to let an adjacent intact DNA segment pass through, thereby generating negative supercoils upon re-ligation of the DNA break.[20]

Gyrase is a major target for antibacterial strategies because it is indispensable to bacterial cells and absent in human cells; inhibiting gyrase activity impacts the DNA replication and transcription which affect bacterial growth.[21, 22] Additionally, generating a double strand break in DNA, which is lethal to cells if unrepaired, is a necessary step for the gyrase catalytic cycle. Compounds inhibiting gyrase often stabilize the "gyrase- cleavage" complex, which interrupts the re-ligation of the cleaved DNA. [19, 23] Fluoroquinolones (FQ) are widely used antibiotics and are one example of an inhibitor class that stalls the gyrase-DNA complex by

intercalating into the cleavage site of DNA.[24] Other than directly binding to the DNA cleavage site to physically block re-ligation, some compounds exhibit different inhibitory mechanisms against gyrase. The binding site of Thiopene 1 is located in a pocket between GyrA and GyrB subunits and is away from the DNA molecule.[25] Binding of Thiopene 1 triggers an allosteric effect to stabilize the gyrase-DNA cleavage complex.[25] Recently, two phase III approved non-FQ drugs, zoliflodacin and gepotidacin, show distinct bindings to stabilize the cleavage complex. The binding of zoliflodacin occurs at DNA cleavage site. Unlike FQ drugs mainly interacting with GyrA, zoliflodacin, instead, interacts with GyrB to stabilize the cleavage complex, causing double strand break.[26, 27] Gepotidacin belongs to novel bacterial topoisomerase inhibitor (NBTI).[28] Rather than causing DNA double strand break, gepotidacin induces single strand break by occupying at the pocket between two GyrA subunits and the scissile DNA bonds.[27, 28] Taken together, it has been shown that targeting gyrase in different conformations with various inhibitors has proved to be successful for antimicrobial agents.

In addition to developing numerous small molecules to inhibit gyrase, several small proteins have also been identified to have an inhibition effect on gyrase. Some of these peptide-based gyrase inhibitors, including Microcin B17, CcdB and ParE, cause the DNA double strand break to persist, leading to bacterial cell death, [1, 29, 30] while others, such as MfpA, Qnr and GyrI, exhibit a non-damaging, reversible effect on gyrase. We and others have suggested that this reversible inhibition plays a role on regulating bacterial growth or protecting gyrase from damaging inhibition. [31, 32]

The ParDE TA system found on the RK2 plasmid was one of the first identified TA systems.[33-35] Studies revealed that the ParE toxin inhibits DNA gyrase and its expression in bacterial cells caused a filamentous morphology which is consistent with gyrase inhibition.[9, 36] Other studies also showed the *in vitro* gyrase inhibition mediated by ParE toxins encoded chromosomally in *Pseudomonas aeruginosa* (Pa), *Vibrio cholerae* (Vc) and *Mycobacterium tuberculosis* (Mt).[7, 17, 36] The ParE toxins exhibit highly conserved structures but their sequence identity is low, which might explain various levels of ParE toxicity against bacterial cells.[9, 12, 36] The *in vitro* measurements of gyrase inhibition allow calculation of a half maximal inhibitory concentration (IC_{50}), which for VcParE2 from is 1.2μM while PaParE is 3.7μM against *E. coli* gyrase. [16, 36] Moreover, studies about the binding interaction between different ParE toxins and gyrase appear to produce conflicting results.[12, 16, 17] VcParE2 was demonstrated to bind to GyrA59, a GyrA truncation without the CTDs, with affinity approximating to 10nM.[16] Conversely, some ParE toxins show weaker or no interaction with *E. coli* GyrA subunit. *E. coli* ParE2 toxin is reported to have no interaction with GyrA. [11] *M. tuberculosis* ParE2 toxin shows weaker interaction with GyrA, i.e., around 922μM, while having a higher affinity toward MtGyrB, i.e., around 4.75μM[11] These results indicate that even though the ParE toxin family inhibits gyrase, the molecular mechanism of how ParE binds to gyrase remains unknown.

A recent study identified a novel PaParDE homolog and performed computational studies by simulating the structure of ParD - ParE and ParE - GyrA complexes from *P. aeruginosa*.[37] Even though the *in silico* study provides insights for ParE - GyrA interaction, this study only simulated the interaction between ParE and monomeric GyrA subunit, which is unlikely to occur naturally since GyrA is usually in dimeric form. Therefore, experimental structural studies are still needed to characterize ParE activity.

VcParE1 and VcParE2 have shown potent toxicity against both *V. cholerae* cells, causing

approx. 2-log decrease and 4-log decrease on colony forming unit after 2h expression, individually.[7] Moreover, the VcParE toxins encoded on chromosome II of *V. cholerae* induce the degradation of chromosome I, which contains most of the organism's essential genes, following loss of chromosome II, which encodes excess of hypothetical and uncharacterized open reading frames. This suggests that chromosomal ParDE TA systems also trigger postsegregational killing.[7] The interaction between VcParE2 and gyrase has also been reported. Yuan et al., showed that VcParE2 interacts with GyrA subunit with a biphasic binding.[16] Taken together, VcParE toxins exhibit potent toxicity against bacterial cells and show a biphasic interaction with GyrA subunits.

The objective of this study is to capture DNA gyrase complex bound with ParE toxin, which we hypothesize must only occur mid-way through the catalytic cycle. Because DNA gyrase undergoes multiple large conformational changes in its catalytic cycle, it is uncertain which state of gyrase ParE is able to bind to. Isolation of this complex will allow further studies to be conducted by cryo - electron microscopy (cryo-EM) for structural analysis. The challenge is in generating the highly toxic ParE proteins using recombinant protein expression. Our results show that this is a feasible method to obtain sufficient amount of purified ParE proteins via co-expression of gyrase B+A chain fusion which is able to lessen the ParE toxicity.

Method

Recombinant Plasmid construction and transformation.

The *VcparDE2* genes were cloned and inserted after the ribosome binding site in the pET28a vector using HiFi DNA Assembly kit (NEB). The pBAD33::strep-VcParE1 was constructed by inserting the sequence of strep - tag to the pBAD33::VcParE1 via Q5 mutagenesis kits (NEB). The resulting constructs were validated by DNA sequencing.

The transformation of recombinant plasmids into *E. coli* cells was proceeded via heat shock. 0.1-100ng of plasmid containing the target gene was added and mixed with 50μL aliquot of competent cells and kept on ice for 30 min. The mixture was then heated at 42°C for 30 second. Following a 5-minute incubation on ice, 1mL of S.O.C. outgrowth media (NEB) was added, and the cells were incubated at 37°C for 1 hr with shaking to allow recovery. A successful transformation was validated by growth of cultures on selective plates. Resulting strains were isolated from single colony and store as glycerol stocks at -80°C.

Expression and Purification of GyrA and GyrB subunit

These methods follow standard procedures adopted from the literature and established by previous members of the Bourne lab. Briefly, plasmids pET30a::*EcgyrA-His* and ::*EcgyrB-His* were transformed into BL21(DE3) pLys competent cells (NEB), and a starter culture in LB was diluted at a 1:20 ratio into 2X YT media with 50μg/mL kanamycin. This was grown to an optical density at 600 nm (OD_{600}) equaling to 0.6 - 0.8 and was subsequently induced for the expression with 1.0mM Isopropyl ß-D-1-thiogalactopyranoside (IPTG) at 30°C 180rpm overnight (16-18hrs).

Cells were harvested by centrifuging. Pellets were resuspended in 50mM HEPES pH8.0,300mM NaCl, 5mM imidazole and 0.2mM PMSF, and lysed using an Emulsiflex-C3 homogenizer (Avestin Inc). The resulting lysate was clarified at 22000 x g at 4°C for 40min. Clarified lysate was loaded onto a 5mL HisTrap FF nickel Sepharose column (GE Healthcare) equilibrated in the same buffer and captured proteins were washed with 50mM HEPES pH8.0,

750mM NaCl to remove residual bound DNA. Protein was eluted gradiently with 50mM HEPES pH8.0,300mM NaCl, 500mM imidazole and 0.2mM PMSF. Protein fractions were collected and after concentrating were loaded onto a HiPrep sephacryl S400 16/60 column (GE Healthcare) equilibrated with 50mM HEPES pH8.0, 200mM NaCl, 2mM PMSF.

Purification of VcParE2 using denaturation-refolding method

Attempts to purify VcParE2 follow previously reported procedures.[4, 38] BL21(DE3) cells were transformed with a pET-28a plasmid encoding the *VcparDE2* gene with C-terminal 6x His tag appended to the *VcparE2*. A starter culture was incubated overnight (16-18hrs) at 37° C 200rpm in LB media supplemented with 50μg/mL kanamycin and was subsequently diluted at a 1:20 ratio into LB media. The expression of the VcParDE2 complex was induced by adding 1mM IPTG when the optical density reached 0.6 – 0.8. The culture was then incubated at 18° C, 180rpm overnight (16-18hrs). Cells were harvested by centrifuging at 10,000 x g at 4°C for 15 min. Pellets were resuspended in 50mM Tris pH8.0, 300mM NaCl, 25mM imidazole. Cells were lysed using Emulsiflex-C3 homogenizer (Avestin Inc). The resulting lysate was clarified at 16000 x g at 4°C for 40min. Clarified lysate was loaded onto a 5mL HisTrap FF nickel Sepharose column (GE Healthcare) equilibrated in the same buffer. After column wash, the VcParDE2 complex was eluted gradiently with 50mM Tris pH8.0, 300mM NaCl, 500mM imidazole. Protein fractions were collected and after concentrating loaded onto a Superdex 75 10/300 GL (GE Healthcare) column pre-equilibrated with 50mM Tris pH8.0, 300mM NaCl.

Following the published protocol, [38, 39] the purified VcParDE2 complex was reloaded onto a 5mL HisTrap FF nickel Sepharose column (GE Healthcare). The column was then washed with 25mL with 20mM Tris pH8.0, 500mM NaCl, 10% ethylene glycol. The bound VcParDE2 complex subsequently underwent denaturation process using a step-gradient wash with 50% and 100% of 20mM Tris pH8.0; 500mM NaCl; 10% ethylene glycol; 5M denaturant (urea or Guanidinium hydrochloride, GdHCl), respectively, resulting in the dissociation of VcParD2. The bound VcParE2 was refolded on-column via washing with 25mL of 20mM Tris pH8.0, 25mM NaCl, 5%glycerol, 2mM β-Mercaptoethanol (BME); then washing with 25mL of 20mM Tris pH8.0, 1mM NaCl, 10% ethylene glycol and finally washing with 25mL of 20mM Tris pH8.0; 250mM NaCl; 2mM BME. The refolded VcParE2 was eluted from the nickel column with 50mM Tris pH8.0, 300mM NaCl, 500mM imidazole. Protein fractions were collected and concentrated to the required volume prior to running through a Superdex 75 10/300 GL (GE Healthcare) column pre-equilibrated 50mM Tris pH8.0, 300mM NaCl.

***In vitro* protein synthesis and purification via heparin agarose**

A commercial transcription - translation kit (PURExpress *In Vitro* Protein Synthesis Kit, NEB) was used and followed manufacturer's procedures. Reactions were done by incubating 250ng of plasmid DNA encoding Green Fluorescent Protein (GFP), MtParE1 and VcParE2 sequences, individually, with the reaction solution supplementing with 20U RNase inhibitor at 37°C for 3h. The protein production was monitored by measuring the fluorescent signal arising from GFP (excitation at 485nm, emission at 528nm).

To purify the protein from the reaction mixture, protein samples were added to the heparin resin pre-equilibrated with 50mM Tris pH7.5, 100mM NaCl and shaken at room temperature for 30min. The resin was washed with 50mM Tris pH7.5, 150mM NaCl and 250mM NaCl. The captured proteins were then eluted by adding 50mM Tris pH7.5, 500mM NaCl. The flow through at each step was collected and electrophoresed with visualization by coomassie staining.

Purification of GST-VcParE2 in the absence of ParD antitoxin.
The plasmid was transformed into BL21(DE3) competent cells (NEB). The expression and purification of GST-VcParE2 protein followed the procedure and buffers used for purification of VcParDE2 complex. Purified GST-VcParE2 was then cleaved to remove the GST fusion tag via adding 1U of PreScission protease per 500μg of the target protein and incubated at 4˚C overnight (16-18 hrs). VcParE2 was then purified from GST using a 5mL GSTrap FF column (GE Healthcare) pre-equilibrated with Tris pH8.0, 500mM NaCl, and 2mM BME. After column wash, the VcParE2 was collected in the flow through and concentrated prior to running through a Superdex 75 10/300 GL (GE Healthcare) column pre-equilibrated with50mM Tris pH8.0, 300mM NaCl.

DNA gyrase supercoiling assay
The DNA gyrase supercoiling assay followed previously reported procedures.[36] The reaction mixture consisted of assay buffer(final concentrations at 64mM Tris pH8.0, 44mM KCl, 7mM $MgCl_2$, 3.5mM DTT, 3mM spermidine and 0.168mg/mL BSA), 500ng of commercial relaxed pHot plasmid (Inspirialis), 5mM ATP, and purified DNA gyrase A and B with required concentrations (final concentration at 5nM or 10nM) and inhibitors (if necessary), typically in a total volume of 30μL. The reaction was incubated at 37˚C for 1hr then quenched by adding equal volumes of buffer containing 100mM Tris pH8.0, 500mM NaCl, 1% SDS, 1mM EDTA and 40% sucrose and further incubated at 50˚C for 30min to ensure release of the covalent protein-DNA intermediate. After centrifuging at 16,000 x g for 5min, samples were loaded onto 1% agarose gels, in a 1x TAE buffer and electrophoresed at 40V for 4h. Gels were subsequently stained with SYBR safe (Invitrogen) and imaged. Band intensity was quantified using ImageJ, and the supercoiling activity was determined by calculating the percentage of the intensity of the supercoiled DNA relative to the total lane intensity.

Result

Purification of VcParE2 toxin using denaturation-refolding method produces limited active VcParE2

The VcParE2 toxin shows potent toxicity against bacterial cells,[7, 16] meaning that it is lethal to directly overexpress VcParE2 in *E. coli* recombinant expression systems. However, by co-expression of VcParE2 with VcParD2, the cognate antitoxin that neutralizes VcParE2 toxicity, VcParE2 can be overexpressed and purified using *E. coli* cells. Several studies regarding the purification of toxin proteins have shown that the cognate antitoxin can be dissociated from the toxin by utilizing denaturants, e.g. urea or guanidinium hydrochloride (GdHCl), where the unfolded toxin protein can be refolded by removing these denaturants.[4, 38, 39] Therefore, in this study, we aimed to obtain purified VcParE2 via denaturation-refolding method (Figure 3.1.)

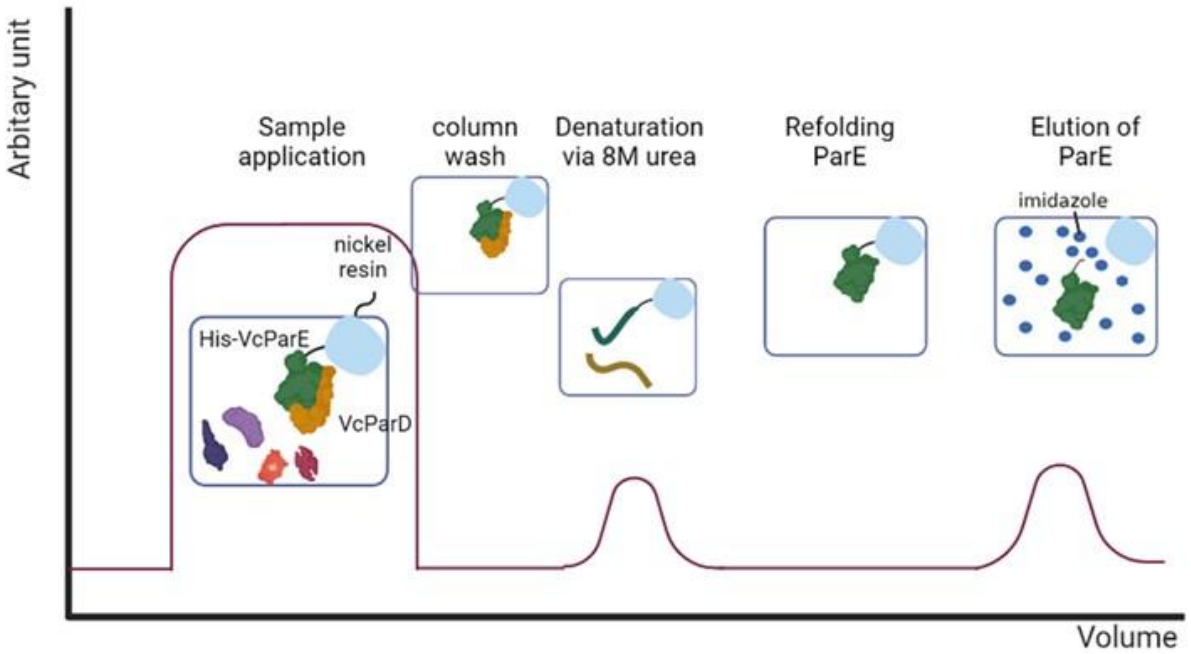

Figure 3.1. the overview of denaturation-refolding method. The lysate containing VcParDE2 complex with 6x His-tag at C-terminus of VcParE2 is loaded onto a nickel affinity column. After column wash with low concentration (25mM) of imidazole, the VcParDE2 complex remains bound to the column and most nonspecific proteins are removed. The column is than washed with denaturant, e.g. urea or GdHCl, to denature the VcParDE2 complex, leading to the dissociation of VcParD2 from VcParE2. After washing with refolding buffers, the VcParE2 returns to its native folded state and is eluted from the column by high concentration (500mM) of imidazole. Protocol adapted from [39]

The VcParDE2 complex was purified using nickel affinity chromatography followed by size exclusion chromatography. (Figure 3.2A - B) The resulting VcParDE2 complex was reloaded back to a nickel affinity column again. After column wash, a gradient wash with 4.0M and 8.0M urea was performed to unfold VcParDE2 complex. The unfolded VcParE2 with C-terminal 6x His-tag remained associated to the nickel column while the unfolded VcParD2 was eluted. The unfolded VcParE2 underwent a refolding process and eluted from the column with imidazole and was further purified and analyzed via size exclusion chromatography.

In our trials, VcParD2 only dissociated partially from VcParE2 after washing with high concentrations of urea, and residual VcParD2 co-eluted with VcParE2 (Figure 3.2D, lane 7 and lane 9) Additionally, the refolding process was likely not fully successful as aggregation was observed with a significant amount of protein eluting in the void volume during size exclusion chromatography analysis. (Figure 3.2F lane 11)

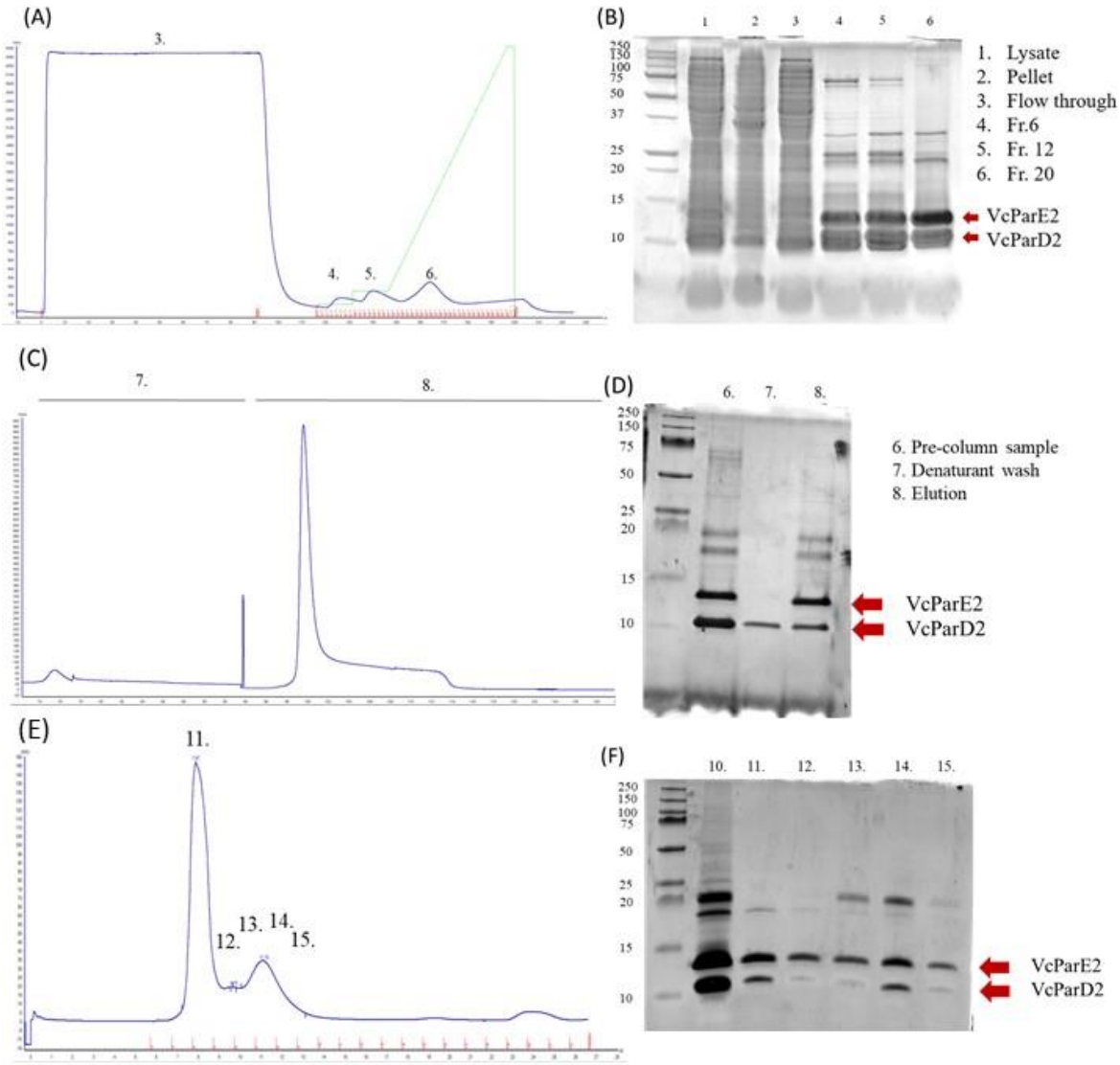

Figure 3.2. Obtaining purified VcParE2 via on-column denaturation-refolding purification. (A) Nickel affinity chromatogram of purified VcParDE2 complex and (B) shows the corresponding species in each step. (C) Nickel affinity chromatogram representing the denaturation-refolding process and (D) shows the corresponding species in each step. (E) Size exclusion chromatogram verifying the refolding of proteins and (F) shows the corresponding species in each step. All samples collected in each step were load into 12% tris-tricine gels and visualized by Coomassie staining.

To fully remove VcParD2 from VcParE2, we conducted multiple trials of denaturant wash. The reason for this approach is to disrupt the equilibrium between the folded and unfolded states of VcParDE2 complex so that VcParD2 would completely dissociate from VcParE2. Instead of continuous wash with 8M urea, the unfolded proteins were eluted from nickel affinity column and loaded back to the nickel column for another trial of the 8M urea wash.

As Figure 3.3 shows, even undergoing the second trial of denaturant wash, there were still VcParD2 that remained bound to VcParE2. Additionally, there was no further removal of VcParD2 after the urea wash. (lane 2 and 3 in the right panel.)

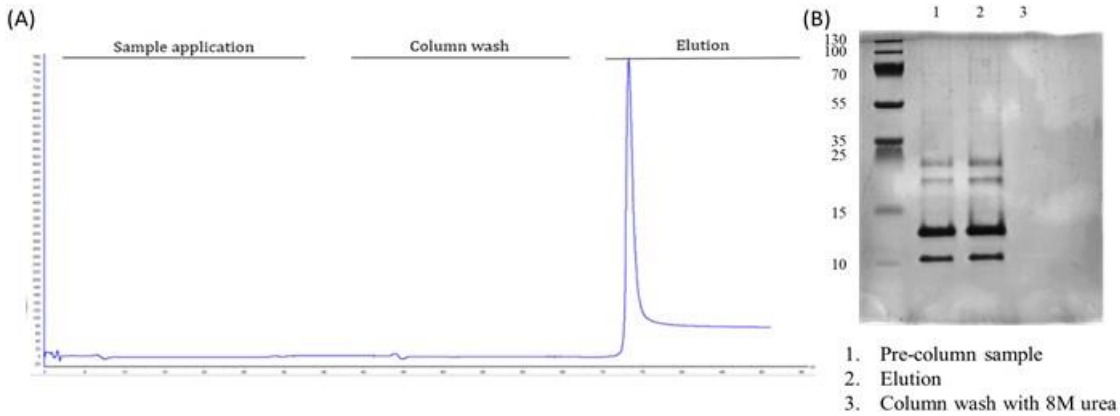

Figure 3.3. An additional trial of an 8M urea wash was not able to remove residual VcParD2 from VcParE2. Because VcParD2 was not fully dissociated from VcParE2 upon the initial washed with urea, a second trial was conducted. (A) The nickel affinity chromatogram of the on-column denaturation. (B) The gel result to visualize the protein species in each step.

The refolding step also plays a vital role in the purification process. Yamaguchi et al., states that directly removing denaturant from high to low concentration may increase chances for protein aggregation, whereas gradual removal of denaturant may facilitate protein refolding to return to the native state.[40] As figure 5 shows, to improve VcParE2 refolding, buffers used in refolding contain a gradient of urea to gradually decrease its concentration in the sample. Additionally, dialysis was used in the process to more gradually exchange the buffer while removing urea. The resulting chromatogram from size exclusion chromatography shows that the peak in the void volume decreased (Figure 4B), indicating that protein refolding has improved. However, the sample still contained residual VcParD2 and the yield is less than 0.1mg per 1L of bacterial culture. (Figure 4.4C)

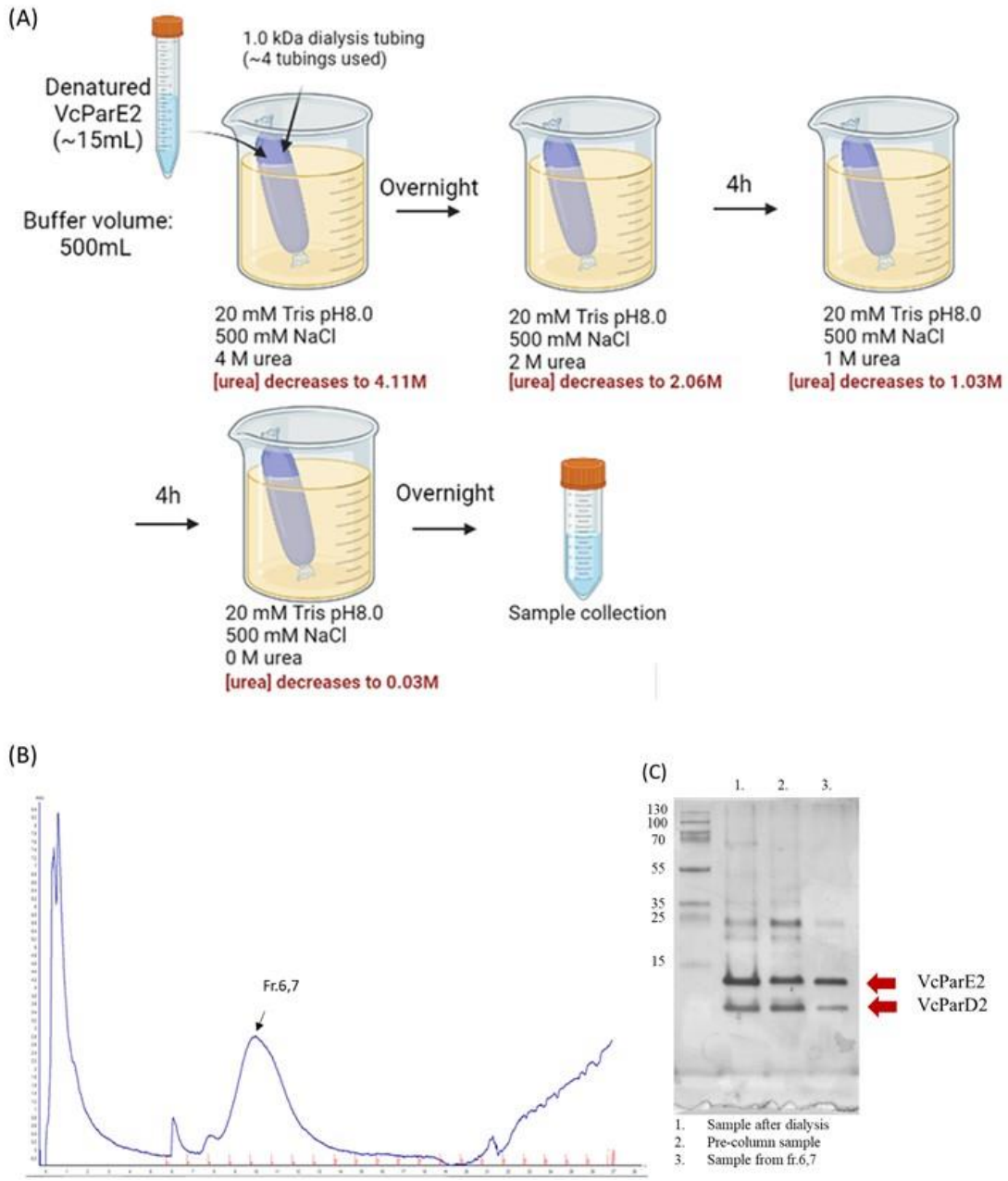

Figure 3.4. A dialysis method to refold VcParE2. (A)Schematic overview of this alternative refolding method. (B) Size exclusion chromatogram of the resulting protein. (C) Gel result to visualize the protein species in each step.

We also used GdHCl as an alternative denaturant to urea to denature VcParDE2 complex. The denaturation-refolding was carried out with the sample remaining bound to the nickel column rather than using a dialysis step. Compared to the utilization of urea, denaturation of VcParDE2 by GdHCl hardly removed VcParD2 from VcParE2, as the samples from the elution fractions still contained VcParD2 with VcParE2 (Figure 3.5C lane 4-8) However, compared to previous attempts, the on-column refolding did not produce aggregation even though the refolding process directly removed GdHCl from high to low concentration (Figure 3.5B), implying that refolding with higher amount of VcParD2 might prevent VcParE2 from aggregation. Taken together, our results suggest that urea is a better choice to denature the VcParDE2 complex compared to GdHCl. However, VcParD2 cannot be completely removed from VcParE2 since some residual VcParD2 remain bound to VcParE2. Our results also indicate that gradient removal of urea improves VcParE2 refolding that prevents aggregation. Lastly, refolding of VcParE2 with increased amount of VcParD2 might prevent the formation of aggregation. (Figure 3.5)

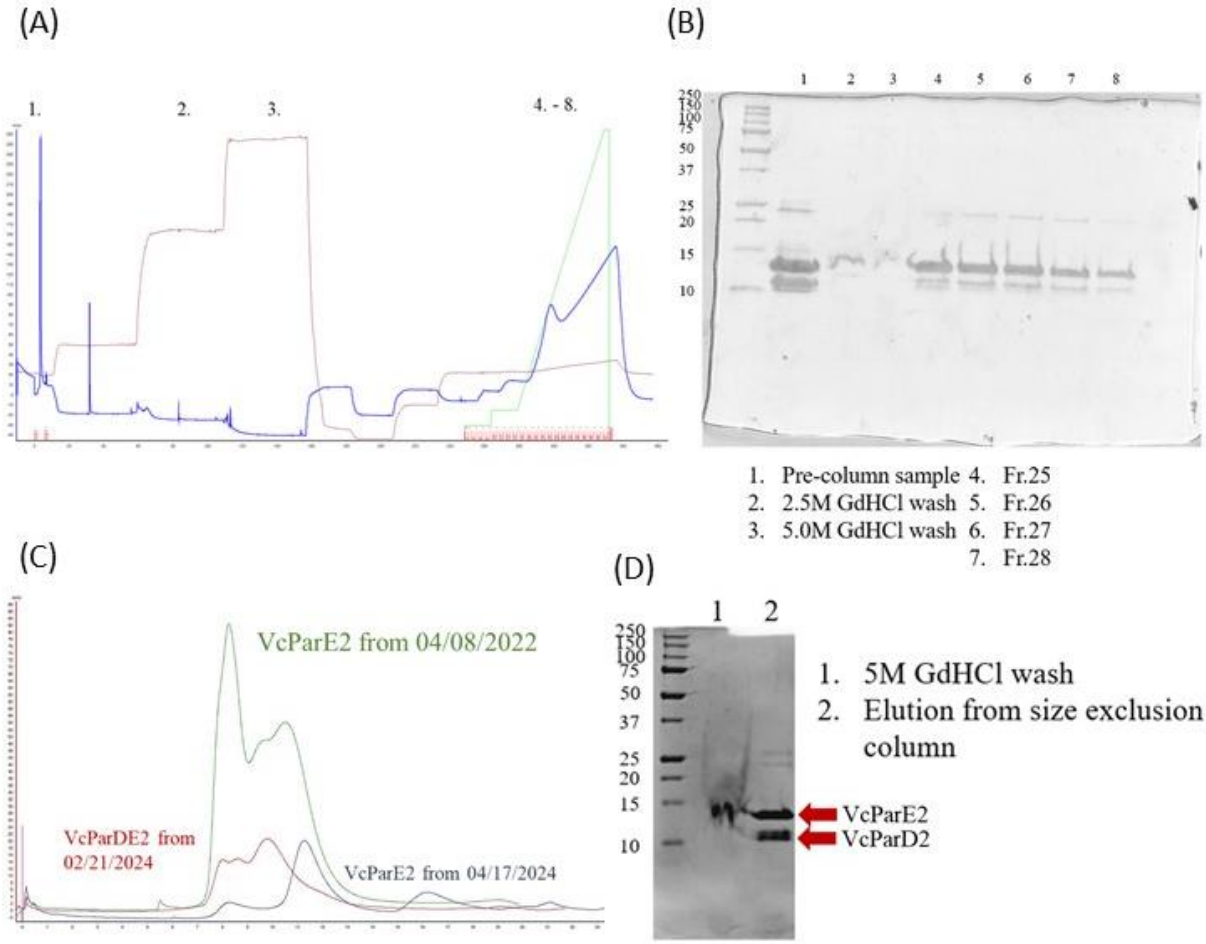

Figure 3.5. On-column denaturation-refolding using GdHCl to unfold VcParDE2. (A)The nickel affinity chromatogram of the on-column denaturation (B) protein gel representing the protein species in each step indicated in (A). (C) Superposition of the size exclusion chromatogram of refolded proteins from each attempt. (D)The protein gel showing the final refolded protein using the on-column denaturation-refolding by GdHCl

Generating ParE toxins using *in vitro* protein synthesis produced insufficient amount of proteins for further analysis.

Because ParE toxins exert potent toxicity to *E. coli* cells, we then considered using *in vitro* protein synthesis to produce ParE proteins without expressing in cells. To monitor the efficiency of protein synthesis, the plasmid containing GFP sequence was also included, and the green fluorescence was detected as the function of protein production. The signal of the green fluorescence reached to the plateau at 150min, indicating the entire synthesis should be completed. (Figure 6A) The reaction samples were subsequently collected and assessed by electrophoresis. Because there were other proteins involved in the synthesis, such as ribosomal proteins, it is indistinguishable to identify proteins of interest. (Figure 6B)

Since the ribosomal proteins in the synthesis kit also contain a His-tag, their separation was carried out using heparin resins, with samples collected at each step. As Figure 6C showed, most proteins, including ribosomal proteins, did not bind to the heparin resins. Additionally, the limited yield of target proteins from the synthesis made them difficult to identify on the gel. Taken together, while *in vitro* protein synthesis is capable of producing proteins, evidenced by the detection of green fluorescence from GFP, the overall protein yield was insufficient for further analysis.

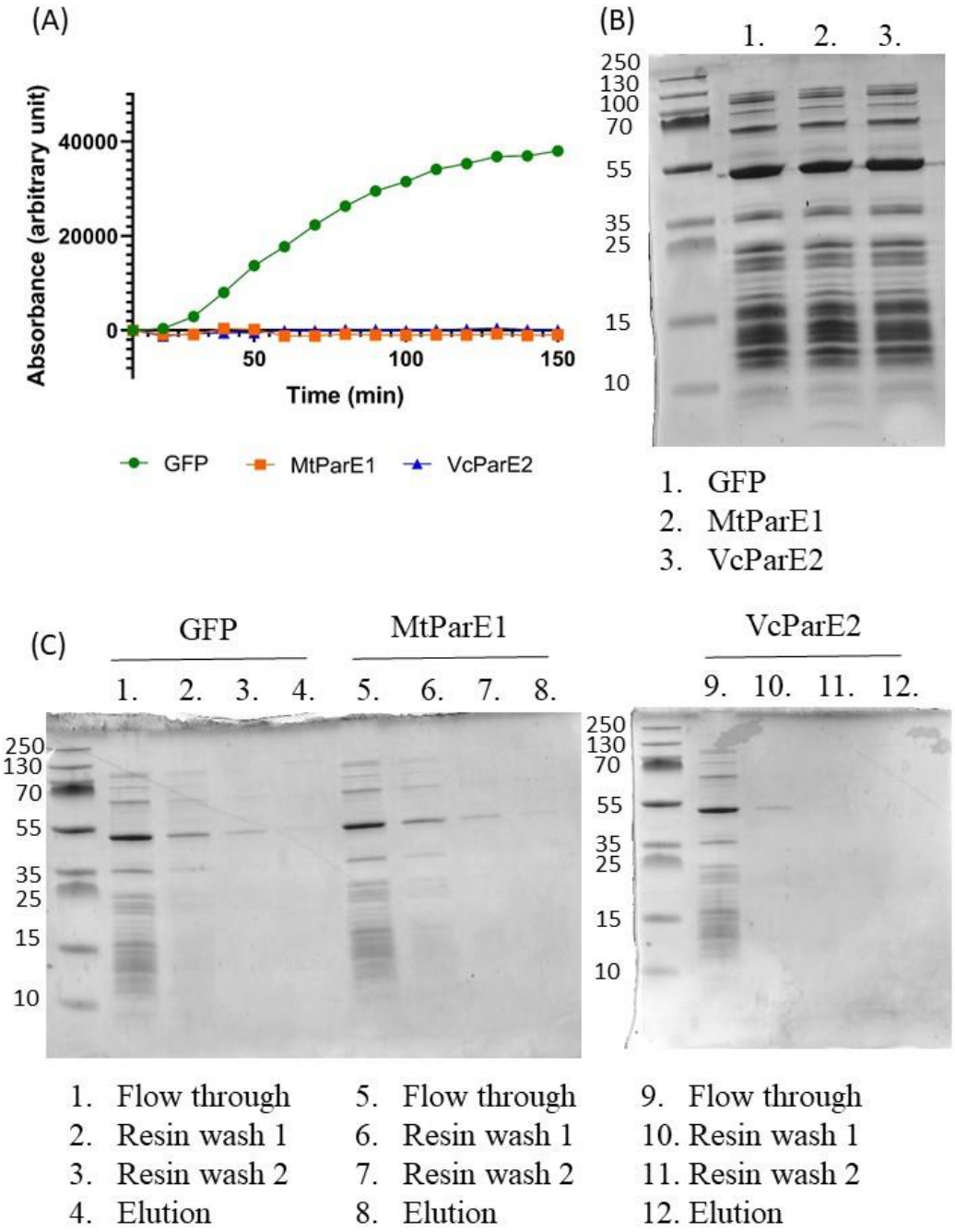

Figure 3.6. Producing ParE toxins using in vitro protein synthesis. (A) Monitor the Absorbance of green fluorescence over 150 min interval. The excitation is 485nm and emission is 528nm. (B) Samples after the reaction were collected and checked on a 15% tris tricine gel. (C) Samples were collected during each step of heparin resin purification and were checked on a 15% tris tricine gel.

Addition of a GST fusion protein to the N-terminus of VcParE2 mitigates toxicity, but cleavage of GST also results in a cleavage site in VcParE2.

Because the size of GST (approx. 28kDa) is larger than VcParE2 (approx. 12kDa), implying GST might be able to physically block VcParE2 action, including a GST tag is one of the strategies to overcome the toxicity of VcParE2. Our result indicated that *E. coli* BL21(DE3) cell is not impacted by toxicity associated with VcParE2. The purification of GST-VcParE2 utilized nickel affinity and size exclusion chromatography, and purity was assessed before linker cleavage. (Figure 3.7B) To cleave the linker between GST and VcParE2, the purified GST-VcParE2 was incubated with PreScission protease at 4°C overnight (16-18h). The protein gel indicated a successful cleavage with two protein bands shown on the gel. (Figure 7C) However, the size of VcParE2 on the protein gel was slightly smaller than the expected 12kDa.

The cleaved protein was first separated via nickel affinity column because only GST contained 6x His-tag. However, even though VcParE2 did not have a His-tag, it still remained bound to the nickel column and eluted with GST. (Figure 3.8A, B) We then tried to separate VcParE2 from GST using GSTrap column, in which VcParE2 would be collected in the flow through while GST remained bound in the column. The protein gel showed that VcParE2 was successfully washed from the GSTrap column even though some of the GST was also in the flow through. Pure VcParE2 was able to be obtained by size exclusion chromatography. (Figure 8C - F)

To examine the inhibitory effect of VcParE2 against DNA gyrase, the supercoiling activity assay was performed. As Figure 7G shows, incubating up to 4μM VcParE2 with 5nM gyrase produced no inhibition, and the supercoiled topology of DNA was still formed, suggesting that this truncated form of VcParE2 is not active as a gyrase inhibitor.

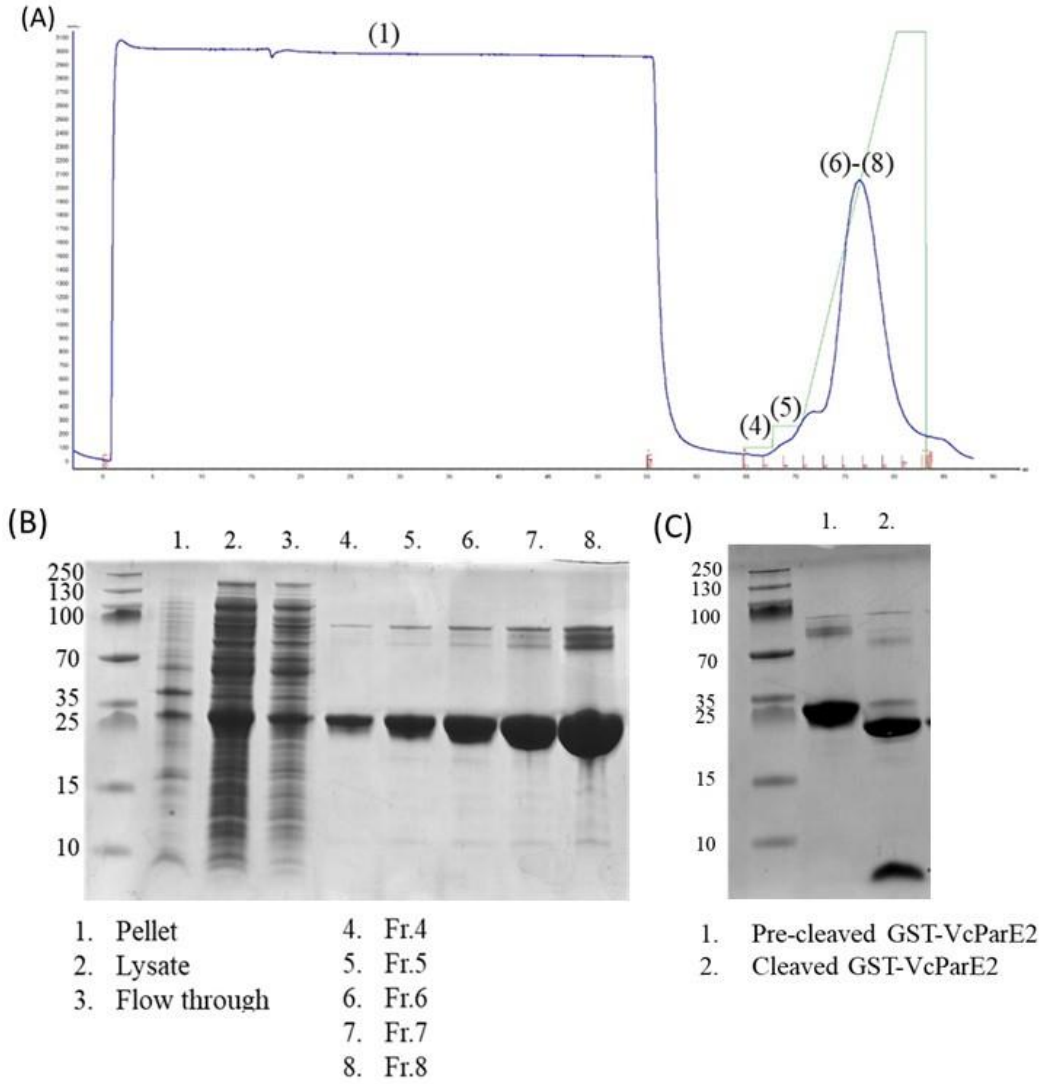

Figure 3.7. Purification of GST-VcParE2 proteins and cleavage via PreScission protease. (A) The nickel affinity chromatogram of GST-VcParE2 and (B) samples in the corresponding steps was shown on the 12% tris-glycine gel. (C) The 12% tris-tricine gel showed the cleavage of GST-VcParE2 after incubation with PreScission protease.

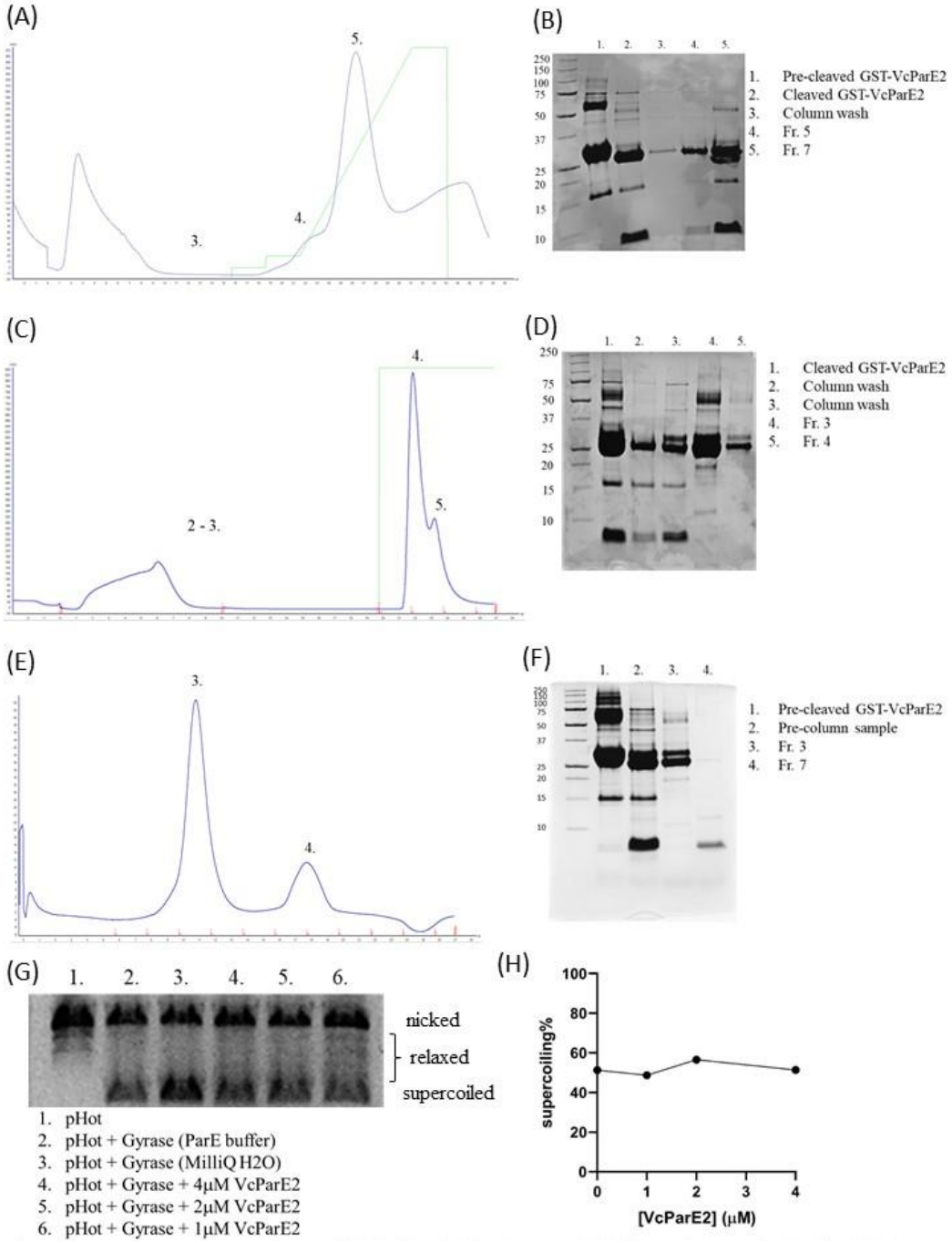

Figure 3.8. Separation of VcParE2 from GST using nickel affinity and GSTrap column. (A) Nickel affinity chromatogram of cleaved VcParE2 and GST and (B) the corresponding species in each step was collected and ran on a 12% tris-tricine gel. (C) GSTrap chromatogram of separating VcParE2 and GST and (D) the corresponding species in each step was collected and ran on a 12% tris-tricine gel. (E) Size exclusion chromatogram of separating VcParE2 and GST. and (F) the corresponding species in each step was collected and ran on a 12% tris-tricine gel. (G) Truncated VcParE2 at concentration of 1, 2, and 4mM, was incubated with 5nM gyrase during a test for supercoiling activity and (H) plot the quantification of supercoiled DNA as a function of VcParE2 concentration

Co-expression of VcParE1 and a DNA Gyrase B+A chain fusion blocks toxicity and purified VcParE1 inhibits gyrase supercoiling.

The concept of covering the toxicity of the ParE protein by larger proteins to allow overexpression seemed promising. As an alternative approach, we sought to express excess gyrase with a Strep-tagged construct encoding-VcParE1. While the culture did experience certain effects of toxicity, a limited amount of VcParE1 could be captured. The purification of VcParE1 started with an affinity step on a Strep-Trap column (Figure 3.9A and C). The eluted sample was collected and subjected to size exclusion chromatography. As Figure 3.9B and D indicated, even though there appears to be degradation of the sample, evident as species below 10kDa, some purified VcParE1 was still acquired and confirmed by western blot. The yield of purified VcParE1 is approx. 0.5mg per 1L culture.

The purified VcParE1was subsequently assessed if it could stabilize gyrase-mediated cleavage complex to inhibit the formation of supercoiled DNA. Incubation of *E. coli* gyrase with VcParE1 in the presence of relaxed pHot plasmids inhibited gyrase supercoiling ability. (Figure 3.9E) As the concentration of VcParE1 increased, the intensity of the band representing supercoiled DNA diminished and became smeared, demonstrating that the purified VcParE1 is active and capable of inhibiting gyrase activity.

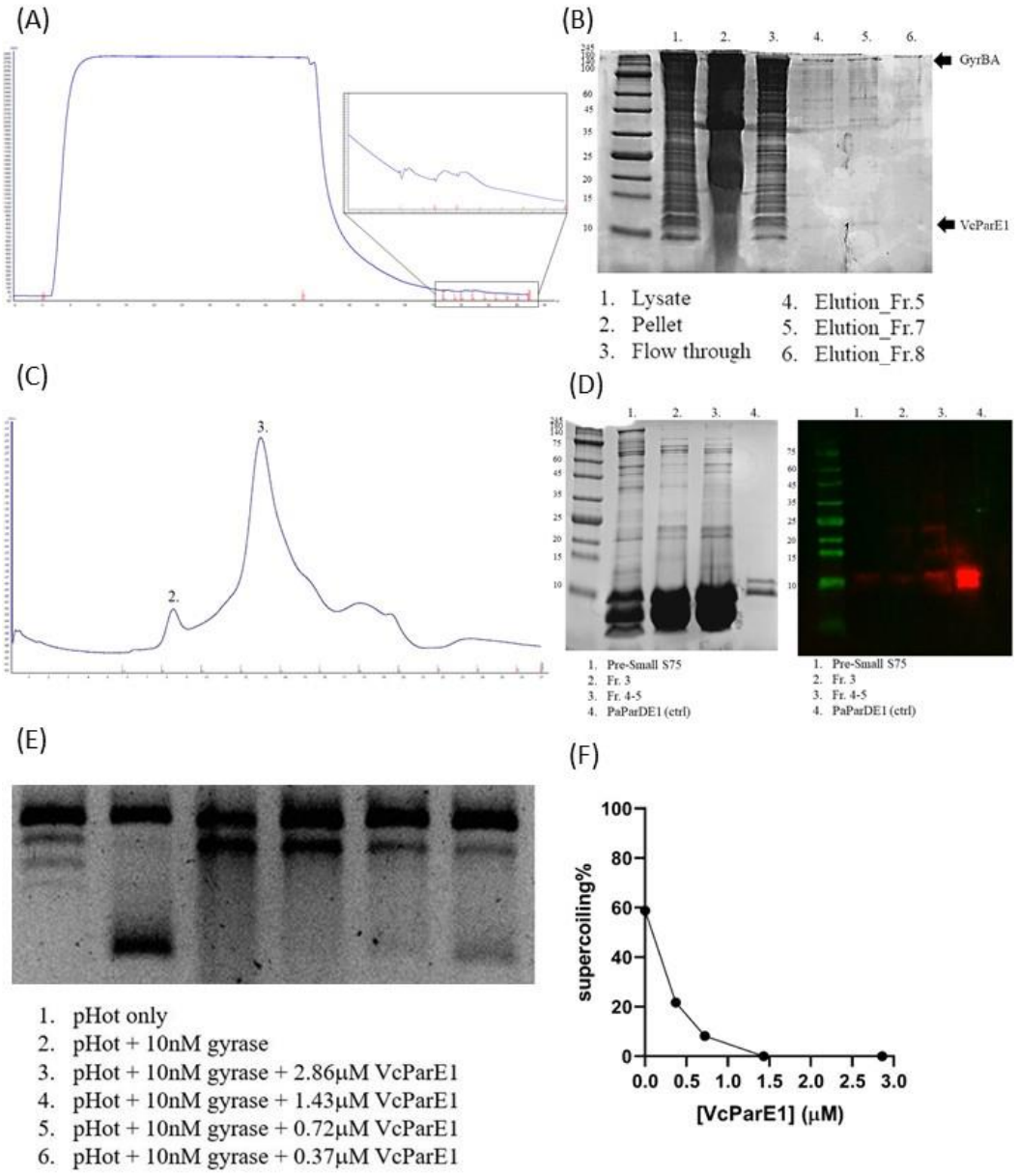

Figure 3.9. Purification of VcParE1 through StrepTrap column and size exclusion chromatography. (A) The StrepTrap chromatogram of purifying VcParE1 and (B) samples in the corresponding steps was shown on the 15% tris-tricine gel. (C) Size exclusion chromatogram of purified VcParE1 and (D) samples indicated in the corresponding peaks was shown on a 15% tris-tricine gel visualized via coomassie staining and western blot. (E) VcParE1 at concentrations of 0.37mM, 0.72mM, 1.43mM and 2.86mM were incubated with gyrase; it is evident that as the concentration increases, supercoiled DNA was no longer formed. (F) plot of the quantification of supercoiled DNA as a function of VcParE1 concentration

Discussion

The ParE toxin family has been shown to target DNA gyrase with a different mechanism to other known inhibitors, including quinolone antibiotics and CcdB toxin, indicating the significant research value for investigating the interaction between ParE and DNA gyrase.[16] However, acquisition of purified ParE proteins, especially those that exert high toxicity, via an *E. coli* expression system is challenging. My work sought to develop an optimal protocol to produce purified ParE protein samples for further biochemical and biophysical studies. The denaturation-refolding method has been proven for several toxin proteins, including bacteriophage P1 Doc toxin from the Phd-Doc system, *E. coli* MazF toxin from the MazEF system, *V. cholerae* HigB2 toxin from the HigAB2 system, and *E. coli* ParE2 toxin from the PaaA2-ParE2 system.[39] VcParE2 has also been reported as purified via this method[4]; however, we encountered several issues during the purification of VcParE2 using this method and were not successful in generating purified sample.

First, successfully removing the majority of VcParD2 from VcParE2 is challenging. The VcParDE2 complex has been shown to contain an equilibrium between $VcParD2_6$-$VcParE2_2$ hexadecamer, where additional VcParD2 (auxiliary VcParD2) bind to the VcParDE2 complex, (primary VcParD2) and $VcParD2_2$-$VcParE2_2$ tetramer.[38] Even though denaturation was able to liberate VcParD2 antitoxin in the flow through, there was still VcParD2 associated with VcParE2 toxin, suggesting that denaturation may have only disrupted the binding between the primary VcParD2 and the auxiliary VcParD2 but not the binding between VcParD2 and VcParE2. To fully dissociate VcParD2 from VcParE2, slowing down the flow rate and extending the denaturation process is a feasible direction for future testing.

A second challenge was encountered with incomplete protein refolding that caused aggregation of VcParE2. Removing denaturants from the denatured protein is a critical step for refolding the protein back to its native state.[40] Our result showed that removal of denaturants directly from a high to a low concentration from denatured VcParE2 leads to protein aggregation. However, gradually decreasing the concentration of the denaturant reduced aggregation, but could not completely prevent aggregation. Surprisingly, Sterckx et al., showed that their on-column refolding procedure that proceeded through the direct removal of the denaturant on-column was able to obtain active, refolded toxin proteins.[39] Additionally, Girardin et al., also presented the feasibility to obtain an active VcParE2 via on-column refolding through directly removing the denaturant without decreasing the denaturant concentration using a gradient.[4] Those results imply there must be a critical concentration for loading onto the affinity column, and if the concentration exceeds this, as was likely the case in our experiments, aggregation likely occurs as denaturant is removed.

A final challenge is that the protein yield via the denaturation-refolding method did not produce sufficient quantities of protein for further biochemical/biophysical analysis. In our study, while 10mg of VcParDE2 was obtained from 4L culture grown in a Terrific Broth media, only 0.09mg of refolded VcParE2 was acquired after the denaturation-refolding process. Girardin et al., states that 0.5mg of VcParE2 was obtained per liter of culture using this denaturation-refolding method.[4] Alternatively, they also overexpressed VcParE2 in *Spodoptera frugiperda* (Sf9) insect cells, which lack the VcParE2 target, DNA gyrase. The yield of expression in Sf9 cells produces up to 2.4mg of VcParE2 per liter of culture.[4] This might be an indication that overexpression of ParE toxin proteins in the expression systems other than *E. coli* is a practical way to obtain sufficient amounts of purified proteins for future biochemical and biophysical studies.

Expression of VcParE2 with a bulky fusion protein, such as GST tag, was another strategy to overcome toxicity to the host *E. coli* expression system. The concept of sterically blocking ParE toxicity via a large GST was first used in the expression of the highly toxic ParE toxin from the plasmid RK2.[41] Using a similar strategy, a GST-VcParE2 fusion protein could be purified. However, the size of GST-VcParE2 was smaller than expected. Following cleavage with PreScission protease and separation from GST, VcParE2 was smaller than expected and failed to inhibit gyrase activity, suggesting that the truncated form of VcParE2 is not active as a gyrase inhibitor.

Consistent with the concept of neutralizing ParE toxicity with large proteins to enable overexpression in *E. coli* cells, an alternative strategy involves co - transformation of two plasmids, one encoding a Gyrase B chain fused to the A fusion at the gene level, and the other encoding VcParE1, into the expression cells. This partially masked VcParE1 toxicity, allowing modest expression in *E. coli* cells. The activity of purified VcParE1 was confirmed by the inhibition of gyrase-mediated supercoiling activity, and preliminary results suggest the VcParE1 - Gyrase complex can be directly isolated from the supercoiling activity assay.

In conclusion, obtaining purified, active ParE protein through *E. coli* expression systems is challenging due to the toxicity against bacterial cells. The denaturation-refolding method, which has been shown to be effective to purify other toxin proteins as well as two ParE toxins, still encounters limitations. Alternatively, our study presents another strategy by co-transformation of the ParE toxin with its target, i.e., gyrase, as an effective way to express ParE toxin in *E. coli* and produce sufficient quantities of active, purified ParE. The ParE-gyrase complex is also potentially able to be isolated from the supercoiling assay. Future direction will be scaling up the quantity of the assay to obtain sufficient ParE-gyrase complex for structural analysis via cryo-EM.

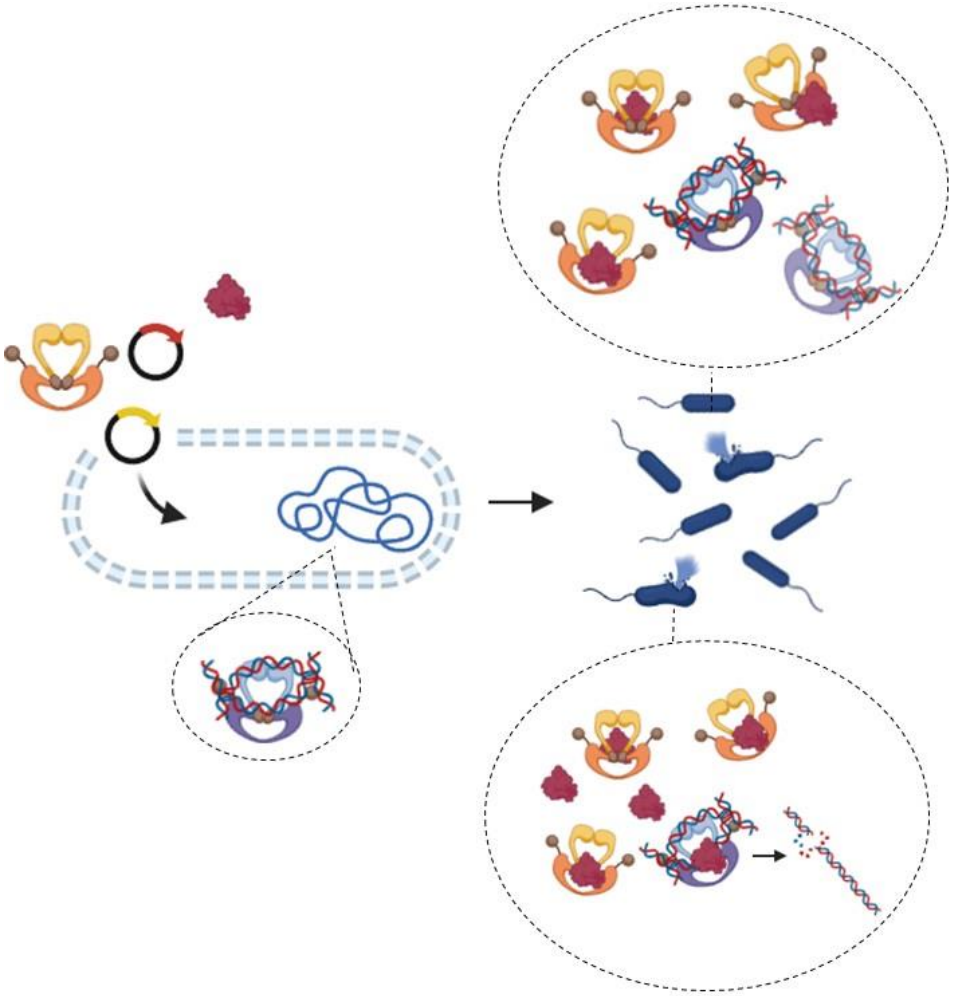

Figure 3.10. Co-expression of gyrase B+A chain fusion with VcParE1 toxin mitigates the toxic effect. The VcParE1 toxicity can be blocked by the co-expressed gyrase B+A chain fusion. However, cells still experience certain toxic effects due to the leaking of VcParE1 from the gyrase B+A chain fusion or excessive expression of VcParE1 than that of gyrase B+A fusion. Nonethess, utilization of this method is still able to obtain enough amount of cell pellet and acquire sufficient amount of purified VcParE1 protein.

Data Availability

All data are included in this manuscript and supplement document; DNA clones for constructs made in this work are available upon request

Author Contributions

C.H.T. collected all data reported in this manuscript; C.H.T. and C.R.B. participated in the project design, data processing, manuscript drafting, and editing.

Acknowledgements

We appreciate the assistance from the OU Protein Production and Characterization Core facility for assisting with protein purification and access for the equipments. The OU Protein Production and Characterization Core facility is supported by Institutional Development

Awards from the National Institute of General Medical Sciences of the National Institutes of Health Grants P20GM103640 and P30GM145423, the OU Vice President for Research and Partnerships, and the OU College of Arts and Sciences)

Reference

1. Jurėnas, D., et al., *Biology and evolution of bacterial toxin-antitoxin systems.* Nat Rev Microbiol, 2022. **20**(6): p. 335-350.
2. Pandey, D.P. and K. Gerdes, *Toxin-antitoxin loci are highly abundant in free-living but lost from host-associated prokaryotes.* Nucleic Acids Res, 2005. **33**(3): p. 966-76.
3. Makarova, K.S., Y.I. Wolf, and E.V. Koonin, *Comprehensive comparative-genomic analysis of type 2 toxin-antitoxin systems and related mobile stress response systems in prokaryotes.* Biol Direct, 2009. **4**: p. 19.
4. Girardin, Y., et al., *Evaluation of different strategies to produce Vibrio cholerae ParE2 toxin.* Protein Expr Purif, 2024. **215**: p. 106403.
5. Roberts, R.C. and D.R. Helinski, *Definition of a minimal plasmid stabilization system from the broad-host-range plasmid RK2.* Journal of Bacteriology, 1992. **174**(24): p. 8119-8132.
6. Fraikin, N., F. Goormaghtigh, and L. Van Melderen, *Type II Toxin-Antitoxin Systems: Evolution and Revolutions.* J Bacteriol, 2020. **202**(7).
7. Yuan, J., Y. Yamaichi, and M.K. Waldor, *The three vibrio cholerae chromosome II-encoded ParE toxins degrade chromosome I following loss of chromosome II.* J Bacteriol, 2011. **193**(3): p. 611-9.
8. Guglielmini, J. and L. Van Melderen, *Bacterial toxin-antitoxin systems: Translation inhibitors everywhere.* Mob Genet Elements, 2011. **1**(4): p. 283-290.
9. Ames, J.R., et al., *Expression of different ParE toxins results in conserved phenotypes with distinguishable classes of toxicity.* Microbiologyopen, 2019. **8**(10): p. e902.
10. Aakre, C.D., et al., *Evolving new protein-protein interaction specificity through promiscuous intermediates.* Cell, 2015. **163**(3): p. 594-606.
11. Sterckx, Y.G., et al., *A unique hetero-hexadecameric architecture displayed by the Escherichia coli O157 PaaA2-ParE2 antitoxin-toxin complex.* J Mol Biol, 2016. **428**(8): p. 1589-603.
12. Fiebig, A., et al., *Interaction specificity, toxicity and regulation of a paralogous set of ParE/RelE-family toxin-antitoxin systems.* Mol Microbiol, 2010. **77**(1): p. 236-51.
13. Dubiel, A., et al., *ClpAP protease is a universal factor that activates the parDE toxin-antitoxin system from a broad host range RK2 plasmid.* Sci Rep, 2018. **8**(1): p. 15287.
14. Brzozowska, I. and U. Zielenkiewicz, *Regulation of toxin-antitoxin systems by proteolysis.* Plasmid, 2013. **70**(1): p. 33-41.
15. Jiang, Y., et al., *ParE toxin encoded by the broad-host-range plasmid RK2 is an inhibitor of Escherichia coli gyrase.* Mol Microbiol, 2002. **44**(4): p. 971-9.
16. Yuan, J., et al., *Vibrio cholerae ParE2 poisons DNA gyrase via a mechanism distinct from other gyrase inhibitors.* J Biol Chem, 2010. **285**(51): p. 40397-408.
17. Gupta, M., et al., *The Chromosomal parDE2 Toxin-Antitoxin System of Mycobacterium tuberculosis H37Rv: Genetic and Functional Characterization.* Front Microbiol, 2016. **7**: p. 886.
18. Vanden Broeck, A., et al., *Cryo-EM structure of the complete E. coli DNA gyrase nucleoprotein complex.* Nat Commun, 2019. **10**(1): p. 4935.
19. Michalczyk, E., et al., *Molecular mechanism of topoisomerase poisoning by the peptide antibiotic albicidin.* Nat Catal, 2023. **6**(1): p. 52-67.

20. Ruan, S., C.H. Tu, and C.R. Bourne, *Friend or Foe: Protein Inhibitors of DNA Gyrase.* Biology (Basel), 2024. **13**(2).
21. Bielińska, A. and D. Hulanicka, *Effect of DNA gyrase inhibitors and urea on the expression of cysB, the regulatory gene of the cysteine regulon.* J Gen Microbiol, 1986. **132**(9): p. 2571-6.
22. Briffotaux, J., S. Liu, and B. Gicquel, *Genome-Wide Transcriptional Responses of Mycobacterium to Antibiotics.* Front Microbiol, 2019. **10**: p. 249.
23. Jacoby, G.A., *Mechanisms of resistance to quinolones.* Clin Infect Dis, 2005. **41 Suppl 2**: p. S120-6.
24. Aldred, K.J., R.J. Kerns, and N. Osheroff, *Mechanism of quinolone action and resistance.* Biochemistry, 2014. **53**(10): p. 1565-74.
25. Chan, P.F., et al., *Thiophene antibacterials that allosterically stabilize DNA-cleavage complexes with DNA gyrase.* Proc Natl Acad Sci U S A, 2017. **114**(22): p. E4492-e4500.
26. Morgan, H., et al., *A 2.8 Å Structure of Zoliflodacin in a DNA Cleavage Complex with Staphylococcus aureus DNA Gyrase.* Int J Mol Sci, 2023. **24**(2).
27. Nicholls, R.A., et al., *How Do Gepotidacin and Zoliflodacin Stabilize DNA-Cleavage Complexes with Bacterial Type IIA Topoisomerases? 2. A Single Moving Metal Mechanism.* Int J Mol Sci, 2024. **26**(1).
28. Gibson, E.G., et al., *Mechanistic and Structural Basis for the Actions of the Antibacterial Gepotidacin against Staphylococcus aureus Gyrase.* ACS Infect Dis, 2019. **5**(4): p. 570-581.
29. Collin, F. and A. Maxwell, *The Microbial Toxin Microcin B17: Prospects for the Development of New Antibacterial Agents.* J Mol Biol, 2019. **431**(18): p. 3400-3426.
30. Dao-Thi, M.H., et al., *Molecular basis of gyrase poisoning by the addiction toxin CcdB.* J Mol Biol, 2005. **348**(5): p. 1091-102.
31. Chatterji, M. and V. Nagaraja, *GyrI: a counter-defensive strategy against proteinaceous inhibitors of DNA gyrase.* EMBO Rep, 2002. **3**(3): p. 261-7.
32. Jacoby, G.A., M.A. Corcoran, and D.C. Hooper, *Protective effect of Qnr on agents other than quinolones that target DNA gyrase.* Antimicrob Agents Chemother, 2015. **59**(11): p. 6689-95.
33. Jensen, R.B., et al., *Comparison of ccd of F, parDE of RP4, and parD of R1 using a novel conditional replication control system of plasmid R1.* Mol Microbiol, 1995. **17**(2): p. 211-20.
34. Roberts, R.C., A.R. Ström, and D.R. Helinski, *The parDE operon of the broad-host-range plasmid RK2 specifies growth inhibition associated with plasmid loss.* J Mol Biol, 1994. **237**(1): p. 35-51.
35. Sobecky, P.A., et al., *Characterization of the stable maintenance properties of the par region of broad-host-range plasmid RK2.* J Bacteriol, 1996. **178**(7): p. 2086-93.
36. Muthuramalingam, M., et al., *The toxin from a ParDE toxin-antitoxin system found in Pseudomonas aeruginosa offers protection to cells challenged with anti-gyrase antibiotics.* Mol Microbiol, 2019. **111**(2): p. 441-454.
37. Gupta, N., et al., *Genomic profiling and molecular dynamics analysis of parDE(Pa) toxin-antitoxin homologs targeting DNA gyrase in Pseudomonas aeruginosa: insights from computational investigations.* J Biomol Struct Dyn, 2025: p. 1-17.
38. Garcia-Rodriguez, G., et al., *Toxin:antitoxin ratio sensing autoregulation of the Vibrio cholerae parDE2 module.* Sci Adv, 2024. **10**(1): p. eadj2403.
39. Sterckx, Y.G., et al., *An efficient method for the purification of proteins from four distinct toxin-antitoxin modules.* Protein Expr Purif, 2015. **108**: p. 30-40.
40. Yamaguchi, H. and M. Miyazaki, *Refolding techniques for recovering biologically*

active recombinant proteins from inclusion bodies. Biomolecules, 2014. **4**(1): p. 235-51.
41. Johnson, E.P., A.R. Strom, and D.R. Helinski, *Plasmid RK2 toxin protein ParE: purification and interaction with the ParD antitoxin protein.* J Bacteriol, 1996. **178**(5): p. 1420-9.

Chapter IV: Investigation of the intrinsic instability of ParD1 antitoxin from *Pseudomonas aeruginosa*

Chih-Han Tu, Christina R. Bourne

Department of Chemistry and Biochemistry, University of Oklahoma, Norman OK USA

This chapter represents unpublished data collected in the Bourne lab.

I collected and processed all of the data, figures with the exception of the mass spectrometry (Figure 4.6) which was performed by Dr. Cynthia Nagy. All figures were produced by myself. Writing of the manuscript was performed by myself with assistance from Dr. Christina Bourne. Editing and feedback on all writing was provided by Dr. Christina Bourne.

Introduction

Toxin-antitoxin (TA) systems can be found in low-copy number plasmids and in the chromosomes of prokaryotes. Canonically, TA systems function in a process called postsegregational killing (PSK) to promote the retention of TA-encoded plasmids in daughter cells during replication.[1, 2] TA systems have also been captured in chromosomes, including in prophages, but any roles for these in normal cell growth or stress responses are still under debate. Some proposed functions include regulating cell growth or inducing cell death during nutrient starvation (e.g., stringent response[3-5], phage defense[6, 7], anti-addiction to protect from retention of other TA-encoded plasmids[8, 9], as well as various roles in pathogenesis.[10] The activation of TA systems resulting in release of the toxin component is based on differential stability of toxins and antitoxins. Toxins typically form stable structures, while antitoxins are relatively unstable, either from an intrinsic characteristic or from targeting by the AAA+ proteases.[11, 12] As the antitoxin level decreases below that of the toxin, an increasing amount of "freed" toxins results, and the TA system begins to impact cell growth. Type II ParDE TA systems contain bicistronic operons that encode ParD antitoxin proteins and ParE toxin proteins. Recent bioinformatics studies highlight the prevalence of ParDE TA systems, with more than 4000 ParDE loci identified within prokaryotic genomes.[13] As noted in earlier chapters, the ParE toxin inhibits DNA gyrase by stabilizing the gyrase-mediated DNA cleavage complex, resulting in persistence of a double strand DNA break. Upon binding to the cognate ParD antitoxin, the ParE toxic effect can be neutralized, forming the ParDE complex.

The structure of ParD antitoxins is composed of an N-terminal ribbon-helix-helix (RHH) DNA binding domain and a C-terminal ParE binding domain. The RHH structure is highly conserved in the ParD antitoxin family, and engages in the formation of ParD dimers and, in some instances, higher order multimers as well as the autoregulation of their own TA operon. The ParDE complex typically forms a 2:2 stoichiometry via dimerization of the ParD antitoxin through the RHH domain.[14-16] However, recent studies have highlighted that some ParDE complexes exhibit different stoichiometry. The ParDE2 complex from *Vibrio cholerae* is capable of forming a $ParD2_6$-$ParE2_2$ hetero-octamer and a $ParD2_2$-$ParE2_2$ hetero-tetramer.[17] The $ParD2_6$-$ParE2_2$ hetero-octamer exhibits the most potent self-repression of its promoter, whereas the ParD2 homodimer has only weak repression. Conversely, the $ParD2_2$-$ParE2_2$ hetero-tetramer has a de-repression effect on this ParDE2's expression.[17] Similarly, the ParDE1 complex from *Mycobacterium tuberculosis* exhibits a dynamic equilibrium between a $ParD1_4$-$ParE1_2$ hetero-hexamer and a $ParD1_2$-$ParE1_2$ hetero-tetramer, and the switch between these different stoichiometries induces the release of ParE1.[18]

Unlike the conserved N-terminal RHH domain, the structure of C-terminal domain is typically disordered until specific interactions with the co-encoded cognate ParE toxin. This disorder in the absence of the ParE toxin is suggested to make ParD more easily targeted by the proteases.[19-21] Our previous study identified that the I68 residue in the C-terminal domain of ParD1 from *Pseudomonas aeruginosa* (PaParD1) played a vital role in altering the structure from disorder to order transition when binding to the cognate PaParE1 toxin.[14]

Aside from *in vivo* proteolytic loss, ParD antitoxins have also been noted to possess an apparent inherent instability. Oberer et al., noted that the ParD antitoxin encoded on the RK2 broad-host range plasmid underwent *in vitro* degradation when stored at either 4°C or ambient temperature. The resulting fragments were shown to be specific peptides, implying there might be mechanistic explanation for this ParD "intrinsic" degradation.[22] Our previous result also detected degraded fragments from PaParD1 that were identified by Direct-infusion mass spectrometry (DIMS).[23] This study revealed that the point of breakage is specific to a glutamine-rich region in the α-helix 2, which bridges the RHH and ParE-toxin interaction regions,[23] suggesting that glutamine residues were potentially of importance to the process of intrinsic cleavage.

The role of glutamine side chains is reminiscent of the intrinsic cleavage observed in some inteins.[24-26] These protein-excising domains exist in many proteins, where they cleave themselves out from the host protein and ligate the remaining portions, (N-extein and C-extein) to form a new peptide bond.[26, 27] In addition, a long-lived human lens protein also undergoes spontaneous cleavage via a glutamine-mediated mechanism.[24] Therefore, multiple examples highlight glutamine side chains as mediating "self-cleavage" within a protein.[24, 26]

Mechanistically, it is proposed that the nitrogen atom on the side chain amide of a glutamine residue attacks the carbonyl group of the peptide backbone, resulting in the cleavage of the peptide bond and formation of a glutarimide ring. After hydrolysis, a C-terminal glutamine is generated.[24] In addition, such a glutamine residue is proposed to potentially also undergo a deamidation reaction as well as crosslinking in an intermediate.[28] The nitrogen atom of the peptide backbone attacking the carbonyl group of the glutamine side chain leads to the formation of a glutarimide intermediate.[28] The resolution of such a glutarimide ring intermediate is suggested to be via opening through hydrolysis, leading to the formation of C-terminal glutamic acid or iso-glutamic acid, or by attack from a nitrogen atom from a lysine side chain or the amide group of another peptide, leading to protein-protein crosslinking.[28]

In this study, we sought to follow-up earlier studies on the degradation of PaParD1 with a goal of deducing a molecular mechanism for this instability. We establish that the kinetics of PaParD1 loss is affected both by temperature and pH value, with maximal degradation observed at physiological pH and temperature. Additionally, we found that higher concentrations of PaParD1 correlate with increased kinetics of the degradation rate. Interestingly, we established that ionic strength affects PaParD1 dimerization and degradation, such that the degradation rate increases as monomeric PaParD1 increases. However, mutation of glutamine amino acids failed to impact degradation, suggesting that the proposed intein-like mechanism may not be applicable to this system. Lastly, a 20-25kDa species observed during PaParD1 degradation was identified as degraded fragments of the molecular chaperone DnaK, suggesting it is a pervasive co-purifying contaminant and that its fragmentation coincides with that of PaParD1 through an unknown mechanism, suggesting that the intrinsic instability is somehow coupled with co-purifying chaperone.

Method

Construction of Recombinant Plasmid and transformation

A pET-15b vector encoded PaParD1 gene is already available from our lab inventory. The Site-directed mutant PaParD1 were generated via a Q5 mutagenesis kits (NEB) using primers listed in Table S1. Verification of the resulting constructs was done by DNA sequencing. Transformation of pET-15b vector encoding the desired PaParD1 gene into *Escherichia coli* (*E. coli*) BL21 DE3 competent cells was conducted following a standard heat shock protocol. The resulting strains were stored as glycerol stocks at -80°C and fresh inoculations from these stocks were used in all experiments.

Expression and purification of ParD1 antitoxin from *Pseudomonas aeruginosa*

To induce the expression of PaParD1, *E. coli* BL21 DE3 pLys competent cells (NEB) containing the pET15b::*PaparD1* plasmid were grown at 37°C shaking at 200rpm. LB broth supplemented with 100μg/mL carbenicillin was used as the growth media for the overnight liquid cultures (16-18hrs). The resulting dense cultures were then diluted at a 1:20 ratio into LB broth or 2x YT media with 100 μg/mL carbenicillin and grown aerobically at 37°C. When the optical density at 600nm reached 0.6 – 0.8, protein expression was induced by adding 1.0mM IPTG to the culture with 5hrs incubation at 25°C, 180rpm shaking.

Cells were harvested and resuspended in "buffer A" (50mM Tris pH8.0, 300mM NaCl, 25mM imidazole). Cell lysis was conducted using an Emulsiflex-C3 homogenizer (Avestin Inc). After centrifugation at 16,000 x g at 4°C for 40min, the supernatant was passed over a 1mL HisTrap FF nickel Sepharose column (GE Healthcare) equilibrated with buffer A. After the column was washed with the same buffer, the ParD1 protein was eluted from the column by a step gradient of 5% and 10% "buffer B", followed by a gradient elution from 10% to 100% of buffer B (50mM Tris pH8.0, 300mM NaCl, 500mM imidazole). The eluted ParD1 was concentrated to the required volume and loaded to a HiLoad 16/60 Superdex 75 pg column (GE Healthcare) equilibrated in "buffer C" (10mM Hepes pH7.5; 150mM NaCl). The purity of ParD1 was monitored by electrophoresis through Tris-Tricine acrylamide gels.

In vitro degradation assay

The purified PaParD1 proteins were incubated at either 4°C or 37°C. To monitor the degradation, PaParD1 aliquots were collected at the designated time points by taking 18μL from the overall sample, and mixing with 6μL of reducing SDS loading dye (62.5mM Tris-HCl, pH6.8, 2.5% SDS, 5% beta-mercaptoethanol, and 10% glycerol). As a series from all times points were collected, samples were heated at 95°C for 5mins and loaded onto 15% acrylamide gels with a tris-tricine buffer system (Cathode buffer: 0.1M Tris pH8.5, 0.1M Tricine, 0.1% SDS. Anode buffer:0.2M Tris, pH8.5). The protein bands were separated by electrophoresis by running at 150V for 50min and visualized via Coomassie blue staining. ImageJ was used to estimate relative band intensities. The degradation percentage was determined by the ratio between the intact ParD1 band and the degradation band in each lane.

Native gel electrophoresis

The purified PaParD1 samples in different buffer conditions were collected by taking 18μL from the overall sample and mixing with 6μL of the sample buffer (100mM Tris-HCl, pH8.6, 10% glycerol and 0.1% bromophenol blue). The mixtures were subsequently loaded onto a 6% native gel with the running buffer containing 45mM Tris pH8.3, and 192mM glycine. Electrophoresis was carried out on ice to separate protein bands by running at 100V for 3h.

The bands were visualized by staining with Coomassie blue.

Passively Elution Proteins from Polyacrylamide Gel as Intact species (PEPPI)
Sample lanes of the stained tris-tricine acrylamide gels were sliced by a craft knife at the regions of interest based on molecular weight. The excised pieces were transferred into protein LoBind tubes and pulverized finely using plastic pestles. 100 mM ammonium bicarbonate pH 9.0 with 0.1% SDS was added into each tube and shaken at 25°C, 1100rpm for 20min. The residual gel was removed by transferring samples into centrifugal filters and centrifuging at 4° C, 14,000 x g for 10min. The resulting solution was used for the subsequent LC-MS analysis.

Liquid Chromatography Mass Spectrometry(LC-MS)
The PEPPI fractions were analyzed via LC-MS/MS by Dr. Cynthia Nagy, a member of the Fornelli group at OU, as follows:

Samples were buffer exchanged using Zeba spin desalting column into solvent A (95% Optima water, 5% acetonitrile, 0.1% formic acid.) The sample was then concentrated down to 20 µM using a 3kDa molecular weight cut-off (MWCO) Ultra-15 concentrator (Amicon) and underwent LC analysis with a Dionex Ultimate 3000 (Thermo Scientific) using a MAbPac EASY-Spray column (150 mm x 1mm i.d., particle size: 4 µm, Thermo Scientific). The total runtime was 45 minutes with the following settings for gradient elution: 6% solvent B (5 % water, 94.8 % acetonitrile, and 0.1 % formic acid) from 0 to 6 min; 40 % B at 30 min; and then increased to 80% B in 2 mins and a two-step condition of the column for proper reproducibility between runs. The applied flow rate was 1.5 µL/min. 26 ng sample was injected onto the column for each experiment. Data dependent acquisition was performed using an Orbitrap Eclipse Tribrid MS instrument (Thermo Scientific). Both MS1 and MS2 data were collected with an Orbitrap resolution of 120K (at 200m/z).

Results

The intrinsic degradation is affected both by temperature and pH.
The unstable nature of antitoxins potentially results from both disordered structures and targeting by ATP-dependent proteases.[11, 12, 20-22, 29] While the degradation of ParD antitoxins by ATP-dependent proteases in cells has been documented,[11, 20, 21] the intrinsic instability of the ParD structure even in the purified form is surprising and not understood. This instability necessitates fresh purifications for each experiment with antitoxins. Thus, we evaluated the impact of both temperature and pH on the PaParD1 antitoxin degradation. Our result showed the intrinsic instability of purified wild type PaParD1 over a 10-day window. Compared to physiological-like conditions, *i.e.*, 37°C, and pH7, the lower temperature, *i.e.*, 4° C, and acidic environment, *i.e.*, pH5, likely disfavor the degradation of PaParD1(Figure. 4.1).

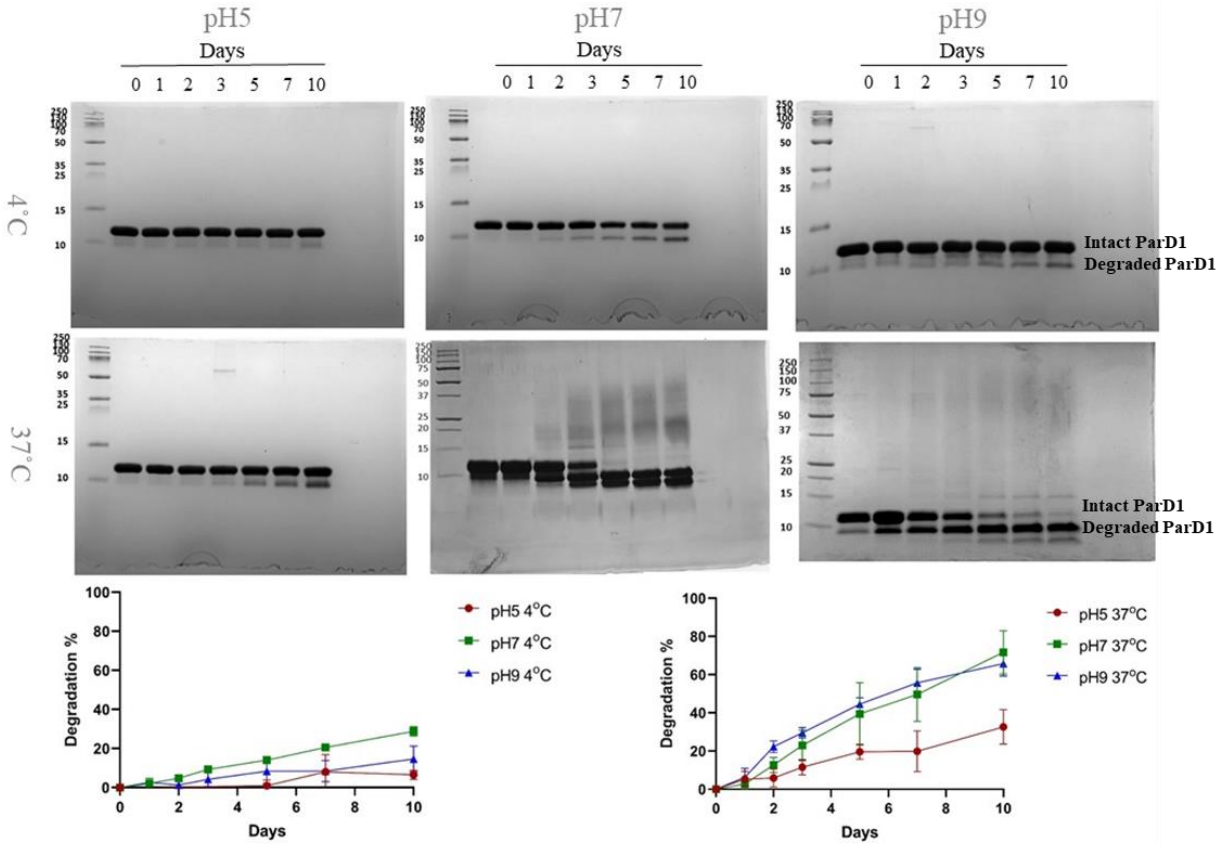

Figure 4.1. The degradation of PaParD1 is temperature and pH dependent. The analysis of PaParD1 degradation was conducted via incubating at indicated temperature and pH environments. Each condition was conducted with three independent replicates. The molecular weight of intact PaParD1 is approx. 11kDa. The band intensities were measured using ImageJ, and the degradation percentage was determined by the ratio between the overall ParD1 band and the degradation band in each lane. Average values are graphed with standard error of the mean (SEM).

The dimerization of PaParD1 is affected by ionic strength

The structure of PaParDE1 (PDB ID:6XRW) displays a conserved N-terminal RHH domain in PaParD1 and its role in mediating dimerization. Upon analysis, hydrophobic interactions contribute to the stabilization of PaParD1 dimer.(Table S4.1)[14] In our study, size exclusion chromatograms reveal that when PaParD1 is purified in a buffer with 300mM NaCl, denoted as higher ionic strength, there was only one peak and this corresponds to dimeric PaParD1. However, when the same sample is instead purified using a buffer containing 150mM NaCl, denoted as lower ionic strength, not only did the peak corresponding to dimeric PaParD1 appear, but the chromatogram also revealed a distinct peak corresponding to monomeric PaParD1. (Figure 4.2A)

The stoichiometry of PaParD1 in different salt concentrations was also confirmed using native gel electrophoresis, where PaParD1 in lower ionic strength existed as two distinct bands while in higher ionic strength, or containing glycerol in lower ionic strength, one predominant band is seen. (Figure 4.2B) Taken together, these results indicate that ionic strength impacts the stability of the PaParD1 dimer, as low ionic strength, is expected to modestly decrease the strength of hydrophobic interactions between PaParD1 monomers, leading to some dissociation of dimeric PaParD1 complex. Interestingly, we note that the dimeric PaParD1 in a low ionic strength is stabilized and can be maintained if 20% glycerol is included, which mimics a typical longer-term storage condition.

We then assessed if the monomeric PaParD1 in low ionic strength was able to reform as a dimer when ionic strength was again increased. Purified PaParD1 was first loaded into size-exclusion column pre-equilibrated with the buffer with low ionic strength. As expected, two major peaks corresponding to PaParD1 dimer and monomer appeared in the chromatogram. Fractions within those peaks were collected, concentrated and loaded onto the size exclusion column pre-equilibrated at the buffer at higher ionic strength. Surprisingly, only one peak representing the PaParD1 dimer is seen in the chromatogram, indicating that the formation and dissociation of PaParD1 dimer is dynamic, and altering ionic strength impacts the status of PaParD1.

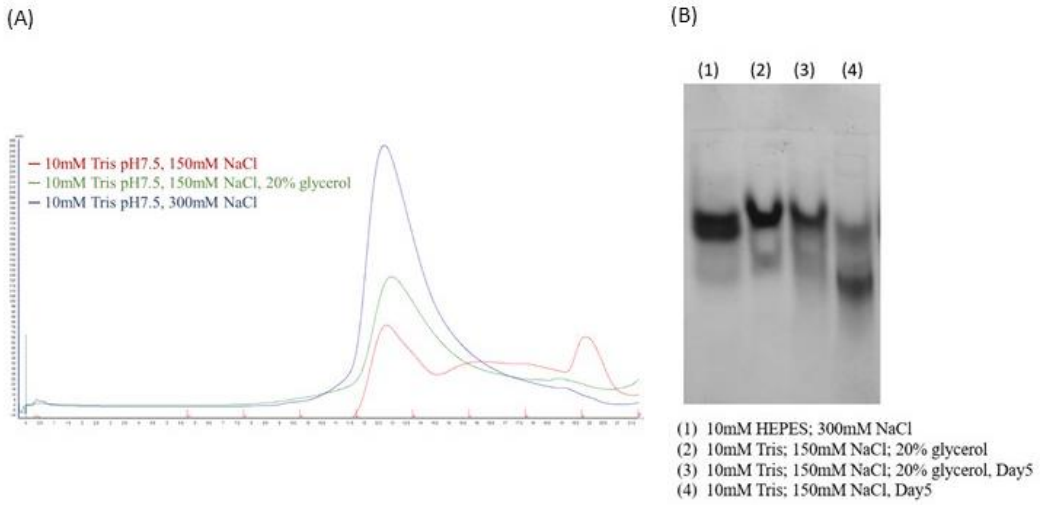

Figure 4.2. Buffer conditions affect the stability of PaParD1 dimer. (A) The size exclusion chromatogram reveals changes in the stoichiometry of PaParD1 in different ionic strengths. The first peak (from the left) corresponds to PaParD1 dimer, while the second peak (only visible for the red trace) represents PaParD1 monomer. (B) A native gel confirms dimeric and monomeric PaParD1 in different buffer conditions.

The degradation rate increases as the ratio of monomeric PaParD1 increases.

To evaluate the degradation of PaParD1 in different buffer conditions, PaParD1 in high ionic strength, low ionic strength and low ionic strength with glycerol were incubated at 37˚C. As Figure 4.3 shows, after 5 days of incubation at low (150mM) ionic strength, degraded PaParD1 increased to approx. 40% of the total sample. However, at a higher (300mM) ionic strength, only approx. 15% of the total sample consists of degraded PaParD1 at the same timepoint. The degradation of PaParD1 was also mitigated to approx. 15% by inclusion of glycerol to 20% in lower ionic strength. Lastly, PaParD1 showed identical degradation rate in both Tris and HEPES buffer, suggesting that ionic strength rather than functional groups on the buffer, such as the primary amines in Tris, is the factor that correlated with the extent of degradation.

Our previous results revealed that the dissociation of the PaParD1 dimer occurs in the lower ionic strength condition; furthermore, PaParD1 in lower ionic strength is correlated with a higher degradation rate compared to that in higher ionic strength. Therefore, it is possible that the higher the ratio of the monomeric form of PaParD1, the higher the degradation rate. To better assess this, we compared the ratio of monomeric PaParD1 in previous samples and assessed if monomeric PaParD1 affects the degradation. As Figure 4.3C indicates, the degradation rate was less than 15% when the ratio of monomeric PaParD1 was 0%, which was purified from higher ionic strength; however, the degradation rate increased to approx. 50% as the ratio of monomeric PaParD1 reached 44%. All in all, low ionic strength leads to dissociation of PaParD1 from the dimeric form and as the ratio of monomeric PaParD1 increases, the degradation rate increases.

The purification of PaParD1 followed the same procedure but contained various percent monomer in the final sample. It is possible that the concentration before loading to the size exclusion column affects the monomer-dimer equilibrium.

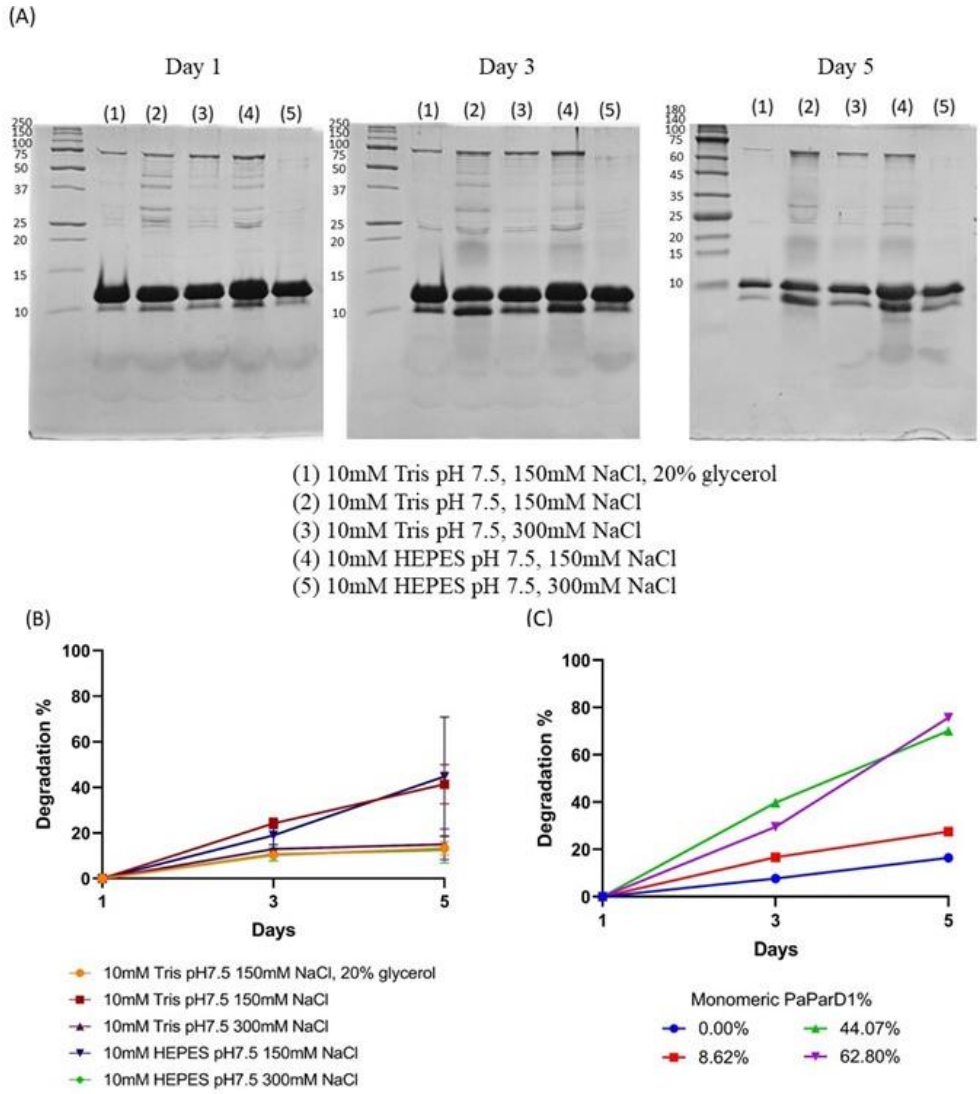

Figure 4.3. Degradation rates are consistent with low ionic strength causing PaParD1 to dissociate into monomers. (A) Assessment of 50μM PaParD1 degradation in different buffer conditions by incubating at 37˚C and sampling at days 1, 3 and 5. Quantitation of the resulting degradation was plotted and shown in (B). The correlation between the ratio of monomeric PaParD1 and degradation rate was also plotted and shown in (C). The trace and resulting degradation were in Figure S4.4. The estimation of band intensities was proceeded using ImageJ, and the degradation percentage was determined by the ratio between the overall ParD1 and degradation band in each lane.

Higher concentrations of PaParD1 increases the degradation rate and promotes the appearance of higher molecular weight species visible by denaturing PAGE.

In monitoring of degradation of PaParD1, we noted a progressive accumulation of an SDS-resistant species with larger molar mass in the 20 - 24 kDa range. In addition, higher concentration might also impact the monomer-dimer equilibrium and the resulting degradation. To address potential concentration-dependence of both degradation and the formation of such species, we incubated PaParD1 at 37˚C, pH7 at three concentrations: 17μM, 71μM and 140μM. As Figure 4.4 indicates, increased concentrations of PaParD1 appeared to increase the degradation rate and extent. At the day 5 timepoint, approximately 40% of PaParD1 at 140μM was degraded; in contrast, only approx. 20% was degraded by day 5 at 17μM. This suggests that higher concentrations of PaParD1 have increased rates of degradation concomitantly with increased formation of species of larger molecular weight.

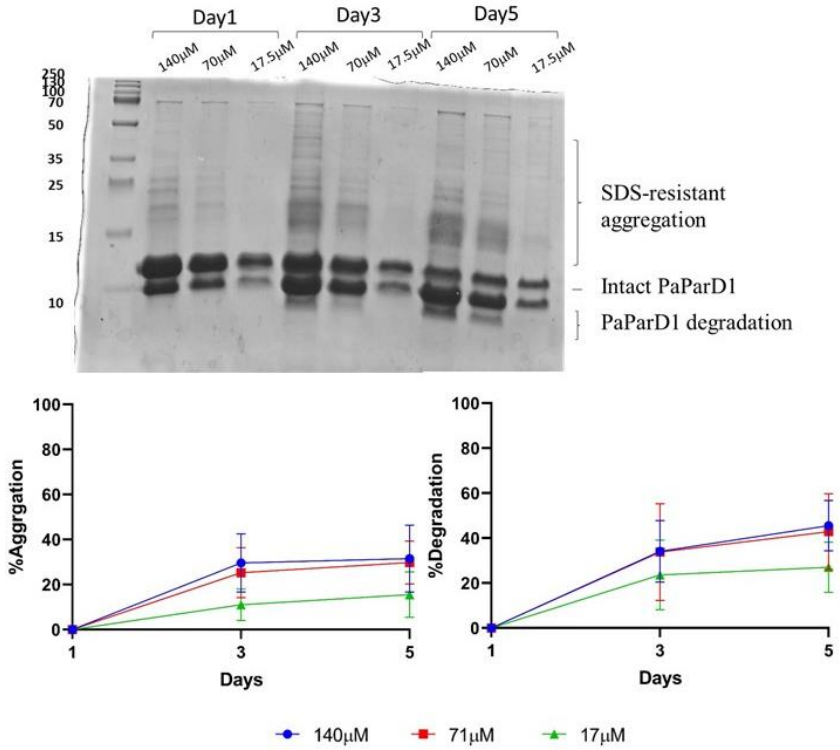

Figure 4.4. The formation of SDS-resistant aggregation and degraded PaParD1 are both concentration- and time-dependent. PaParD1 at three different concentrations, 140μM, 70μM and 17.5μM, was incubated at 37˚C and sampled at day 1, day 3 and day 5. Each condition was conducted with 2 independent replicates. The estimation of band intensities was proceeded using ImageJ, and the aggregation / degradation percentage was determined by the ratio between the overall PaParD1 and aggregation / degradation bends in each lane.

Glutamine residues have minimal impacts on PaParD1 degradation.

Our previous result showed that PaParD1 degradation was enriched at a glutamine-rich region in the α-helix 2 (Figure 4.5.B) In order to investigate if the glutamine side chain could mediate a self-cleavage reaction, point mutants were generated to produce two new PaParD1 proteins: Q43S, Q44S, Q47H (referred to as 3QmutPaParD1) and Q34A, Q38A, Q43S, Q44S, Q47H (referred to as 5QmutPaParD1) The selection of substitutions for residues was based on a sequence alignment of different ParD1 proteins. (Figure S4.6) For these experiments, the PaParD1 wild type and mutant proteins were purified in lower (150mM) ionic strength and monitored for degradation when incubated at 37˚C (Figure 4.5). The degradation rate of wild type and the 3QmutPaParD1 was similar and both reached approx. 70% degradation after 10 days. In contrast, the 5QmutPaParD1 had similar initial kinetics and reached approx. 40% (± 10%) degradation, implying that Q34 and Q38 might contribute to the observed degradation but are unlikely to be directly mediating the degradation.

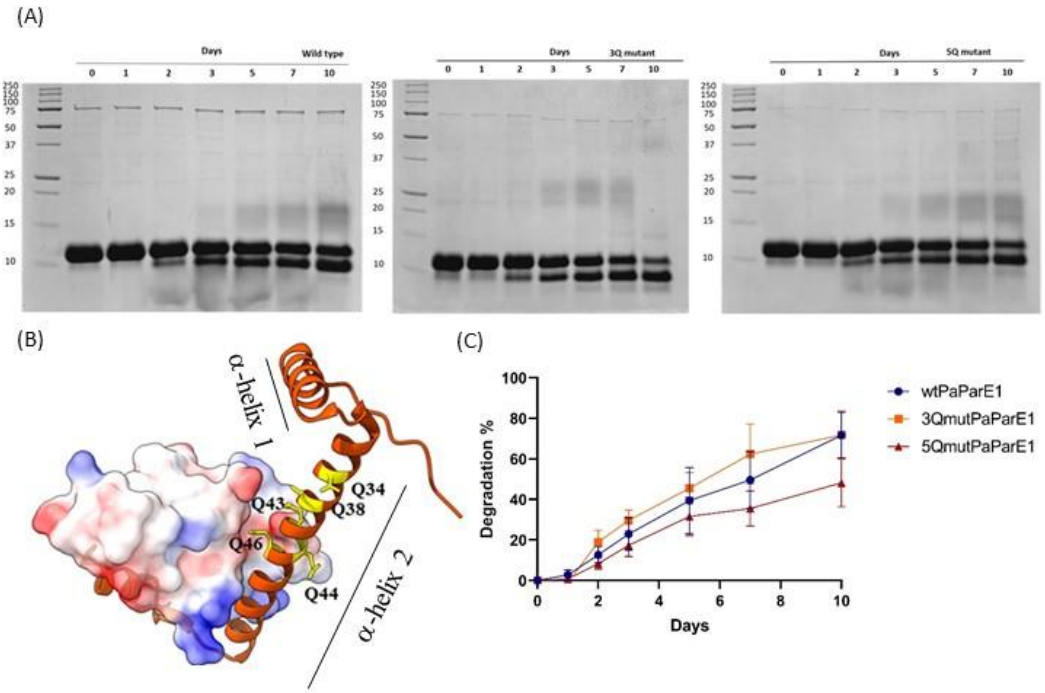

Figure 4.5. PaParD1 degradation still occurred even mutating glutamine residues in the α-helix 2. (A) The 50mM wild type PaParD1, 3QmutPaParD1 and 5QmutPaParD1 were incubated at 37˚C and collected at desired times to assess the degradation. The estimation of band intensities was proceeded using ImageJ, and the degradation percentage was calculated as the ratio between the overall ParD1 and degradation band in each lane and (C) shows the plot of quantitation of the resulting degradation. (B) The PaParDE1 complex (PDB: 6XRW [14]) presents a glutamine-rich region in the second α-helix of PaParD1. The PaParD1 is represented as an orange ribbon, with glutamines presenting in yellow sticks. The PaParE1 is represented as a Coulombic surface.

To elucidate the degradation species as well as the SDS-resistant species at 20 - 25 kDa, we collaborated with the Fornelli lab at the University of Oklahoma for identification by mass spectrometry. Following their protocol, protein samples were isolated from distinct regions of acrylamide gels using a common approach abbreviated as “PEPPI” and the resulting protein fractions were analyzed via the top-down MS approach. The signals from the intact mass spectra for degraded PaParD1 were deconvoluted and the molecular weight of degraded peptides were determined to be around 8.1 - 9 kDa. The band around 70kDa was identified as the DnaK chaperone. Surprisingly, the “SDS-resistant aggregate” species around 20 - 25kDa was identified as fragments of the DnaK chaperone, although the annotated molecular weight for this protein is 69.1kDa.[30] The appearance of these lower molecular weight DnaK contaminants directly correlates with the degradation of the PaParD1 antitoxin.

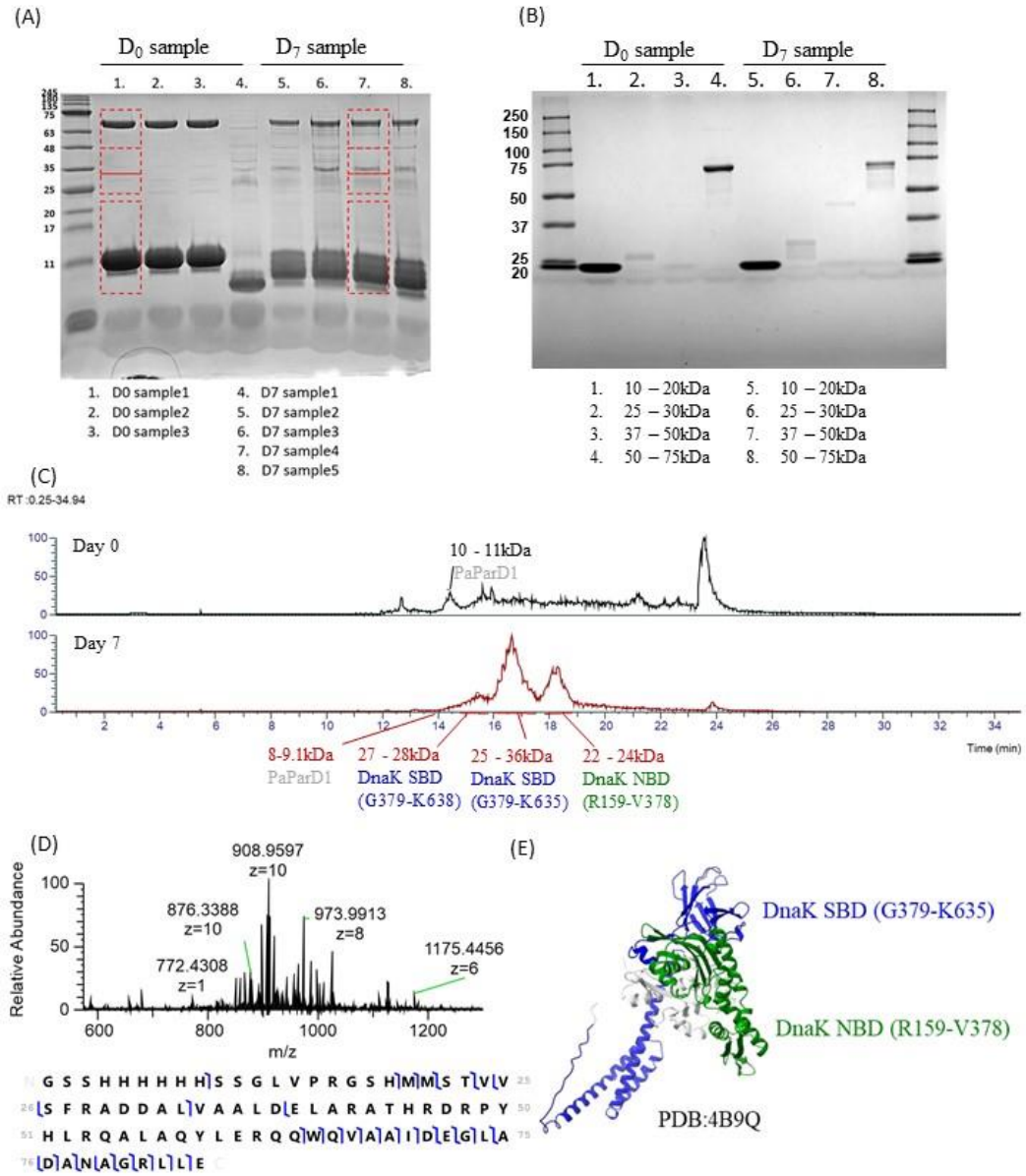

Figure 4.6. PEPPI-MS analysis of wild type PaParD1 after a 10-day incubation at 37˚C reveals the major intermediate species around 20-25kDa. (A) The 50μM wild type PaParD1 proteins incubated at 37˚C were collected at day 0 and day 7 and electrophoresed on a 15% tris tricine gel; dashed red boxes indicate the four regions excised for recovery from the gel. (B) Species extracted from the red boxed regions via the PEPPI method were collected and re-assessed on a 12% tris glycine gel. (C) Chromatogram obtained for the Day0 and Day7 samples (MS1 level). Intact masses of species were revealed by spectral deconvolution and are indicated for specified retention times. Several DnaK fragments were found to be dominating in the chromatogram obtained for the Day7 sample. (D) An MS2 spectrum and corresponding fragmentation map of degraded PaParD1. (E) The structure of DnaK chaperone (PDB:4B9Q [33]) The fragments of DnaK identified were colored accordingly in (C). Peaks at 15.5min and 16.6min were the DnaK substrate binding domain (SBD), colored in blue. Peak at 18.4min was DnaK nucleotide binding domain (NBD), colored in green. The data and images in panel (C) and(D) were acquired from Dr. Nagy from Dr. Fornelli's lab

Removal of DnaK has minimal impact on PaParD1 degradation.

To investigate the influence of DnaK on the degradation of PaParD1, we revisited the purification protocol to remove this contaminant. DnaK has been reported to exhibit low affinity and a fast exchange rate for substrate in the ATP-bound state, and can be removed from substrate proteins via washing with ATP.[31, 32] Thus, samples of PaParD1 were captured on a nickel affinity column and washed with 5mM ATP before elution with imidazole; this sample was further purified by size exclusion chromatography. The contaminant DnaK could be mostly removed by this procedure (Figure 4.7A and B), with the separation appearing only at the size exclusion step. The PaParD1 after this removal procedure was subsequently collected and monitored for degradation. As Figure 4.7C indicates, the extent of PaParD1 degradation was approximately the same in the apparent absence of DnaK. However, the smeared band at approx. 20-25 kDa formed more abundantly after the purification to remove additional contaminants, such as DnaK.

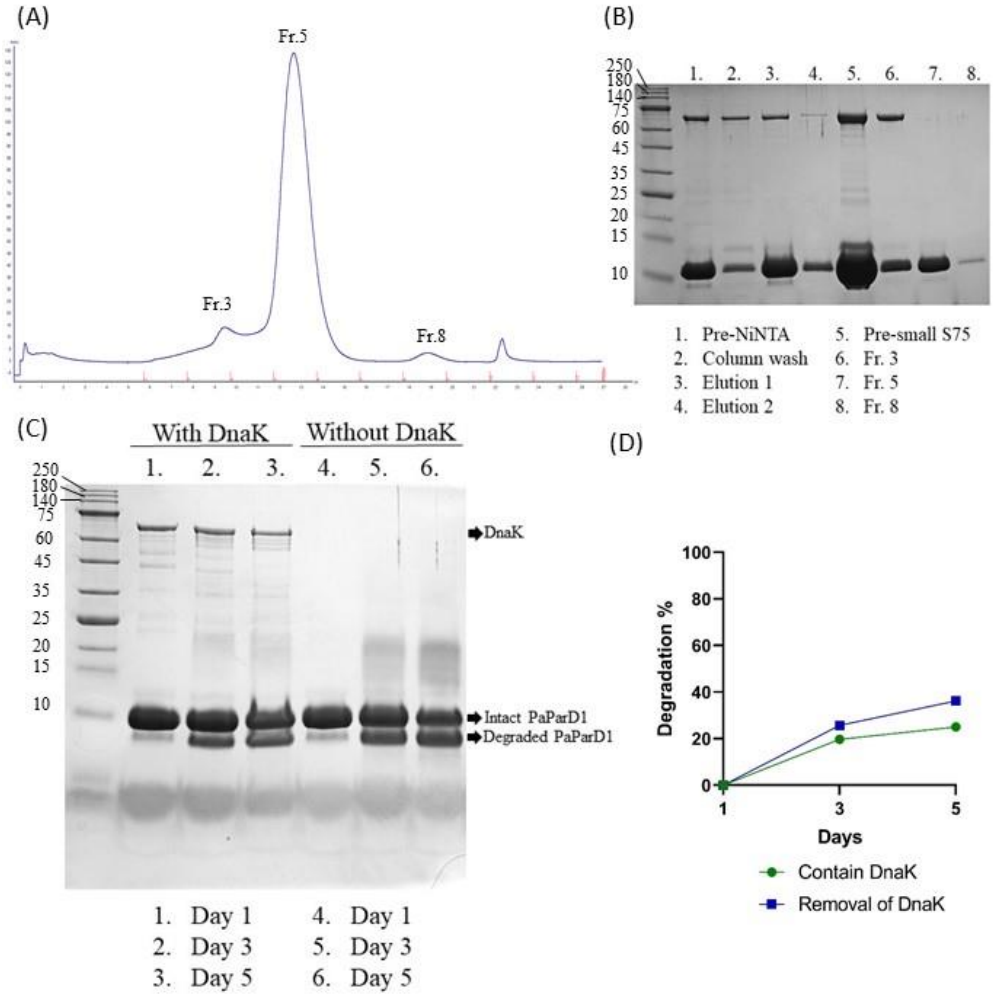

Figure 4.7. Pilot assay: Removal of DnaK has minimal impact on PaParD1 degradation. (A) Size exclusion chromatogram shows the separation of DnaK and PaParD1. (B) Samples collected at each purification step were loaded onto a 15% tris tricine gel and visualized by Coomassie staining. (C) Assessment of 50μM PaParD1 degradation with or without additional purification to remove DnaK. Sample were incubated at 37°C and collected at day1, 3, 5. All collected samples were load into a 15% tris tricine gel an dvisualized by Coomassie staining. (D) The band intensity was quantified using imageJ and the degradation percentage was determined by the ratio between the overall PaParD1 band and degradation band in each lane.

Discussion

The regulation of type II ParDE TA systems relies on the differential half-lives of ParD antitoxins and ParE toxins. Due to the unstable nature of antitoxins, the ParD protein must be continually replenished to keep its cognate ParE toxin neutralized. In the current study, we focused on the *in vitro* intrinsic lability of the PaParD1 antitoxin. We first assessed the impacts of temperature and pH on PaParD1 degradation that we visualized using acrylamide gel electrophoresis. This revealed that the PaParD1 started to degrade resulting in discrete bands around 8 - 9 kDa within 2-days of incubation at 37°C. A similar observation was previously made in our stuies and for the ParD antitoxin encoded on the RK2 plasmid, with the latter resulting in three prominent masses detected by MALDI-TOF-MS.[22] Our results indicate that lower temperatures (4°C), and pH value (pH 5) slowed PaParD1 degradation, to approx. 20% while this increases to 70% degradation at pH 7, 37°C (Figure 4.1). We also observed that the degradation is concentration dependent, meaning the higher the PaParD1 concentration, the higher extent of degradation occurred. Finally, we noted that an SDS-resistant species with higher molecular weight than PaParD1 was generated as degradation occurred, as was especially noted during the 37°C incubation.

The crystal structure of the PaParDE1 complex confirms that hydrophobic interactions stabilize the dimerization of PaParD1 in the N-terminal RHH DNA binding domain.[14] This is consistent with the mode of dimerization of other ParD antitoxins. Our results show that the dimerization of PaParD1 is affected by ionic strength. The PaParD1 forms a dimer in ionic strength higher than physiological condition (e.g., at 300mM), while it dissociates into a dimer-monomer mixture in a lower (physiologic, 150mM) ionic environment. When the ionic strength switches back to high ionic strength, PaParD1 returns to the dimeric form, suggesting the status of PaParD1 between monomeric and dimeric form is dynamic. Additionally, PaParD1 is able to maintain a dimeric form in lower ionic strength if 20% glycerol is included, presumably due to favoring hydrophobic interactions or simply due to a "crowding" type effect. There are examples in the literature of ParD antitoxins that form higher order oligomers.[17] The ParD2 dimer from *V. cholerae* (VcParD2) is able to interact with another VcParD2 dimer to assemble a hexadecamer. Unlike PaParD1 that dissociates from a dimer when in low ionic strength, this condition instead promotes the assembly of the hexadecameric VcParD2 because the interaction between VcParD2 dimer is dictated by hydrogen bonding and salt bridge interaction.[17]

To investigate if glutamine side chains in the α-helix 2 region are critical to the PaParD1 degradation, the glutamine-mutated PaParD1 proteins were generated. Our result showed that the mutated PaParD1 still degraded overtime, though 5Q-mutated PaParD1 exhibited somewhat slowed degradation compared to the wild type and 3Q-mutated PaParD1, suggesting that glutamine is not the only residue affecting PaParD1 degradation. In collaboration with the Fornelli group, we utilized mass spectrometry to analyze PaParD1 degraded products (approx. 8 - 9kDa) and the SDS-resistant species (approx. 20 -25kDa) that appeared as PaParD1 degraded. First, our result showed that degraded PaParD1 truncated at multiple sites. The result of mass spectrometry also identified the SDS-resistant species is degraded DnaK fragments consisting of the substrate binding domain and the nucleotide binding domain. DnaK is shown to have higher affinity to a thrombin cleavage site,[32] which is presented in the PaParD1 construct between the His-tag and PaParD1 protein. This may explain why the DnaK persisted as a contaminant during purification of PaParD1. DnaK could be greatly minimized by washing with ATP and was subsequently separated from PaParD1 via size exclusion chromatography.

However, the PaParD1 degradation occurred at essentially the same rate while the species around 20 - 25 kDa still appeared despite the presumed removal of DnaK. It is possible that the removal procedure reduced intact DnaK while potentially enriching the pool of degraded DnaK fragments, including the truncated substrate binding domain and truncated nucleotide binding domain, making the band around 20-25kDa become more apparent in the PaParD1. This is contraindicated, however, by the lack of any apparent band in the Day 1 sample for re-purified PaParD1. The generation of the smeared bands identified by MS to be cleaved DnaK remains mysterious, as does the mechanistic basis for PaParD1 breakdown.

In conclusion, our study highlights the dynamic nature of PaParD1 stability and key conditions influencing its degradation and dimerization. We found that PaParD1 degradation was affected by concentration, temperature and pH, with lower concentration, lower temperature and acidic conditions all reducing degradation. The ionic strength influenced the dimerization of PaParD1, and its dissociation under physiological ionic strength increased the observed *in vitro* degradation rate. Additionally, mutagenesis of glutamine amino acids combined with mass spectrometry indicated that glutamine has no impact on PaParD1 degradation, suggesting the involvement of other residues in PaParD1 stability. Mass spectrometry also revealed the SDS-resistant species observed in PaParD1 degradation corresponded to degraded DnaK fragments, and the absence of DnaK may have minimal influence on PaParD1 degradation. All in all, our study characterizes the conditions of PaParD1 stability and provides a potential link between ParD stability, oligomeric state, and optimum storage conditions for *in vitro* studies.

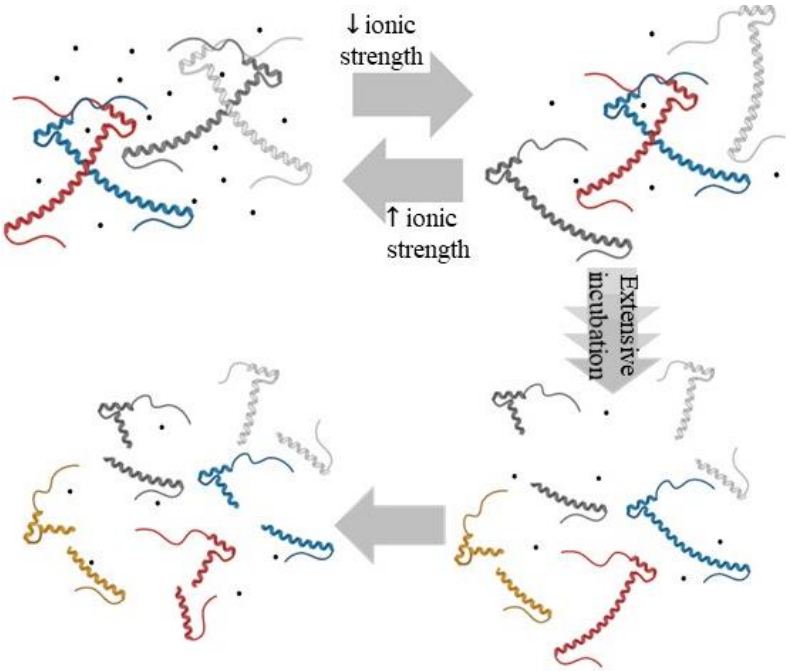

Figure 4.8. The maintance of purified PaParD1 should be lower temperature, pH and higher ionic strength. PaParD1 exhibits a monomer-dimer equilibrium. When the ionic strength decreases, PaParD1 starts to dissociate and become a monomeric form. When incubating at a condition close to the physiological environment (37°C, and pH 7), the monomeric PaParD1 tends to break into 8-9 kDa degraded species.

Data Availability

All data are included in this manuscript and the appendix; DNA clones for constructs made in this work are available upon request

Author Contributions

C.H.T. collected all data except for the data of mass spectrometry shown in Figure 4.6, which was collected by Dr. Cynthia Nagy, in this manuscript; C.H.T. and C.R.B. participated in the project design, data processing, manuscript drafting, and editing.

Acknowledgements

We appreciate the assistance from the OU Protein Production and Characterization Core facility for assisting with protein purification and access to equipment. The OU Protein Production and Characterization Core facility is supported by Institutional Development Awards from the National Institute of General Medical Sciences of the National Institutes of Health Grants P20GM103640 and P30GM145423, the OU Vice President for Research and Partnerships, and the OU College of Arts and Sciences) We also appreciate the expert assistance of Dr. Cynthia Nagy from Fornelli group for mass spectrometry data collection and analysis, which was conducted at the OU Mass Spectrometry, Proteomics & Metabolomics Core

Reference

1. Gerdes, K., P.B. Rasmussen, and S. Molin, *Unique type of plasmid maintenance function: postsegregational killing of plasmid-free cells.* Proc Natl Acad Sci U S A, 1986. **83**(10): p. 3116-20.
2. Ogura, T. and S. Hiraga, *Mini-F plasmid genes that couple host cell division to plasmid proliferation.* Proc Natl Acad Sci U S A, 1983. **80**(15): p. 4784-8.
3. Kamruzzaman, M. and J. Iredell, *A ParDE-family toxin antitoxin system in major resistance plasmids of Enterobacteriaceae confers antibiotic and heat tolerance.* Sci Rep, 2019. **9**(1): p. 9872.
4. Weaver, K., *The Fst/Ldr Family of Type I TA System Toxins: Potential Roles in Stress Response, Metabolism and Pathogenesis.* Toxins (Basel), 2020. **12**(8).
5. Gómez, L.A., et al., *Unraveling the Role of the Zinc-Dependent Metalloproteinase/HTH-Xre Toxin/Antitoxin (TA) System of Brucella abortus in the Oxidative Stress Response: Insights into the Stress Response and Virulence.* Toxins (Basel), 2023. **15**(9).
6. Azam, A.H. and Y. Tanji, *Bacteriophage-host arm race: an update on the mechanism of phage resistance in bacteria and revenge of the phage with the perspective for phage therapy.* Appl Microbiol Biotechnol, 2019. **103**(5): p. 2121-2131.
7. Li, Y., et al., *Prophage encoding toxin/antitoxin system PfiT/PfiA inhibits Pf4 production in Pseudomonas aeruginosa.* Microb Biotechnol, 2020. **13**(4): p. 1132-1144.
8. Tu, C.H., et al., *Evaluating the Potential for Cross-Interactions of Antitoxins in Type II TA Systems.* Toxins (Basel), 2020. **12**(6).
9. Saavedra De Bast, M., N. Mine, and L. Van Melderen, *Chromosomal toxin-antitoxin systems may act as antiaddiction modules.* J Bacteriol, 2008. **190**(13): p. 4603-9.
10. Ramage, H.R., L.E. Connolly, and J.S. Cox, *Comprehensive functional analysis of*

Mycobacterium tuberculosis toxin-antitoxin systems: implications for pathogenesis, stress responses, and evolution. PLoS Genet, 2009. **5**(12): p. e1000767.
11. Diago-Navarro, E., et al., *Cleavage of the antitoxin of the parD toxin-antitoxin system is determined by the ClpAP protease and is modulated by the relative ratio of the toxin and the antitoxin.* Plasmid, 2013. **70**(1): p. 78-85.
12. Van Melderen, L., P. Bernard, and M. Couturier, *Lon-dependent proteolysis of CcdA is the key control for activation of CcdB in plasmid-free segregant bacteria.* Mol Microbiol, 1994. **11**(6): p. 1151-7.
13. Makarova, K.S., Y.I. Wolf, and E.V. Koonin, *Comprehensive comparative-genomic analysis of type 2 toxin-antitoxin systems and related mobile stress response systems in prokaryotes.* Biol Direct, 2009. **4**: p. 19.
14. Snead, K.J., L.L. Moore, and C.R. Bourne, *ParD Antitoxin Hotspot Alters a Disorder-to-Order Transition upon Binding to Its Cognate ParE Toxin, Lessening Its Interaction Affinity and Increasing Its Protease Degradation Kinetics.* Biochemistry, 2022. **61**(1): p. 34-45.
15. Aakre, C.D., et al., *Evolving new protein-protein interaction specificity through promiscuous intermediates.* Cell, 2015. **163**(3): p. 594-606.
16. Dalton, K.M. and S. Crosson, *A conserved mode of protein recognition and binding in a ParD-ParE toxin-antitoxin complex.* Biochemistry, 2010. **49**(10): p. 2205-15.
17. Garcia-Rodriguez, G., et al., *Entropic pressure controls the oligomerization of the Vibrio cholerae ParD2 antitoxin.* Acta Crystallogr D Struct Biol, 2021. **77**(Pt 7): p. 904-920.
18. Beck, I.N., et al., *Toxin release by conditional remodelling of ParDE1 from Mycobacterium tuberculosis leads to gyrase inhibition.* Nucleic Acids Res, 2023.
19. Klemencic, M., A. Haluzan Vasle, and M. Dolinar, *The Cysteine Protease MaOC1, a Prokaryotic Caspase Homolog, Cleaves the Antitoxin of a Type II Toxin-Antitoxin System.* Front Microbiol, 2021. **12**: p. 635684.
20. Ziemski, M., et al., *Genome-wide interaction screen for Mycobacterium tuberculosis ClpCP protease reveals toxin-antitoxin systems as a major substrate class.* Febs j, 2021. **288**(1): p. 111-126.
21. Dubiel, A., et al., *ClpAP protease is a universal factor that activates the parDE toxin-antitoxin system from a broad host range RK2 plasmid.* Sci Rep, 2018. **8**(1): p. 15287.
22. Oberer, M., et al., *Thermodynamic properties and DNA binding of the ParD protein from the broad host-range plasmid RK2/RP4 killing system.* Biol Chem, 1999. **380**(12): p. 1413-20.
23. Snead, K.J. and C.R. Bourne, *Intrinsic Degradation of the Type-II Antitoxin ParD from Pseudomonas aeruginosa.* bioRxiv, 2021: p. 2021.03.29.437564.
24. Friedrich, M.G., et al., *Spontaneous Cleavage at Glu and Gln Residues in Long-Lived Proteins.* ACS Chem Biol, 2021. **16**(11): p. 2244-2254.
25. Ramsoomair, C.K., et al., *Coordination of the third step of protein splicing in two cyanobacterial inteins.* FEBS Lett, 2017. **591**(14): p. 2147-2154.
26. Amitai, G., B. Dassa, and S. Pietrokovski, *Protein splicing of inteins with atypical glutamine and aspartate C-terminal residues.* J Biol Chem, 2004. **279**(5): p. 3121-31.
27. Patel, S., *Drivers of bacterial genomes plasticity and roles they play in pathogen virulence, persistence and drug resistance.* Infect Genet Evol, 2016. **45**: p. 151-164.
28. Friedrich, M.G., et al., *Spontaneous protein-protein crosslinking at glutamine and glutamic acid residues in long-lived proteins.* Biochem J, 2021. **478**(2): p. 327-339.
29. Loris, R. and A. Garcia-Pino, *Disorder- and dynamics-based regulatory mechanisms in toxin-antitoxin modules.* Chem Rev, 2014. **114**(13): p. 6933-47.
30. Richards, A. and T.J. Lupoli, *Peptide-based molecules for the disruption of bacterial*

Hsp70 chaperones. Curr Opin Chem Biol, 2023. **76**: p. 102373.
31. Bukau, B. and A.L. Horwich, *The Hsp70 and Hsp60 chaperone machines.* Cell, 1998. **92**(3): p. 351-66.
32. Rial, D.V. and E.A. Ceccarelli, *Removal of DnaK contamination during fusion protein purifications.* Protein Expr Purif, 2002. **25**(3): p. 503-7.
33. Kityk R, Kopp J, Sinning I, Mayer MP. Structure and dynamics of the ATP-bound open conformation of Hsp70 chaperones. Mol Cell. 2012;48(6):863-874. doi:10.1016/j.molcel.2012.09.023

Chapter V

Research Impact and Future directions

The research reported in chapters II-IV of this dissertation provide novel insights into the field of toxin-antitoxin (TA) systems spanning cellular to structural levels. Chapter II provides new insights on the influence of induced ParE toxin expression on native bacterial host cell mutagenesis resulting from ParE-mediated gyrase inhibition as well as subsequent sensitization to antibiotic treatments. In addition, the C-terminus of ParE toxins, which have been suggested to be a determinant of ParE toxicity, was found to not alter their potency through generation and testing of chimeric ParE toxins. In chapter III, we explored the feasibility of acquiring purified ParE toxins using previously reported methods and developed our own optimized approach for purification. We found that co-expression of the ParE toxin with a construct encoding ab altered version of its target, a GyrB-GyrA DNA gyrase fusion, is an effective way to express VcParE1 toxin in *E. coli* and produce sufficient quantities of active, purified toxin for on-going cryo-EM studies. It is likely that the conformation of gyrase recognized by ParE toxins is a transient intermediate, and previous attempts to mitigate toxicity through expression of just GyrB or GyrA were unsuccessful (M. Muthuramalingam, unpublished) as these would not have been catalytically competent. Lastly, we investigated conditions affecting the *in vitro* stability of purified PaParD1 antitoxin in chapter IV. We determined the ionic strength impacts the dimerization of PaParD1 and the status between monomer and dimer also impacts the degradation rate of PaParD1. Through a collaboration with local mass spectrometry experts Dr., Cynthia Nagy and Luca Fornelli, a pervasive protein chaperone DnaK was surprisingly found to co-purify with PaParD1, although it is unclear if its presence correlates with protection from degradation.

TA systems have been shown to pause growth or kill bacterial cells when the toxin interacts with its cellular target.[1] In the ParDE TA system, the ParE toxin binds DNA gyrase resulting in stabilization of the gyrase-mediated DNA cleavage complex, causing an DNA double strand break.[2-5] If the ParE-mediated inhibitory mechanism can be utilized, our data in chapter II suggest it could serve as an effective antibacterial strategy without negatively affecting current antibiotic treatments. Based on the research in chapter II, the future direction will be developing ParE mimics. Screening for compounds or small peptides that resemble the structure of ParE toxins could be novel antimicrobial reagents that repress the function of DNA gyrase. In addition, our data indicate that ParE-mediated inhibition sensitizes antibiotics treatments, supporting that developing ParE mimics is a promising direction for counteracting antimicrobial resistance. Our result in chapter II also presents that C-terminal region of the ParE toxin does not contribute to its toxicity, which provides directions for designing the mimics.

In chapter III, our results highlight that co-transformation of the ParE toxin with its target, DNA gyrase B+A chain fusion, lessened the toxic effect to *E. coli* cells, enabling it to modest expression of the ParE protein. The future direction will assess if this strategy also mitigates the toxicity of other ParE toxins in *E. coli* cells. Even though co-expressed DNA gyrase B+A chain fusion was able to cover most ParE-exerted toxic effect, cells still encountered ParE toxicity, leading to decreased cell pellet for purification. Since ParE toxins exhibit various level of toxicity, it is intriguing to assess if our method also works on other ParE toxins.

The future direction beyond this chapter will also focus on elucidation of the interaction between gyrase and ParE toxin. We have result from pilot experiments that successfully capture

a ParE-bound gyrase complex directly from a gyrase-mediated supercoiling assay. Optimize of this method, including ensuring stability of this complex, should permit success in visualizing the ParE-bound gyrase complex structure through cryo-electron microscopy.

The inherent instability of antitoxins is widely recognized in the field of TA system,[13-15] and our study at chapter IV provides more details into conditions that affect the stability of the PaParD1 antitoxin. Future direction will examine the stability of other ParD antitoxins that have been reported to undergo oligomerization, such as VcParD2. Comparing the stability of ParD antitoxins in the presence of cognate ParE toxins under the physiological condition is another direction that can provide deeper insight to understand how ParE toxin releasing from the ParD antitoxin.

We also identified DnaK chaperone co-purified with PaParD1. Known for its stable nature, the DnaK, however, broke into substrate-binding domain an nucleotide-binding domain, forming an intermediate band around 20-25kDa, when incubating at 37°C with PaParD1. While DnaK is known for assisting the degradation of other proteins,[17] its own degradation is less characterized. Therefore, exploring the role of DnaK chaperone on ParD stability, both *in vivo* and *in vitro*, will be the future direction of chapter IV.

Taken together, the research in this dissertation extends the knowledge in the field of TA system research, spanning from the impact of bacterial growth, ParE toxins purification, and to ParD antitoxin stability. We demonstrated that ParE-mediated DNA cleavage leads to increased mutation frequency but does not inherently drive antibiotic resistance, suggesting its potential as an antibacterial strategy. We also demonstrated that the ParE C-terminal region, previously suggested to influence its toxicity, is insufficient to determine ParE potency. In addition, we optimized methods for purifying ParE toxins, establishing the effectiveness of co-transformation with DNA gyrase to overcome ParE toxicity. Lastly, we explored the instability of the PaParD1 antitoxin, identifying key factors and oligomeric states that affect its degradation. These studies contribute to a deeper understanding of the ParDE TA systems, and provide new methodology that will be useful as we continue to explore potential usage of these toxin mechanisms as antibacterial approaches.

Reference

1. Jurėnas, D., et al., *Biology and evolution of bacterial toxin-antitoxin systems.* Nat Rev Microbiol, 2022. **20**(6): p. 335-350.
2. Muthuramalingam, M., et al., *The toxin from a ParDE toxin-antitoxin system found in Pseudomonas aeruginosa offers protection to cells challenged with anti-gyrase antibiotics.* Mol Microbiol, 2019. **111**(2): p. 441-454.
3. Beck, I.N., et al., *Toxin release by conditional remodelling of ParDE1 from Mycobacterium tuberculosis leads to gyrase inhibition.* Nucleic Acids Res, 2023.
4. Yuan, J., et al., *Vibrio cholerae ParE2 poisons DNA gyrase via a mechanism distinct from other gyrase inhibitors.* J Biol Chem, 2010. **285**(51): p. 40397-408.
5. Gupta, M., et al., *The Chromosomal parDE2 Toxin-Antitoxin System of Mycobacterium tuberculosis H37Rv: Genetic and Functional Characterization.* Front Microbiol, 2016. **7**: p. 886.
6. Ames, J.R., et al., *Expression of different ParE toxins results in conserved phenotypes with distinguishable classes of toxicity.* Microbiologyopen, 2019. **8**(10): p. e902.
7. Fiebig, A., et al., *Interaction specificity, toxicity and regulation of a paralogous set of*

ParE/RelE-family toxin-antitoxin systems. Mol Microbiol, 2010. **77**(1): p. 236-51.
8. Klemenčič, M., A. Halužan Vasle, and M. Dolinar, *The Cysteine Protease MaOC1, a Prokaryotic Caspase Homolog, Cleaves the Antitoxin of a Type II Toxin-Antitoxin System.* Front Microbiol, 2021. **12**: p. 635684.
9. Gupta, K., et al., *Contribution of the Chromosomal ccdAB Operon to Bacterial Drug Tolerance.* Journal of Bacteriology, 2017. **199**(19): p. 10.1128/jb.00397-17.
10. Snead, K.J., L.L. Moore, and C.R. Bourne, *ParD Antitoxin Hotspot Alters a Disorder-to-Order Transition upon Binding to Its Cognate ParE Toxin, Lessening Its Interaction Affinity and Increasing Its Protease Degradation Kinetics.* Biochemistry, 2022. **61**(1): p. 34-45.
11. Sterckx, Y.G., et al., *An efficient method for the purification of proteins from four distinct toxin-antitoxin modules.* Protein Expr Purif, 2015. **108**: p. 30-40.
12. Garcia-Rodriguez, G., et al., *Toxin:antitoxin ratio sensing autoregulation of the Vibrio cholerae parDE2 module.* Sci Adv, 2024. **10**(1): p. eadj2403.
13. Johnson, E.P., A.R. Strom, and D.R. Helinski, *Plasmid RK2 toxin protein ParE: purification and interaction with the ParD antitoxin protein.* J Bacteriol, 1996. **178**(5): p. 1420-9.
14. Fraikin, N., F. Goormaghtigh, and L. Van Melderen, *Type II Toxin-Antitoxin Systems: Evolution and Revolutions.* J Bacteriol, 2020. **202**(7).
15. Loris, R. and A. Garcia-Pino, *Disorder- and dynamics-based regulatory mechanisms in toxin-antitoxin modules.* Chem Rev, 2014. **114**(13): p. 6933-47.
16. Sterckx, Y.G., et al., *A unique hetero-hexadecameric architecture displayed by the Escherichia coli O157 PaaA2-ParE2 antitoxin-toxin complex.* J Mol Biol, 2016. **428**(8): p. 1589-603.
17. Blaszczak A, Georgopoulos C, Liberek K. On the mechanism of FtsH-dependent degradation of the sigma 32 transcriptional regulator of Escherichia coli and the role of the Dnak chaperone machine. Mol Microbiol. 1999;31(1):157-166. doi:10.1046/j.1365-2958.1999.01155.x

Appendix A

Chapter II Supporting information

Table S2.1. Primer sequences used for cloning

Name	Sequence (5' – 3')[a]
pBAD33_VcD2_F	aaaacattcgTCTAGAGTCGACCTGCAG
pBAD33_VcD2_R	ttttagccatAACTAGGCTCCTTACTGG
VcD2_F	gagcctagttATGGCTAAAAATACAAGTATCAC
VcD2_R	cgactctagaCGAATGTTTTCACTATCGAG
pBAD33_VcE2_F	cggcgcataaTCTAGAGTCGACCTGCAG
pBAD33_VcE2_R	atggtttcatAACTAGGCTCCTTACTGG
VcE2_F	gagcctagttATGAAACCATTTAATCTTACCG
VcE2_R	cgactctagaTTATGCGCCGAATATTGG
pBAD33_VcDE2_F	cggcgcataaTCTAGAGTCGACCTGCAG
pBAD33_VcDE2_R	ttttagccatAACTAGGCTCCTTACTGG
VcDE2_F	gagcctagttATGGCTAAAAATACAAGTATCAC
VcDE2_R	cgactctagaTTATGCGCCGAATATTGG
pBAD33_VcDE1_F	tgtttcttagATGCACACACTAACAGCAAATG
pBAD33_VcDE1_R	aaacgctcaaAAGCTTGCATGCCTGCAG
VcE1_F	atgcaagcttTTGAGCGTTTACCTCAATATG
VcE1_R	gtgtgtgcatCTAAGAAACAAAGCGTGAC
PaParE1-Vc_F	CCAATATTCGGCGCATAGGAAATTACCCCCTGAGGATC
PaParE1-Vc_R	GTTCACATCCATGCTCTTGACTCTGTCGATGCGCAA
PaParE1-Cc_F	GGCTCACCTTGGCTGAGAAATTACCCCCTGAGGATC
PaParE1-Cc_R	CTGGCGTTCATGCTTTGGACTCTGTCGATGCGCAA

[a.] lower case indicates the overlapping part for Gibson Assembly.

Table S2.2. The component of M9 minimal media

M9-cas medium				
Component	$CaCl_2$	$MgSO_4$	Casamino acid	5x M9 salts
Concentration	0.1mM	2mM	0.20%	1x

5x M9 salts				
Component	Na_2HPO_4	KH_2PO_4	NaCl	NH_4Cl
Concentration	240mM	110mM	43mM	93mM

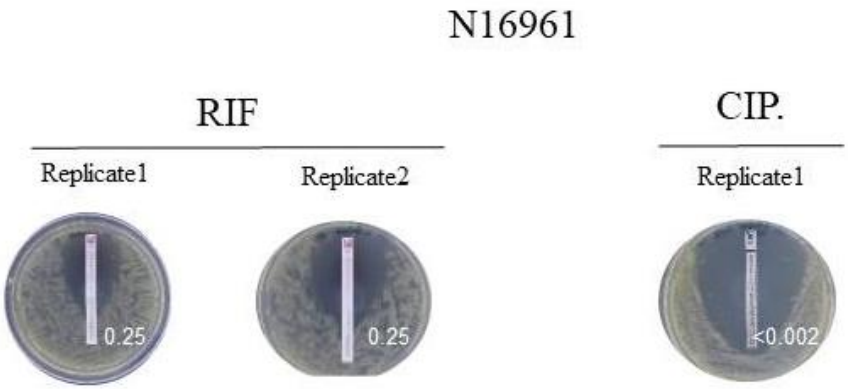

Figure. S2.1. Determination of MIC of RIF and CIP using antibiotics strips. The cultures of V. cholerae N16961 were streaked on LB agar plates after overnight incubation (18 - 24hrs). The antibiotic strip containing RIF or CIP were placed in the center of the plates. The MIC is determined by reading the scale on the strips at the point at which bacterial growth begins. RIF: rifampicin; CIP: ciprofloxacin.

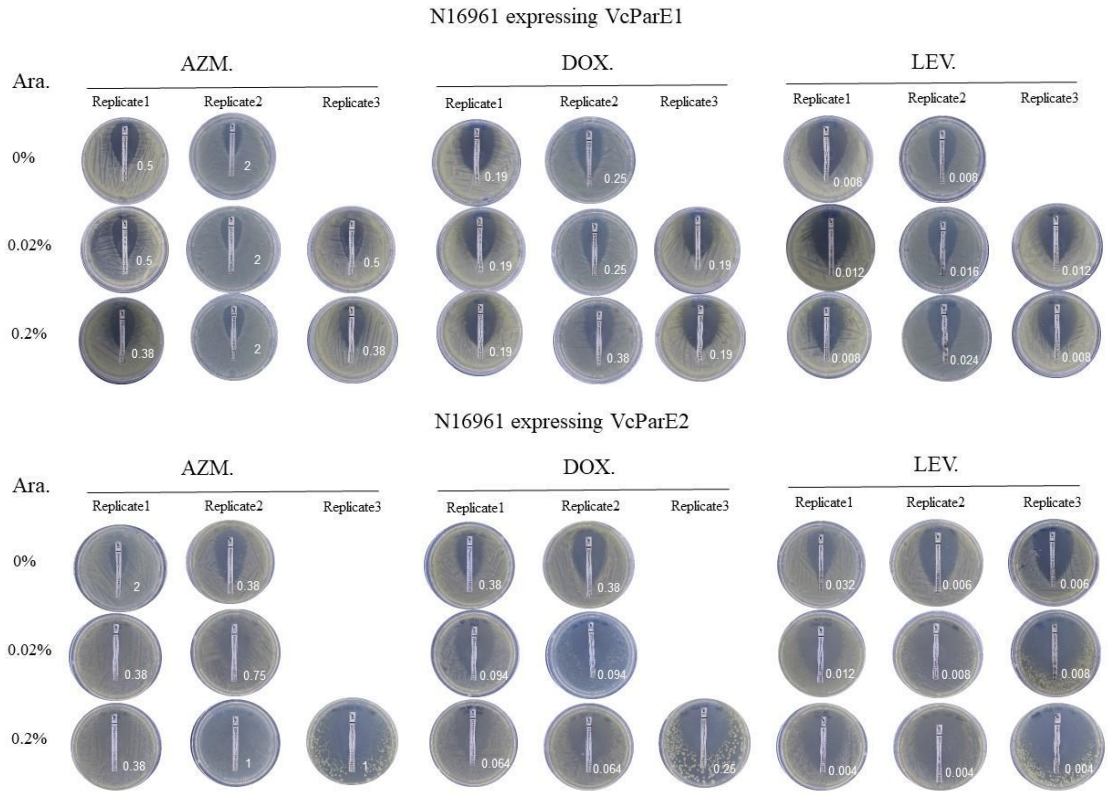

Figure S2.2. Impact of VcParE toxin expressions on *V. cholerae* N16961 antibiotic susceptibility. The cultures of *V. cholerae* N16961 were streaked on LB agar plates after 8hrs expression of VcParE1 and VcParE2. The antibiotic strip containing RIF or CIP were placed in the center of the plates. The MIC is determined by reading the scale on the strips. AZM: azithromycin; DOX: doxycycline; LEV: levofloxacin.

Appendix B

Chapter III Supporting information

Table S3.1. Primer sequences used for cloning

Name	Sequence (5' – 3')[a]
His_pET28a_F	attcggcgcaGAGCACCACCACCACCAC ttttagccat
His_pET28a_R	GGTATATCTCCTTCTTAAAGTTAAACAAAATTATTCTAGA ATCC
VcDE2_His_F	gagatataccATGGCTAAAAATACAAGTATCACTCTTG
VcDE2_His_R	ggtggtgctcTGCGCCGAATATTGGGTTC
pBAD33_Strep_VcE1_F	gcagtttgaaaaaATGCAAAATAAACAATATAAGC
pBAD33_Strep_VcE1_R	ggatggctccacatATTGAGGTAAACGCTCAATC

[a.] lower case indicates the overlapping part for Gibson Assembly.

Appendix C

Chapter IV supporting information

Table S4.1. Primer sequences used for cloning

Name	Sequence (5' – 3')[a]
3Q_PaD1_Fwd	gcacgtcGCTGCCATCGATGAAGGC
3Q_PaD1_Rev	caactactCCTTTCCAGGTACTGCGC
5Q_PaD1_Fwd	ctcgcggcaTACCTGGAAAGGAGTAGTTGG
5Q_PaD1_Rev	cgctgcccgCAGGTGGTAGGGTCGGTC

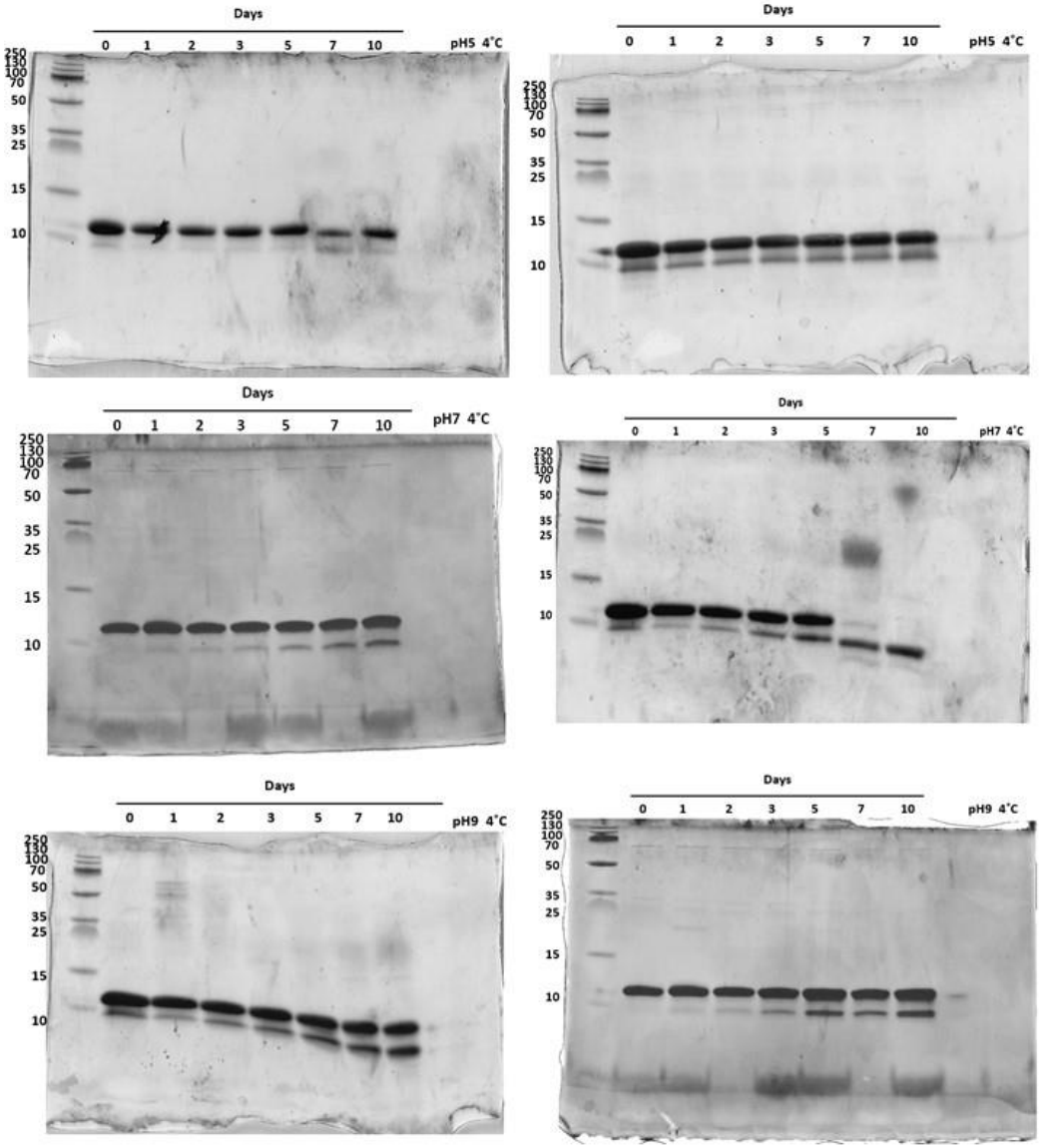

Figure S4.1. Replicate gels for monitoring PaParD1 degradation at pH5, pH7, and pH9 at 4˚C. These data are summarized in the text, Figure 4.1. The estimation of band intensities was proceeded using ImageJ, and the degradation percentage was determined by the ratio between the overall ParD1 band and the degradation band in each lane.

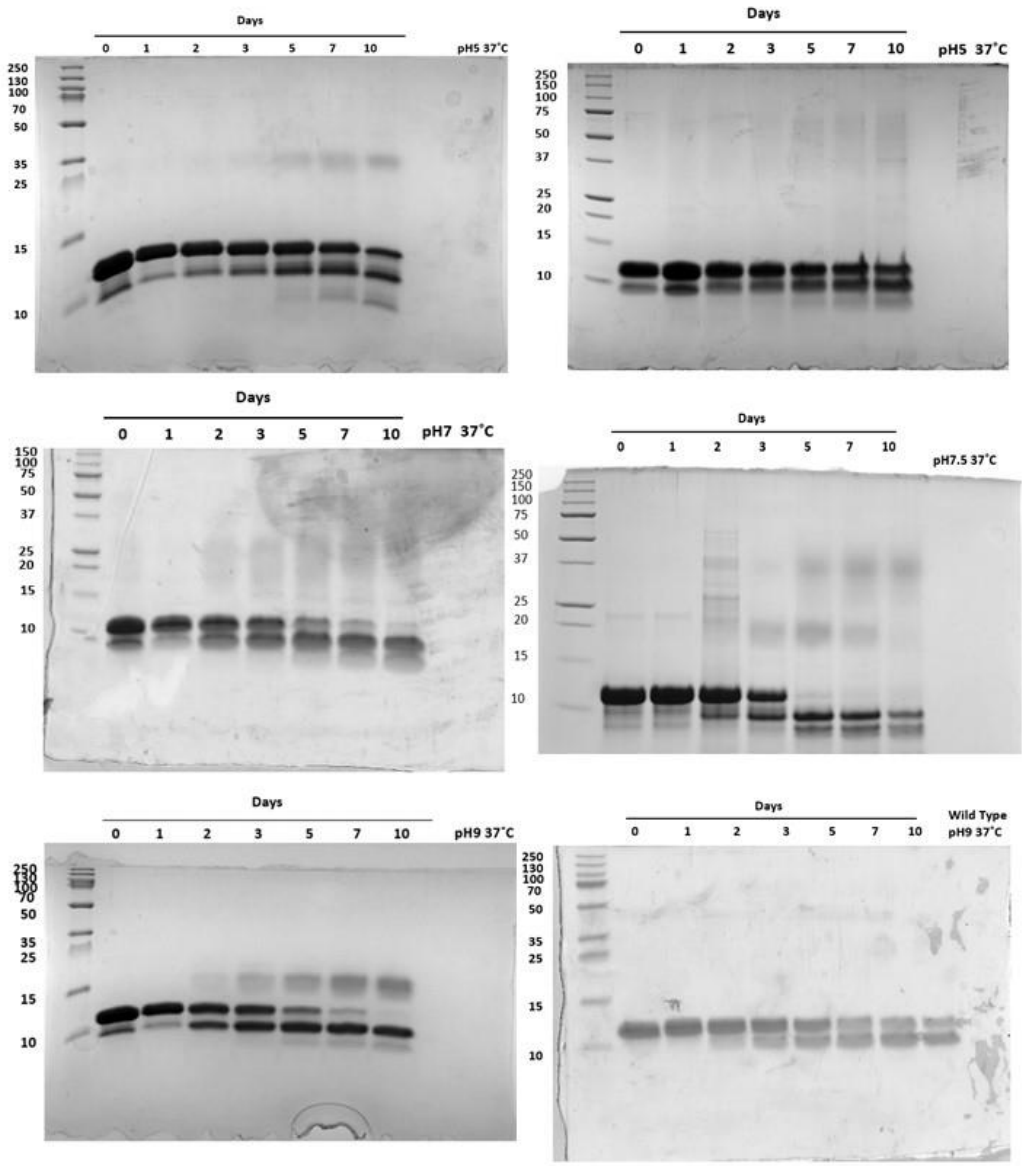

Figure S4.2. Replicate gels for monitoring PaParD1 degradation at pH5, pH7, and pH9 at 37˚C. These data are summarized in the text, Figure 4.1. The estimation of band intensities was proceeded using ImageJ, and the degradation percentage was determined by the ratio between the intact ParD1 band and the degradation band in each lane.

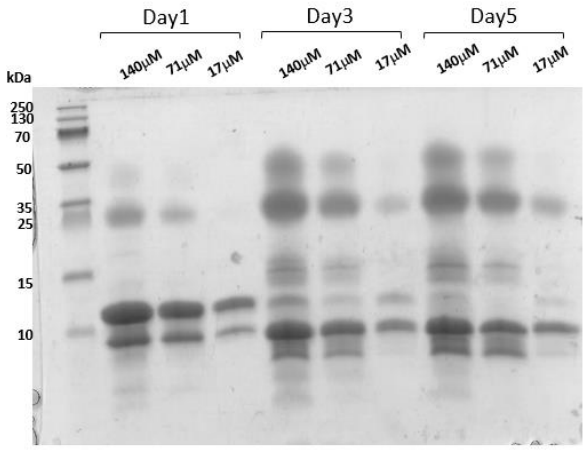

Figure S4.3. Replicate gel for monitoring PaParD1 degradation with three different concentrations at 37˚C. These data are summarized in the text, Figure 4.2. The estimation of band intensities was proceeded using ImageJ, and the degradation percentage was determined by the ratio between the overall ParD1 band and the degradation band in each lane.

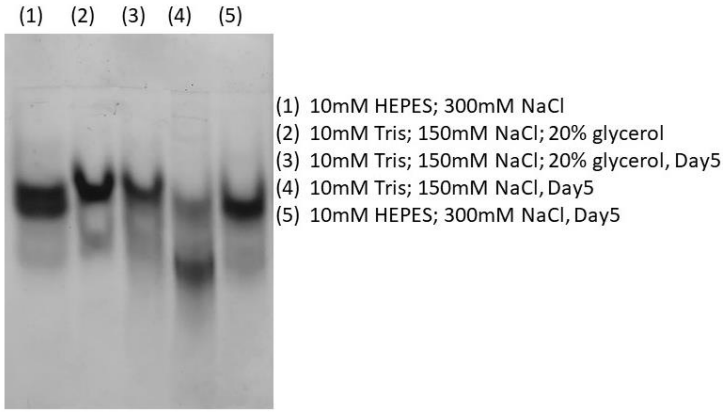

Figure S4.4. Replicate native gel for assessing PaParD1 status at different buffer conditions. These data are summarized in the text, Figure 4.3.

Monomeric PaParD1 ratio = 0.0%

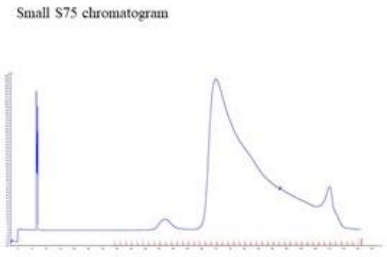

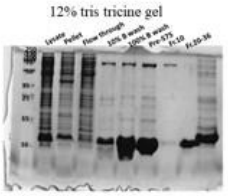

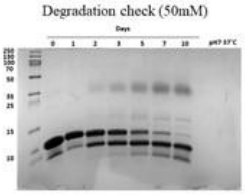

Monomeric PaParD1 ratio = 8.62%

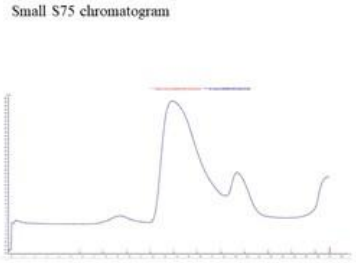

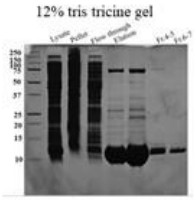

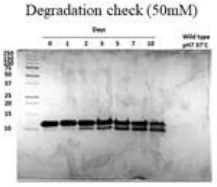

Monomeric PaParD1 ratio = 62.8%

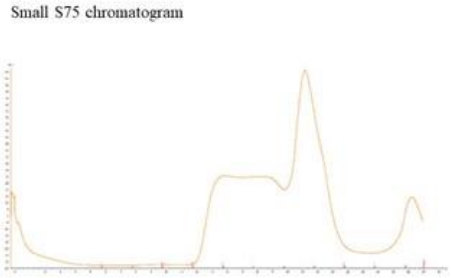

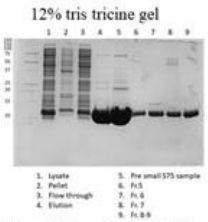

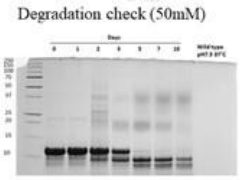

Monomeric PaParD1 ratio = 44.1%

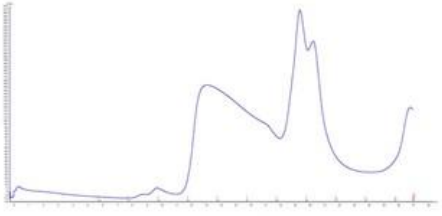

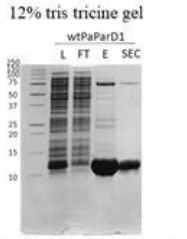

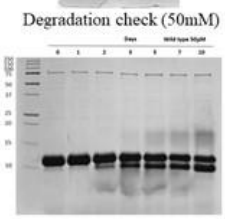

Figure S4.5. The chromatogram and corresponding protein gels regarding to the monomeric ratio of PaParD1. These data are the details of Figure 4.4.C and summarized in the text, Figure 4.4. The ratio of monomeric PaParD1 is determined by the area of peak representing monomeric PaParD1 to the area of peak representing dimeric PaParD1.

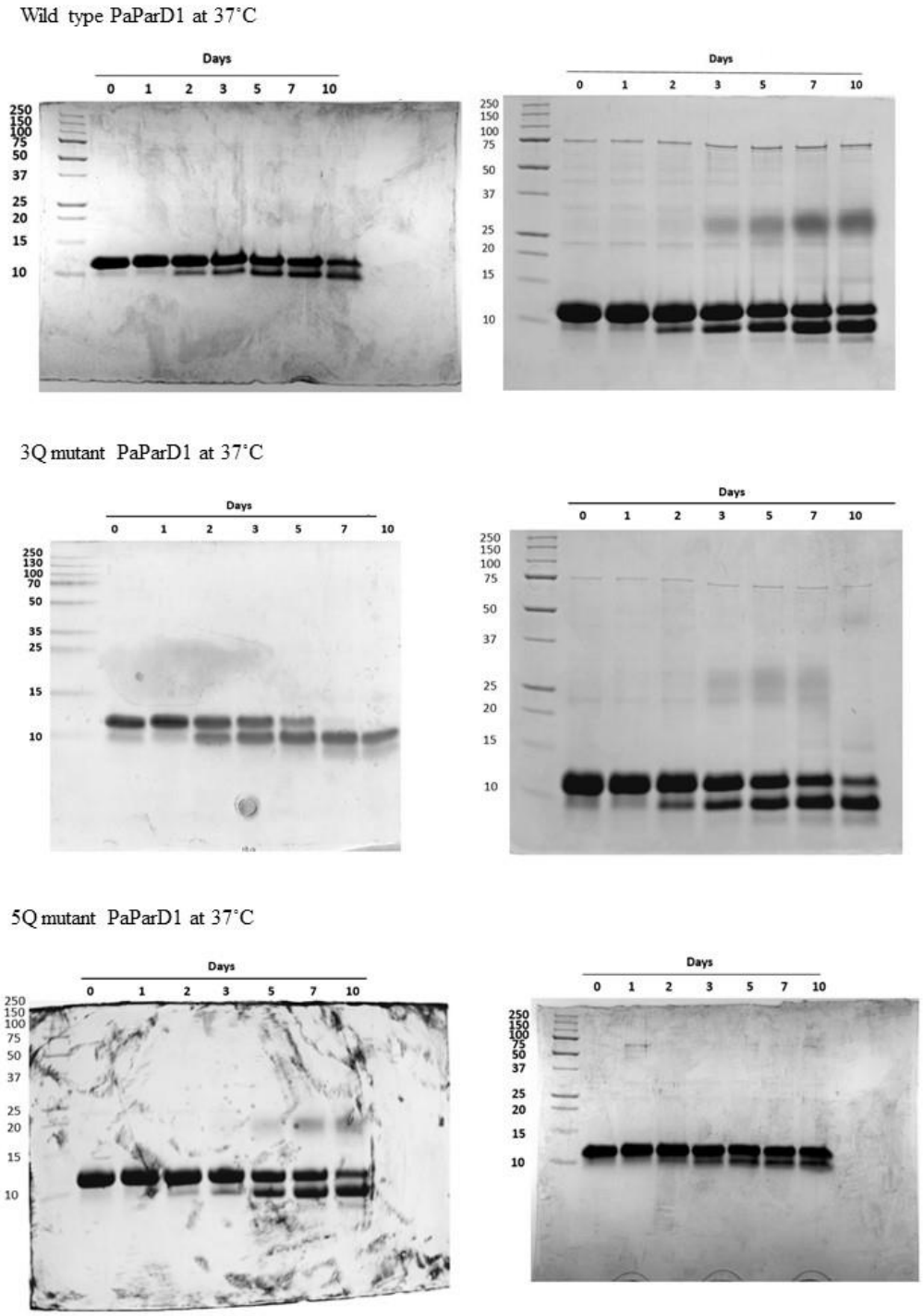

Figure S4.6. Replicate gels for monitoring wild type, 3Q mutant, 5Q mutant PaParD1 degradation at pH7, 37˚C. These data are summarized in the text, Figure 4.5. The estimation of band intensities was proceeded using ImageJ, and the degradation percentage was determined by the ratio between the intact ParD1 band and the degradation band in each lane.

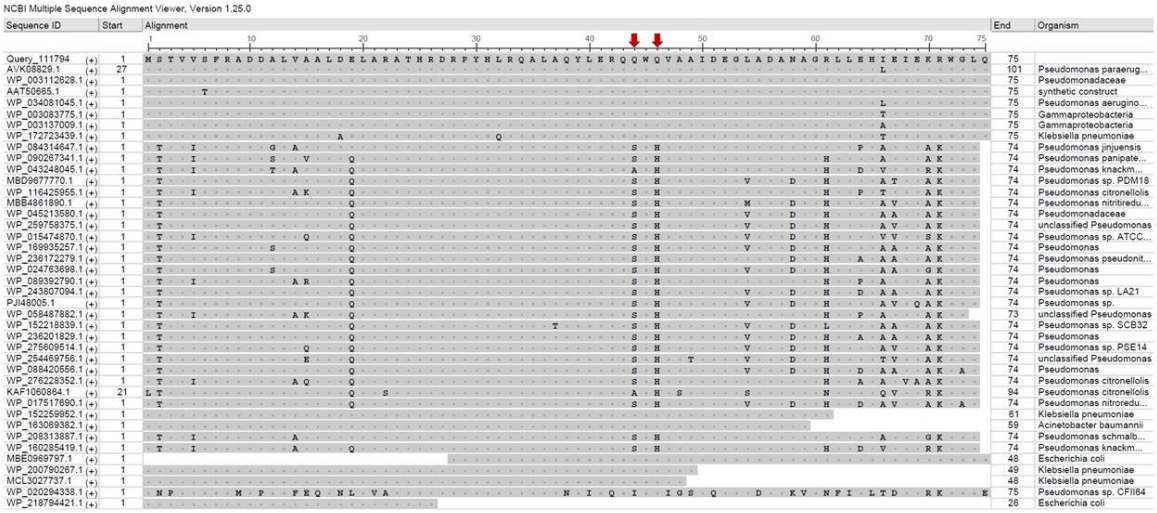

Figure S4.7. Sequence alignment shows the sequence similarity between PaParD1 and the other ParD proteins. The alignment was processed through NCBI blast. (https://blast.ncbi.nlm.nih.gov/) p The sequence search was based on the database of non-redundant protein sequences and the algorithm used in the search was Quick BLASTP (Accelerated protein-protein BLAST) The Q44 and Q47 of PaParD1 were highlighted by red arrows.

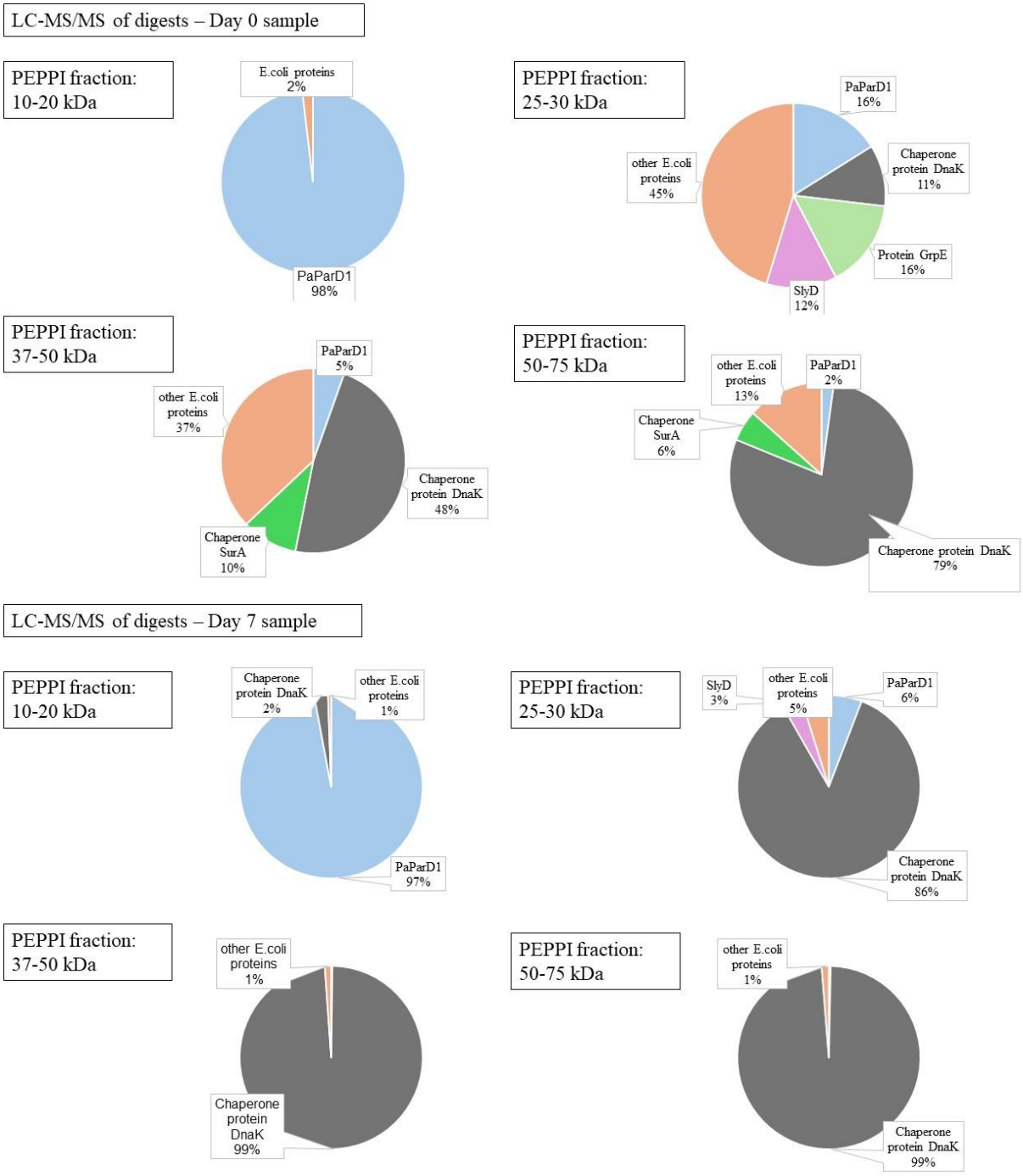

Figure S4.8. The distribution of protein speices in each molecular weight in PaParD1 degradation monitor at Day 0 and Day7. The pie charts presented the abundance of each protein species in different molecular weight at Day 0 and Day 7 PaParD1 degradation. The identification of each species was approached via LC-MS/MS and processed by Dr. Cynthia Nagy from Fornelli group.

Table S4.1. Primer sequences used for cloning

Name	Sequence (5' – 3')[a]
3Q_PaD1_Fwd	gcacgtcGCTGCCATCGATGAAGGC
3Q_PaD1_Rev	caactactCCTTTCCAGGTACTGCGC
5Q_PaD1_Fwd	ctcgcggcaTACCTGGAAAGGAGTAGTTGG
5Q_PaD1_Rev	cgctgcccgCAGGTGGTAGGGTCGGTC

Table S4.2. Profiles showing potential hydrogen bonding in the PaParD1 dimer. The data was calculated using PDBePISA(https://www.ebi.ac.uk/pdbe/pisa/). It shows that the solvent-accessible area of the interface (1736 Å ^{2}) accounts for 22.9% of total surface area (7575.5 Å ^{2}). It also shows details of specific residues involving in the formation of hydrogen bonding, including distance and ΔG value. Right panel shows the corresponding residues in PaParD1 dimer. The major interaction is from N-terminal RHH domain, highlighted in black dash box. The structure is from PaParDE1 (PDB entry: 6XRW) removed PaParE1.

PaParD1_1	Dist. [Å]	PaParD1_2	ΔG (kcal/M)
ASP 11[N]	2.96	MET 1[O]	-0.38
ALA 9[N]	2.89	THR 3[O]	0.1
PHE 7[N]	2.89	VAL 5[O]	1.5
SER 6[OG]	2.36	SER 6[OG]	0.12
VAL 5[N]	2.85	PHE 7[O]	1.07
ARG 33[NH1]	2.84	ARG 8[O]	0.13
THR 3[N]	2.85	ALA 9[O]	-0.06
ARG 42[NH2]	2.76	GLN 38[OE1]	0.06
HIS 31[ND1]	2.77	TYR 39[OH]	0.12
MET 1[O]	2.96	ASP 11[N]	0.07
THR 3[O]	2.89	ALA 9[N]	-0.06
VAL 5[O]	2.89	PHE 7[N]	1.07
PHE 7[O]	2.85	VAL 5[N]	1.5
ARG 8[O]	2.84	ARG 33[NH1]	0.61
ALA 9[O]	2.85	THR 3[N]	0.1
ASP 11[OD1]	3.52	THR 3[N]	-0.38
GLN 38[OE1]	2.76	ARG 42[NH2]	-0.49
TYR 39[OH]	2.77	HIS 31[ND1	0.78

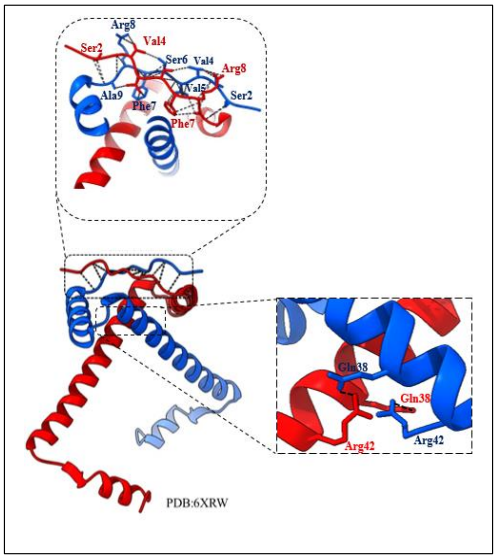

Table S4.3. Profiles showing mass and relative abundance of truncated PaParD1 around 8.1 – 11kDa in Day1 and Day7. Data was obtained from Dr. Nagy from Dr. Fornelli's lab

Day 1.

	Monoisotopic mass (Da)	Average mass (Da)	Rel. abundance (%)
MetOFF	10725.443	10732.17	100
1× oxidation, MetOFF	10741.443	10748.17	31.91
2× oxidation, MetOFF	10757.437	10764.18	25.36
	10903.487	10910.29	22.61
	10772.442	10779.19	12.26
	10983.475	10990.31	10.27
	10788.443	10795.19	8.48
	10919.483	10926.29	7.92
MetOFF trunc. (2-92)	10241.195	10247.63	6.88
	10999.479	11006.32	6.15
	10935.497	10942.31	5.74
	11015.463	11022.31	4.2
MetON	10854.445	10861.22	3.22

Day 7.

	Monoisotopic mass (Da)	Average mass (Da)	Rel. abundance (%)
MetOFF trunc. (2-85)	9335.667	9341.53	100
MetOFF trunc. (2-75)	8396.19	8401.55	84.06
	28081.25	28098.79	68.02
	14683.11	14692.33	41.3
	27711.04	27728.36	40.1
1× oxidation, trunc (2-85)	9351.653	9357.52	33.18
2× oxidation, trunc (2-85)	9367.657	9373.54	25.22
	27726.04	27743.37	21.69
	8411.175	8416.55	20.3
	8210.129	8215.35	19.82
	30897.88	30917.18	19.53
	30995.91	31015.26	16.64
	30928.84	30948.15	15.22
	30929.84	30949.16	15.21
	30913.85	30933.16	14.79
MetOFF	10725.44	10732.16	14.54

Table S4.4. Profiles showing mass and relative abundance of truncated DnaK at retention time approx. 18.4 min and 14 – 16min. Data was obtained from Dr. Nagy from Dr. Fornelli's lab.

Retention time approx. 18.4min

Mono mass (Da)	Avg mass (Da)	Rel. abund. (%)	Mono mass (Da)	Avg mass (Da)	Rel. abund. (%)
26052.4	26068.75	7.17	22885.83	22900.2	6.54
22940.9	22955.32	27.2	23818.39	23833.32	5.97
23736.35	23751.24	17.17	23182.04	23196.6	5.2
22811.88	22826.19	4.18	23026.95	23041.42	4.46
26093.59	26109.96	2.99	24121.55	24136.69	4.41
23346.11	23360.77	1.54	22910.84	22925.23	1.33
23720.35	23735.23	35.28	22854.82	22869.16	33.03
23110.02	23124.54	21.55	22427.59	22441.62	5.36
22869.82	22884.17	17.07	22837.82	22852.15	2.7
23009.9	23024.36	13.46	22930.87	22945.27	1.78
22187.45	22201.34	8.69	23679.25	23694.1	1.64
23339.1	23353.75	7.21	22952.89	22967.31	8.88

Retention time approx. 14-16min

Mono mass (Da)	Avg mass (Da)	Rel. Abund (%)	Mono mass (Da)	Avg mass (Da)	Rel. Abund (%)
27678.05	27695.36	100	28148.30	28165.89	15.14
28050.27	28067.80	99.89	27791.12	27808.49	14.68
27694.03	27711.35	86.84	27062.72	27079.67	14.29
6646.35	6650.55	65.52	27664.00	27681.29	13.42
28065.25	28082.78	61.31	7342.74	7347.48	13.27
27711.03	27728.36	42.91	28163.32	28180.91	12.94
28081.25	28098.79	39.83	30897.87	30917.17	12.87
27045.71	27062.64	36.92	6678.34	6682.58	12.24
7585.83	7590.72	34.04	26868.58	26885.41	11.85
27724.04	27741.37	33.87	30913.84	30933.15	11.3
27777.08	27794.44	30.45	27656.00	27673.29	10.03
27239.81	27256.85	29.96	30995.87	31015.22	9.87
27792.10	27809.47	19.68	27807.08	27824.46	8.65
27740.04	27757.38	19.62	28101.30	28118.85	7.8
7255.70	7260.38	19.42	27210.74	27227.77	7.46
6662.36	6666.58	19.33	27752.03	27769.38	7.32
6589.32	6593.49	19.14	27382.83	27399.97	7.09
27238.81	27255.85	19.06	27076.71	27093.67	6.76
14683.10	14692.32	17.49	27774.10	27791.46	5.89
27321.81	27338.91	15.55	6946.50	6950.93	5.68